LABORATORY COLUMN SOLUTE CONCEN-

TRATION MEASUREMENT USING X-RAY

FLUORESCENCE SPECTROSCOPY
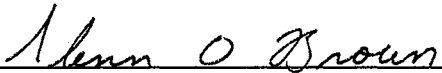
By

JACK E. GAZIN

Bachelor of Science
Oklahoma State University
Stillwater, Oklahoma
1984

Master of Science
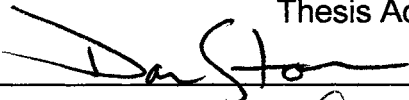Oklahoma State University
Stillwater, Oklahoma
1992

Submitted to the Faculty of the
Graduate College of the
Oklahoma State University
in partial fulfillment of
the requirements for
the Degree of
DOCTOR OF PHILOSOPHY
May, 1998

LABORATORY COLUMN SOLUTE CONCEN-

TRATION MEASUREMENT USING X-RAY

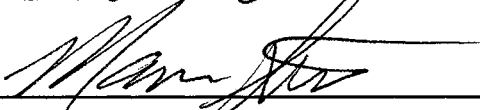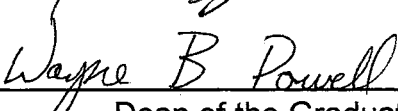# FLUORESCENCE SPECTROSCOPY

Thesis Approved:

Glenn O Brown

Thesis Advisor

Dan Storm

David R. Thompson

Phil Barta

Marvin Stone

Wayne B Powell

Dean of the Graduate College

ACKNOWLEDGEMENTS

I would like to express appreciation to Dr. Glenn Brown for his advice, encouragement, and friendship throughout my graduate studies and research. Dr. Brown also deserves credit for enduring my irreverent attitude toward life in general. Kudos are extended to Dr. Marvin Stone for teaching me the ins and outs of instrumentation and hardware-software interfacing. Thanks also go to the other members of my committee: Dr. David Thompson, Dr. Dan Storm, and Dr. Nick Basta.

Now that my tenure as student is ended, I would also like to extend my appreciation to the faculty and staff of the Department of Biosystems and Agricultural Engineering. I would especially like to thank Wayne Kiner, Manager, Research Instrument Laboratory, as well as Robert Harshman and Robert Harrington of the Biosystems and Agricultural Engineering Laboratory.

My deepest appreciation is extended to Dr. Tamara Walkingstick. We have now seen each other through the doctoral process. Neither of us would have succeeded without one another. Finally, I would like to thank my parents for their support and confidence in me.

TABLE OF CONTENTS

Chapter

LIST OF TABLES

LIST OF FIGURES

CHAPTER 1

INTRODUCTION

New techniques of evaluating solute transport and distribution in saturated

and unsaturated systems are always needed. These techniques can either be

variations of existing methods or completely new and unique. Innovative metho-

dology and technology may be in the form of advancing the governing equations

or variations of an existing apparatus. Examples of areas under current research

include: macropore affects, fingering, multiphase flow in unsaturated systems,

and transport and flow in nonhomogeneous systems.

The original motivation for research presented here was to non-intrusively

study steady-state flow of solutions in saturated porous media using gamma-ray

transmission and computed tomography methods. This would include the study

of macropore effects, preferential flow, and variation in soil density in laboratory

columns due to packing. System error analysis was to be investigated during the

course of the various experiments.

Background

Prior to this investigation Brown, Stone, and Gazin (1993) designed and

built a gamma scanner and quantitatively evaluated it in terms of accuracy,

resolution, and sensitivity. Additionally, Brown et al. (1994) studied small-scale

1

density variations and macropores in 50.8 mm driven cores. Initial research using a parallel beam gamma scanner quickly showed that a solution does not, in fact, infiltrate uniformly into a "homogeneous" soil. An acrylic test column was packed with an aeolian soil and scanned at intervals to establish density variations. A flux of water was then uniformly applied and allowed to equilibrate over a period of time. Subsequent imaging of the column over the same intervals showed that the distribution of moisture had assumed a "finger" geometry.

Refinements in the scanner led to a non-collinear, dual-source, dual-energy scanner with a second source-detector pair placed at an angle of 48 degrees to the primary source-detector pair. This configuration would have allowed the simultaneous measurement of dry bulk density and moisture content of the test soil. Typical arrangements, however, have the sources in line with one another.

A solution of 100,000 ppm sodium iodide was used in the next series of experiments to enhance the density contrast between the solution and soil. A low-energy peak was found during preliminary analysis of the offset detector data. Subsequent investigation determined it to be the result of primary-energy photons interacting with iodide K-shell electrons to produce fluoresced x-rays. This peak would have been obscured by Compton haze with an inline, dual-source, single-detector system.

At this point it occurred to the author that a repacked laboratory column could be analyzed simultaneously, in terms of moisture distribution as well as analyte concentration, with a single radioisotope source.

Objectives

The research presented will develop and verify a new technique for the analysis of high-Z (atomic number) salt solutions in porous media. It combines gamma-ray attenuation and x-ray fluorescence spectroscopy (XRF). All data was acquired simultaneously with one source and provided a comprehensive tool for analysis of the column physical properties, moisture content, and analyte concentration. This approach reduces the time needed for a priori information as well as expense and regulatory requirements needed for a second radioisotope source.

During the course of the investigation an attempt was made to: (1) calibrate analyte x-ray intensity with concentration and position in the sample; (2) determine the location of x-ray generation using Monte Carlo modeling of radiation transport theory; (3) obtain information concerning the feasibility of simultaneous image and XRF data acquisition; (4) perform system error analysis; (5) determine the optimum configuration for a dual purpose, single source apparatus to be used for both imaging and XRF; and (6) determine the types of experiments for which this system will be practical (static or dynamic flow).

The end result of this research is intended to enable researchers to have access to a relatively low cost multifaceted laboratory tool to supplement more traditional means of analyses.

CHAPTER 2

PHOTON INTERACTIONS

AND

GENERATION OF FLUORESCED X-RAYS

Introduction

X-ray fluorescence occurs when a beam of photons is impinged on a
target. Generally, the fluoresced x-rays are of too low an energy to detect unless
an extremely sensitive detector is being used. If fluoresced x-rays are being
produced because of the presence of a high-Z element they may not be observed
due to low intensity and/or a noisy background.

Fluorescent x-rays can be viewed as an easily obtainable additional source
of information when doing gamma attenuation or tomography research. The only
other needed components are an offset detector and a relatively high concen-
tration of a high-Z salt to serve as the target analyte. A brief summary of gamma
attenuation and computed tomography research in the soil sciences is given to
provide background prior to a discussion of basic photon interactions.

Gamma Attenuation

Since van Bavel's (1957) use of gamma-ray attenuation principles for the

4

determination of bulk density in dry soil, numerous researchers have applied this technology for the determination of soil-water content. De Vries (1969) used attenuation data gathered in situ in conjunction with a low impedance tensiometer to construct a partial water retention curve. He also discussed the effect of collimation (restriction of the beam on both the source and detector) on photon counting statistics. Topp (1969) used gamma attenuation to measure the soil-water content of a repacked column (sandy loam) for his soil-water hysteresis studies. Fritton (1969) evaluated the resolving time, mass absorption coefficient, and water content of soils. Gardner et. al. (1972) used a dual-source (two sources, two photon energies) arrangement for the simultaneous determination of water content and soil bulk density as well as evaluating the systematic error involved in dual-source measurements. Reginato and Jackson (1971) measured soil-water content under field conditions using temperature-compensated gamma-ray transmission. A gamma-ray transmission method was also used by Elzeftawy and Mansell (1975) to determine soil-water content during the course of their study of unsaturated steady-state and transient flow in sand. Nofziger (1978) thoroughly evaluated errors associated with dual-source determinations of soil-water content and bulk density in non-uniform soils. Grismer (1984) used a dual-source gamma-ray configuration to investigate the transport of various salts in unsaturated soils. Stillwater and Klute (1988) presented a method for the determination of the precision and accuracy of soil-water content and bulk density using a collinear, dual-source system.

Gamma attenuation devices allow non-destructive determination of soil-

water content and solute concentration. These values, however, are averaged across the diameter of the sample. The internal properties of the sample within the collimated beam remain unknown. These properties can be determined by constructing a parallel beam gamma-ray computed tomography system. The basic assemblage consists of a 3-axis positioning system (x-y and rotation, x-z and rotation, or y-z and rotation), multichannel analyzer, detector, and appropriate computer software.

Computed Tomography

In computed tomography (CT) attenuation data is taken at intervals across the sample. The sample is then rotated and data again taken. After an N X N matrix of data has been collected it is processed by an image reconstruction algorithm. The resultant image yields a visual map of linear attenuation coefficients throughout the sample. Density values are derived from this data set based on a priori knowledge of the sample. The original data, represented by the N X N matrix, is the Radon Transform of the attenuation within the sample cross section (Radon, 1917). The reconstructed data is the Inverse Radon Transform of those attenuations. The resolution of the image is based on the density of data points and the diameter of the photon beam. The accuracy of each voxel (volume element) in the image is a function of the reconstruction algorithm and photon statistics.

An example application of this technique is the quantitative determination of soil-water content. A repacked column is imaged to establish the dry bulk

density at a predetermined resolution. A solution is then introduced and allowed to equilibrate. The column is again imaged at the same resolution and compared to the initial data set. The change in density at each position within the sample is directly related to the increase in moisture content and an image of soil moisture can be generated.

CT was first applied to soil investigations using commercial x-ray scanners. Petrovic, Siebert, and Rieke (1982) used an American Science and Engineering CT scanner at the Michigan State University Clinical Center to study the precision, spatial resolution, and limitations with respect to soil bulk density. Hainsworth and Aylmore (1983) used both a commercial x-ray CT scanner as well as a gamma scanner to determine spatial changes in soil-water content with time. Crestana et. al. (1985) initially used a medical CT scanner to evaluate the feasibility of imaging soils and, because of the complexity and cost of a commercial medical scanner, built a gamma-ray miniscanner. Warner and Nieber (1988) used a commercial CT scanner to investigate the size and number of macropores in undisturbed soil cores. Hopmans et. al. (1994) used x-ray CT to study temporal variability of soil moisture in draining soil cores as well as to characterize the variability of porosity in soil cores. Grevers and de Jong (1994) utilized geostatistical analysis on CT data to study the spatial variability of macropores and Peyton et. al. (1994) established a soil-core breakthrough curve using CT.

X-ray Fluorescence

The attenuation effects mentioned above also have bearing on the generation of fluoresced x-rays. If a photon's energy is great enough it is possible to eject a K-shell electron from the target atom's orbit. Subsequent reordering of the remaining electrons yields either an Auger electron or an energy emission. If an emission occurs it is known as a *fluoresced x-ray*. This process lends itself to the non-destructive determination of concentration of certain solutes in solution.

The implication of above is given a typical parallel beam arrangement, it is possible to use a single source to both image the target and perform a laboratory column breakthrough curve experiment. One data set necessarily provides a check against the other. In other words, two independent sets of data can be obtained simultaneously from a single radioisotope source: one data set being attenuation data from the inline detector and the other being fluorescence data from an offset detector.

A primary goal of this chapter, then, is to define the nature of photon interactions as they pass through target material. This will then be applied to the problem of predicting the probability and intensity of x-ray fluorescence events. Consideration will be given to heterogeneous column matrices and target salts in solution. The development of the theory of basic photon interactions in this chapter is based on the current parallel-beam gamma tomography system. The source emits gamma rays with an energy of 0.662 MeV. The detector is a 2"

thallium-activated sodium iodide crystal (Nal) coupled to a photomultiplier and multichannel analyzer.

General Interactions

As a photon travels through matter it will either pass unimpeded or interact in some manner with the atomic structure of the material through which it is passing (Jenkins and De Vries, 1969). A given interaction is classified by the kind of target and the type of event. Targets are electrons, atoms, or nuclei, and events are absorption, scattering, or pair production (Hubbel and Berger, 1968). The sum of these three effects contribute to the mass absorption coefficient; the potential for a photon to be removed from the primary beam.

Photoelectric absorption is dominant at photon energies at or below the K-shell absorption edge energies of high-Z elements. This corresponds to the energy region below approximately 1.1 MeV. Inelastic Compton scattering occurs when the incident photon energy exceeds the absorption edge energy of the target but is not sufficient to initiate pair production. Scattering is dominant in the range of approximately 60 keV to 1.02 MeV. Pair production occurs when an incident photon with an energy of at least 1.02 MeV, the lower threshold energy for pair production, strikes an electron. The photon strikes the electron and moves it into a positive state at which time it becomes a positron. Because positrons are unstable in the presence of free electrons they annihilate one another with the subsequent emission of annihilation radiation. An annihilation emission is composed of two 0.511 MeV photons emitted in opposite directions.

The Mass Attenuation Coefficient

The photoelectric effect, Compton effect, and pair production all contribute to the attenuation of a photon beam as it passes through a substance. These three parameters comprise the mass attenuation coefficient, (μ/ρ, cm^2/g), where μ is the linear attenuation coefficient (cm^{-1}) and ρ is the density (g/cm^3). The mass attenuation coefficient can be calculated for an element, compound, or heterogenous mixture. One way of viewing the mass attenuation coefficient is as the probability of photon absorption and scattering based on the effective atomic weight of the target and the energy of the incident photon.

On a mass basis the attenuation coefficient is the same for an element in the gas, liquid, and solid phases. A more detailed analysis of the components of the mass attenuation coefficient is needed in order to analyze the dependence of μ/ρ on energy and atomic number.

The Photoelectric Absorption Cross Section. The probability of photon absorption is determined by the photoelectric cross section (τ_{pe}, b/atom) of the atom. Photon absorption occurs when the energy of an incident photon approaches the absorption edge energy of an electron shell from the high-energy side. On absorption of a photon by an electron, the electron is either ejected or placed into an outer shell vacancy. In both cases a hole state is created. This results in ionization of the atom. The remaining electrons reorder themselves to accommodate this new vacancy and energy is emitted in the form of an Auger electron or fluoresced x-ray during the reordering process.

The emitted x-ray spectral series is designated by the shell in which the electron transitions finalize (Tertian and Claisse, 1982). For example, if a K-shell electron were ejected the resultant emitted photons would be characteristic K x-rays since electron transitions finalized in the K shell. This x-ray series is the unique spectral signature of each element.

Characteristic x-rays are further subdivided based on their relative intensities with the most intense being the K_α x-ray. This line is the most desirable because of its intensity and energy. The total photoelectric absorption cross section is obtained by summing the contribution of each electron shell (τ_K + τ_L + ...). From this definition it can be seen that the photoelectric cross section is highly dependent on Z.

The Compton Cross Section. The probability of photon scattering is given by the Compton scattering cross section (σ_C, b/atom or b/electron). This cross section is largely dependent on the energy of the incident photon and only weakly dependent on Z. For this reason σ_C is considered to be the same for all elements. The important point about Compton scattering is that an incident photon of energy, E, will have a reduced energy, E', after a scattering event. This, in effect, removes the photon from the beam even if detected since it is no longer a primary energy photon.

The relationship between the photon's angle of scatter (θ) and change in energy is given by

$$\frac{E}{E'} = \frac{1}{1 + (E/mc^2)(1 - \cos\theta)}$$ 2.1

where E and E' are in MeV. The relativistic electron rest energy is denoted by

mc^2. Through the conservation of momentum the kinetic energy imparted to the

electron is $E - E'$.

Generating Detectable Fluoresced X-Rays

Probabilistic parameters must be evaluated when determining whether or

not an analyte is capable of producing a practical number of detectable

fluoresced x-rays. As already mentioned, the probability of a photon being

absorbed or scattered is governed by the mass attenuation coefficient, μ/ρ. The

probability that the photon interacts with an analyte electron in a mixture is

$$C_A \frac{\left(\frac{\mu}{\rho}\right)_{A,E}}{\left(\frac{\mu}{\rho}\right)_{M,E}}$$ 2.2

where C_A is the mass concentration of the analyte, and subscripts A,E and M,E

identify the attenuation coefficients for the analyte and matrix, respectively, at a

given energy.

X-ray generation is based on three factors if an analyte electron is struck

by an incident photon: (1) the absorption jump ratio, (2) fluorescent yield, and (3)

the probability of orbital electron transition. These three terms are generally

combined and called the excitation factor, P_A (Bertin, 1975). Values for items (1)

and (2) may be found in Bertin (1975). Values for determining orbital electron

transition probabilities may be found in ASTM Data Series DS 37 (1965).

Absorption Jump Ratio. Tthe probability of creating an electron vacancy

in the K shell of an analyte atom is known as the absorption jump ratio, J_K, and is

defined as

$$J_K = \frac{r_K - 1}{r_K} \qquad 2.3$$

where r_K is the ratio of the photoelectric absorption cross sections at the K-

absorption edge discontinuity defined by

$$r_K = \frac{T_K + T_{L_I} + T_{L_{II}} + T_{L_{III}} + \cdots}{T_{L_I} + T_{L_{II}} + T_{L_{III}} + \cdots} \qquad 2.4$$

and the subscripts on T refer to the various electron shells and subshells.

Fluorescent Yield. The fluorescent yield (ω) is the ratio of fluoresced x-

rays that actually leave the atom, n_f, to the number of primary photons absorbed,

n, calculated as

$$\omega = \frac{n_f}{n} \qquad 2.5$$

where ω decreases with increasing distance from the K shell and increases with

increasing Z.

Orbital Electron Transitions. The probability of orbital electron transitions for the K shell, $g_{K\alpha}$ is the ratio of the intensity of the K_α lines to all other K lines. It is defined as

$$g_{k\alpha} = \frac{I_{K\alpha_1} + I_{K\alpha_2}}{\Sigma I_K} \qquad 2.6$$

Equations 2.2, 2.3, 2.5, and 2.6 may now be combined to give the total probability of generating a detectable fluorescent x-ray

$$P(Xray) = C_A P_A \frac{\left(\frac{\mu}{\rho}\right)_{A,E}}{\left(\frac{\mu}{\rho}\right)_{M,E}} \qquad 2.7$$

Detecting Fluoresced X-Rays

Fluoresced x-rays are emitted isotropically and are themselves subject to attenuation along their path out of the sample. Factors affecting the detection of fluoresced x-rays include: (1) the intensity (photons/unit time) of the incident beam which affects the number of fluoresced x-rays generated, (2) the mass attenuation coefficient of the matrix; which can be viewed as a mixture of compounds, (3) the mass attenuation of the analyte (either an element or compound), (4) the depth of x-ray production, and (4) detector collimation and position.

Intensity of Primary Photons. The number of primary-energy photons that can be detected at some distance, L, from a point source is a function of the source activity, source and detector geometry, and pathlength. A radioisotope emits photons isotropically into a 4π region at a rate determined by the activity of the source. Source activity is given in Curies (Ci) with one Ci = 3.7 x 10^{10} transformations per second (s^{-1}). The number of photons that can escape the shielding is determined by the angle subtended by the collimator ($d\Omega/4\pi$) multiplied by the source strength.

The photons of a well-collimated source-detector pair can essentially be considered a parallel beam. With increasing distance from the source, photons are further attenuated by divergence before reaching the detector (assuming transmission through air). This form of attenuation follows the inverse square law and defined as

$$I_2 = I_1 \left(\frac{D_1^2}{D_2^2} \right) \qquad \qquad 2.8$$

where I_1 and I_2 are the intensities at distances D_1 and D_2 from the source, respectively.

The number of incident photons penetrating the target is also a function of target density, mass attenuation coefficient as well as depth of penetration. The equation defining the net intensity, I, of incident photons, I_o, reaching a unit volume is known as Lambert's Law and is written

$$I = I_o e^{-(\mu/\rho)\rho x}$$ 2.9

where ρ ($cm^3 g^{-1}$) is the density of the target material.

Calculating Mass Attenuation Coefficients. Since the incident beam and fluoresced x-rays will be attenuated by the matrix which is rarely, or never composed of just one element, it is necessary to evaluate μ/ρ for compounds and mixtures. Attenuation coefficients for the elements and some mixtures may be found in practically any text on radiation shielding (such as Jaeger, 1968) as well as references on nuclear engineering (such as Etherington, 1958). These references also give the method for determining μ/ρ for any compound or mixture for which the chemical formula is known.

The mass attenuation coefficient for a compound is obtained from the expression

$$\left(\frac{\mu}{\rho}\right)_{Compound} = w_i\left(\frac{\mu_i}{\rho_i}\right)$$ 2.10

where w_i is the weight percent of the ith element and μ_i/ρ_i is the coefficient for the constituent elements. Calculating the coefficient for a mixture is similar to that of a compound. In the case of mixtures, μ/ρ for each compound is weighted by the mass fraction present in the mixture.

Detector Collimation and Position. Detector collimation is determined by the desired type of analysis. In a parallel-beam configuration collimation of the detector and source should be the same, especially if computed tomography or attenuation data is desired. Depending on source activity and energy a collinear detector may be neither practical nor efficient for spectroscopy purposes. Data collected with the current configuration indicate that when the energy of the fluoresced line is very much below the energy of the incident beam the line is obscured by Compton scatter.

Evaluation of Equation 2.1 is one means of establishing the ideal detector position. By rearranging and evaluating E' at different values of θ ($0 < \theta < 180$) a symmetric field of Compton-scattered energies (corresponding to a distribution of Compton edges) can be constructed. Making E' the dependent variable yields

$$E' = E\left(1 + \frac{E}{mc^2}(1 - \cos\theta)\right)$$ 2.11

Optimum detector placement would theoretically be at one of the positions of local minima; of course physical constraints could make ideal placement impossible.

Detectable Analytes

Many of the factors affecting the efficiency of fluorescent x-ray production have been discussed. However, one remaining component has yet to be mentioned. As previously noted, each element emits a characteristic line at a particular energy. It may be possible to fluoresce K x-rays from any element but

may not be possible to detect the emissions if the proper detector is not in use.

The type and sensitivity of detector is an important component when considering which analytes are to be used in a study. The NaI(Tl) detectors currently being used in this study are generally most useful at energies above about 6 keV (Jenkins, et al.,1981);however, this is not a practical lower limit in actual practice.

Since x-ray generation is less efficient and yields lower energy x-rays with decreasing Z, a less intense spectrum will be detected because the resultant photons will not have the penetrative energy to escape a thick target. In all likelihood the analyte peak will be masked by the Compton scatter spectrum. For this reason iodide is a good choice for use as a target.

Suggested Analytes

Analytes used in XRF analysis with the current system should have characteristics which contribute to optimum x-ray production. They should have a high excitation potential (ω, J_K, $g_{K\alpha}$) and yield fluoresced photons of high enough energy to penetrate thick targets. Suggested lower and upper bounds in terms of Z are silver (Ag: Z=47) and lead (Pb: Z=82). Several ideal analytes are compounds of iodide, cesium, and tungsten. Compounds that are not acceptable for use with the current system are those with $E_{K\alpha}$ less than approximately 10 keV. These include elements with Z < 30 such as zinc, copper, and iron. Elements in the range 30 < Z < 47 are problematic.

Environmental Contaminants. XRF is particularly useful in the determination of heavy metals. In most aqueous systems mercury, (Hg(aq)) is stable as a free metal (Hem, 1985). Past and present sources of mercury are electrolysis cells, smelting, and automobile emissions. Another heavy metal commonly found in the environment is lead. Until the recent past lead was a common additive in fuels and was also part of auto emissions. Both lead and mercury can be adsorbed by, or complexed with, organics. If in a mobile form both are very good candidates for monitoring solute transport in porous media due to their characteristics.

Summary

Gamma ray attenuation instrumentation can be adapted to more fully utilize the radioisotope source in use. As has been shown, the attenuation process is composed primarily of absorption and scattering. The absorption aspect of attenuation can be used, in conjunction with a suitable analyte, to generate fluoresced x-rays. These x-rays are essentially an additional source that can be used for imaging and quantitative analysis of analyte concentration. Unlike the principal source; however, this induced x-ray source requires no additional licensing, storage, handling, or eventual disposal.

CHAPTER 3

MODELING PHOTON INTERACTIONS

AND

GENERATION OF FLUORESCENT X-RAYS

Introduction

Monte Carlo modeling was implemented to simulate radiation transport and

x-ray generation in test columns. The goal of modeling the system was not to

establish whether or not the generation of fluorescent x-rays was possible since

this had been established in Chapter I. Rather, the aim was to qualitatively

and/or quantitatively answer the following questions based on simulating the

processes involved in x-ray generation:

1. Where are the x-rays generated within the column?
2. Where are the x-rays generated that are detected?
3. What is the expected rate of x-ray generation based on solute concentration?
4. What is the optimum detector placement?
5. Is it possible to construct a calibration curve?
6. How does the modeled response compare to what is actually seen?

Model Background and Development

The Gamma Ray Absorption-Transmission-Emission (GRATE) model was

written by the author and is loosely based on the MONTEREY Mark I (MMI) code

written by Wood (1982) which in turn was apparently based on pseudocode

presented in Jaeger (1968). MMI is a FORTRAN program designed to simulate the transmission and reflection of photons. The system geometry assumes a uniform gamma ray source incident on an infinite homogeneous plane shield of varying thickness. MMI implements the Monte Carlo technique to model the life histories of a large number of photons.

The original program calculated total albedo (a measure of the reflective properties of the shield material) and build-up factor (a measure of how the transmitted photons are altered by Compton scattering processes). Data was output as spectra. Survival weights were assigned to each particle as a means of removing bias at the low-energy range of the spectrum. Neither the photoelectric effect nor pair production were considered.

GRATE was originally MMI translated into Microsoft QuickBasic 4.0. Radical changes were made after debugging and the program eventually evolved to the point that only the program flow resembled MMI. Major changes made include: (1) source geometry, (2) target geometry, (3) target type, (4) scoring, (5) interpolation method, (6) incorporation of the photoelectric effect, (7) incorporation of high-Z salt solutions, and (8) archival of x-ray generation sites.

After successfully implementing GRATE it was again transformed by the author to accommodate the transmission, absorption, and detection of x-rays. As with GRATE, XRAY was written in Microsoft QuickBasic 4.0. XRAY utilizes output from GRATE to model the life histories of x-rays generated as a result of the photoelectric effect. Each site of x-ray generation, stored by GRATE as x,y,z coordinates, is treated as an isotropic point source yielding one x-ray emission

per site. The x-ray is emitted randomly into a 4π solid angle and its life history tracked. XRAY proceeds to the next site after scoring. More than 1.3 billion gamma- and x-rays were simulated using GRATE and XRAY. Minor modifications to both programs were made to improve efficiency at which time they were then reprogrammed in the Microsoft VisualBasic Professional 3.0 environment.

General Overview of Function

GRATE is essentially a statistical reconstruction of photons and the target material through which they are traveling. The physical system being modeled consists of an isotropic point source with pencil beam collimation, a collimated detector aligned with the parallel beam, and a collimated detector placed normal to the beam path. The target consists of a 5.1-cm I.D. acrylic column filled with sand packed to a dry bulk density of 1.68 g/cm^3 and saturated with a solution of potassium iodide. The iodide concentration is changed with each set of simulations in order to establish a theoretical calibration curve.

At the start of each simulation a photon of initial energy, E_o , and position (X_o, Y_o, Z_o) is assigned a randomly determined pathlength, L, to travel. A determination is made at L as to whether or not the particle is in the target. The particle is binned in terms of energy and angular location if it is outside the target and in a scorable position. If the particle is still within the target and has an energy greater than or equal to the energy required to generate an x-ray it undergoes another procedure to determine if an x-ray is generated. On x-ray

generation the coordinates are written to file and a new history is initiated.

If an x-ray is not generated the particle is scattered. At this point a scattering angle and Compton shift in energy is formulated, the particle is given a new path length, and once again tested for position, energy, and probability of generating an x-ray. A particle can be "killed" if its energy falls below a certain cutoff energy, it generates an x-ray, or if it exits the system on a vector which precludes scoring. At the conclusion of the simulation the accumulated contents of each bin are written to file. The contents are then loaded into a spreadsheet and viewed as a spectrum.

Constructing the Model

General Considerations

Factors which must be considered when attempting to simulate this physical system are source-detector geometry, target geometry, and the relationship of the source and detectors to the target. The source must be assigned an initial energy, collimation, and geometry. Detector parameters to be considered are collimation, distance from target, and angular position with respect to the target. Establishing the above parameters is relatively straightforward.

The target components must be constructed in terms of how they appear to incident photons of energy, E. For elements one would go to the tables of photon cross sections found in radiation shielding manuals and find a mass attenuation coefficient for the appropriate energy. While values are given for

some compounds and heterogeneous mixtures, values of interest must usually be calculated from basic data.

Basic Mass Attenuation Coefficients

In the present case the target is composed of sand (assumed to be pure silica - SiO_2), water (H_2O), and potassium iodide (KI). The approach taken for calculating μ/ρ is; (1) find μ/ρ for each component, (2) calculate μ/ρ for the compounds, and (3) calculate μ/ρ for the heterogeneous mixture.

Values of μ/ρ for H, O, Si, K, and I for a range of energies are shown in Table 3.1. Figure 3.1 is a graphical representation of these values for energies ranging from 2.0 to .015 MeV. An additional energy is needed at the K-absorption edge for iodide which occurs at 0.033166 MeV. Any incident photon above this energy is capable of initiating the photoelectric process. Also, at this energy iodide has two values of μ/ρ with the larger value representing the upper absorption edge and the smaller representing the lower.

As the energy of incident photons approaches the upper absorption edge energy (E(photon) > E(absorption edge)) the probability of photoelectric absorption increases and the probability of Compton scattering decreases. Generation of iodide K x-rays is not possible at photon energies below the absorption edge although the photoelectric process is dominant over Compton scattering.

TABLE 3.1

MASS ATTENUATION COEFFICIENTS OF
TARGET ELEMENTS

E (MeV)	μ/ρ (cm^{2}g^{-1})				
	H	O	Si	K	I
2.000	0.0872	0.0444	0.0447	0.0439	0.0409
1.500	0.1028	0.0515	0.0516	0.0505	0.0459
1.000	0.1261	0.0635	0.0633	0.0619	0.0574
0.800	0.1404	0.0706	0.0702	0.0689	0.0660
0.600	0.1595	0.0804	0.0803	0.0786	0.0807
0.500	0.1726	0.0871	0.0868	0.0852	0.0936
0.400	0.1894	0.0952	0.0950	0.0938	0.1160
0.300	0.2109	0.1062	0.1062	0.1060	0.1680
0.200	0.2425	0.1218	0.1232	0.1280	0.3490
0.150	0.2646	0.1331	0.1372	0.1500	0.6730
0.100	0.2940	0.1491	0.1676	0.2160	1.910
0.080	0.3083	0.1583	0.1998	0.2960	3.520
0.060	0.3248	0.1744	0.2802	0.5120	7.550
0.050	0.3341	0.1905	0.3812	0.7770	12.30
0.040	0.3442	0.2244	0.6114	1.390	22.30
0.033	0.3507	0.2917	1.084	1.430	35.83
0.033	0.3507	0.2917	1.084	1.430	6.051
0.030	0.3536	0.3206	1.287	3.140	7.980
0.020	0.3619	0.7441	4.140	10.50	24.70
0.015	0.3648	1.6275	9.783	24.60	53.40
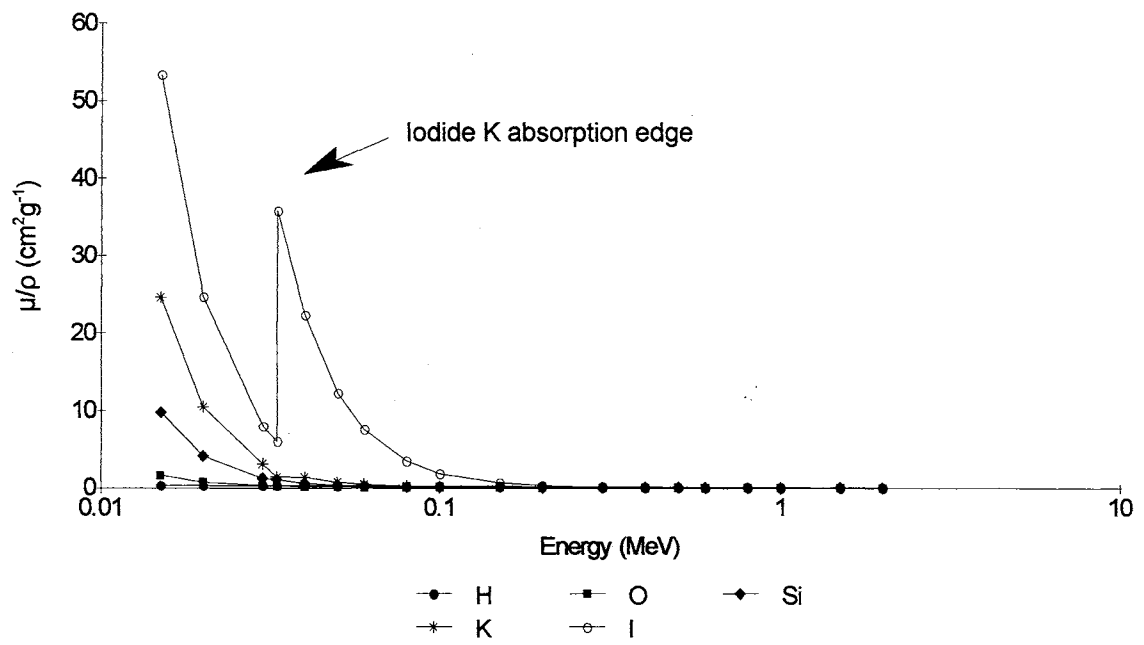
Figure 3.1 Photon Cross Sections of Target Elements.

Calculating Mass Attenuation Coefficients of Compounds and Mixtures

Given the data in Table 3.1, the only additional items needed to calculate

μ/ρ of the constituent compounds are the atomic weights of the elements. These

are found in Table 3.2.

TABLE 3.2

ATOMIC NUMBERS AND WEIGHTS
OF TARGET ELEMENTS

Element	H	O	Si	K	I
Atomic No.	1	8	14	19	53
Atomic Wt.	1.0079	15.9994	28.0855	39.0983	126.9045

Recalling Equation 2.9, the mass attenuation coefficient of a compound is

calculated as

$$\left(\frac{\mu}{\rho}\right)_{Compound} = \sum_{i}^{n} w_i \left(\frac{\mu_i}{\rho_i}\right) \qquad 2.9$$

where w_i is the weight fraction of the ith element. Coefficients for water, silica and

potassium iodide would be calculated in the same manner. Values for 2.0 MeV $\leq$

$E \leq 0.015$ MeV are found in Table 3.3 and the resulting curve in Figure 3.2.

Calculating the attenuation coefficients of mixtures is similar to that of com-

pounds. The process can become tedious, however, when dealing with systems

saturated with a solution of one or more compounds.

TABLE 3.3

MASS ATTENUATION COEFFICIENTS OF
TARGET COMPOUNDS AND MIXTURE

E (MeV)	μ/ρ (cm^{2}g^{-1})			
	H_2O	SiO_2	KI	Mixture
2.000	0.0493	0.0446	0.0416	0.0452
1.500	0.0575	0.0518	0.0470	0.0525
1.000	0.0706	0.0635	0.0585	0.0644
0.800	0.0785	0.0707	0.0667	0.0718
0.600	0.0894	0.0805	0.0802	0.0818
0.500	0.0966	0.0871	0.0916	0.0886
0.400	0.1060	0.0954	0.1108	0.0973
0.300	0.1180	0.1070	0.1534	0.1095
0.200	0.1360	0.1239	0.2969	0.1292
0.150	0.1490	0.1368	0.5498	0.1468
0.100	0.1680	0.1618	1.511	0.1894
0.080	0.1790	0.1836	2.760	0.2339
0.060	0.1970	0.2329	5.892	0.3396
0.050	0.2140	0.2911	9.586	0.4635
0.040	0.2480	0.4225	17.37	0.7318
0.033	0.2845	0.4287	27.73	0.9477
0.033	0.2845	0.4287	4.297	0.4838
0.030	0.3370	0.7907	6.840	0.8418
0.020	0.7110	2.364	21.35	2.490
0.015	1.480	5.523	46.61	5.724

μ/ρ (cm²g⁻¹)

Energy (MeV)

H2O   SiO2   KI
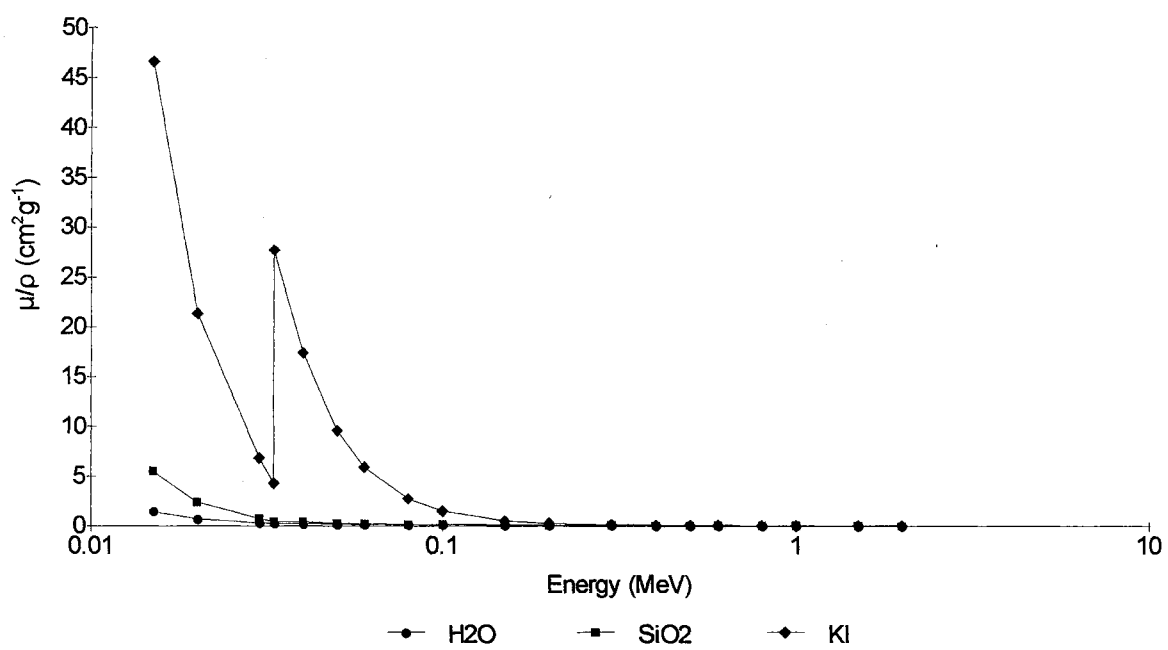
Figure 3.2 Photon Cross Sections of Target Compounds.

GRATE is based on a sand target saturated with a KI solution. Some *a priori* data must be known before calculating the attenuation coefficient of the system. The mass attenuation coefficient of a heterogeneous mixture is a weighted summation of each component based on the mass fraction present. Therefore, to calculate the mass fraction of each component one must have knowledge of the dry bulk density (ρ_b) and porosity (ϕ) of the sand, density of silica (quartz: = 2.65 g/cm³), and concentration of the solute.

The experimental column was designed to be tested with sand packed to a uniform bulk density of 1.68 g/cm³. Assuming constant packing and pure quartz grains the porosity may be estimated (Freeze and Cherry, 1979) by

$$\phi = 1 - \frac{\rho_b}{\rho_s} \qquad\qquad 3.1$$

where ρ_s is the assumed density of quartz in the target material. This yields an estimated porosity of 36.6%. On a unit volume basis the amount of solution present would be 0.366 cm³/cm³, or 0.366 ml/cm³. For the case in which the concentration of KI in terms of I is 100,000 mg/l the mole fractions of both iodine and potassium must be known in order to calculate the mass of K present in a unit volume of solution.

The mass of iodine present in 1 liter is 1g. Since there are 126.9045 g/mole the number of moles iodide is 126.9045⁻¹, or 0.0088 mole. With one mole of potassium per mole iodine there are 0.0088 mole * 39.0983 g/mole K, or 0.3081 g/l K. This yields a total mass (KI) of 1.3081 g/l (0.0013 g/ml). The total

mass of KI present in 0.366 ml would be 0.00048 g (K: 0.113 mg/ml; I: 0.367 mg/ml).

The attenuation coefficient of the target itself can be determined after having calculated the mass attenuation coefficients of the compounds composing the target. The total mass coefficient of the target (H_2O + SiO_2 + KI) is calculated as

$$\left(\frac{\mu}{\rho}\right)_{S,E} = \frac{M_{H_2O}}{M_S} * \left(\frac{\mu}{\rho}\right)_{H_2O,E} + \frac{M_{SiO_2}}{M_S} * \left(\frac{\mu}{\rho}\right)_{SiO_2,E} + \frac{M_{KI}}{M_S} * \left(\frac{\mu}{\rho}\right)_{KI,E}$$ 3.2

where S refers to the target material, M is the mass of the component, and E is the energy at which the coefficient is evaluated. Coefficient values are tabulated in Table 3.3 and shown graphically in Figure 3.3 for $0.015 \leq E \leq 2.0$ MeV.

Defining System Geometry

System geometry is an important component of GRATE because the model tracks photon life histories through 3-dimensional space. A framework must be established in order to provide an absolute reference of the photon to the source, target, and detectors. A photon's coordinates are constantly updated until it is absorbed, scored, or exits the system.

The target is based on the actual laboratory column currently in use. It is an acrylic column with an I.D. of 51 mm. The Y-axis of the model construct is aligned with, and parallel to, the source beam. The target height is defined as one cm and is centered such that the top and bottom of the target is located at Z
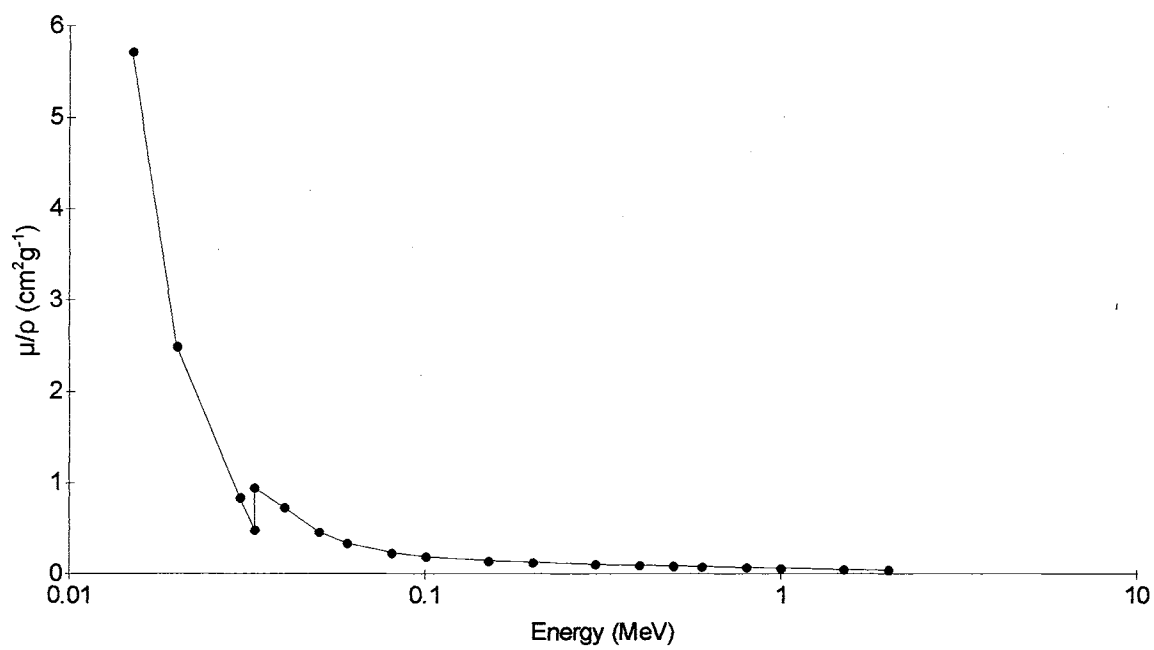
Figure 3.3 Photon Cross Sections of Target Mixture.

= ±0.5 cm. A point source is located at (0, -R, 0) with the photon's initial line of flight being in the positive Y-direction.

A number of angular locations are designated as detectors. The angle subtended at each position is a function of detector collimation and distance of the detector from the target. Collimation was modeled to approximate that of the actual system in which the collimation of the offset detector is 3 cm wide and 1 cm in height. Due to symmetry, counts scored at equivalent angles are summed together. For example, counts scored at 45° and 135° are scored together. This was implemented in order to more quickly build a significant spectrum and is explained in more detail in the next section. A schematic of the system is shown in Figure 3.4.

Translation of Theory into Code

Model efficiency is not necessarily critical if limited simulations are expected to be performed. Efficiency does become important, however, as the complexity of the system and/or the number of simulations increases. For this reason the approach used in MMI was maintained. That is, all constants were precalculated and stored in arrays. Coarse mesh attenuation tables, which are part of the initial input data, are interpolated into fine mesh tables. The same holds with sine and cosine tables used in calculating new azimuthal scattering angles. Also, since a particle's energy can only decrease through its history, flags were formulated in the look up table. These flags mark the point at which to begin a search for an attenuation coefficient based on the new energy after
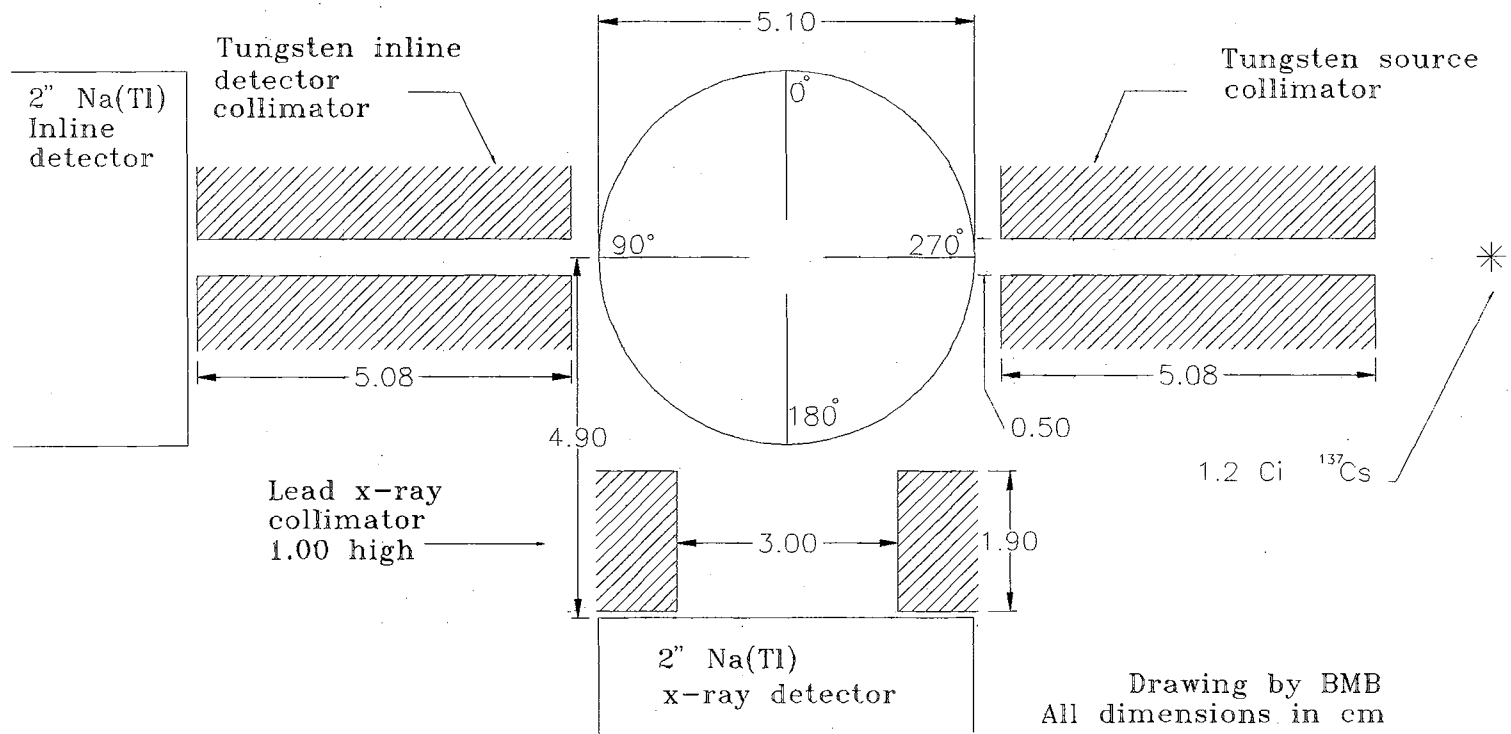
Figure 3.4 Schematic of Modeled System.

scattering.

GRATE is composed of 13 subroutines in addition to the main module. These subroutines can be grouped into three broad functional categories 1) data input, 2) precalculation of the fine mesh energy grid, fine mesh linear attenuation coefficients and data bins, and 3) the actual simulations. The following sections concern the functionality of each subroutine. Any applicable theory is presented concurrently with the code. Variable names are included in parentheses after each item as it is discussed. A complete program listing is located in Appendix A.

Initial Setup Subroutines

Subroutine ConCalc. The ConCalc subroutine is used to construct the mass attenuation coefficient of the target based on: 1) concentration of iodine (ConcI), 2) mass of sand (MassSand), and 3) mass of water (MassWater). Standard stoichiometric procedures are instituted to calculate the total mass of KI (MassKI) present. The total mass of the system (MassSystem) is then calculated which, given the volume of the target (VolumeSample), leads to the calculation of target density (Rho). Mass fractions (MassConcI, MassConcKI, MassConc-Water, MassConcSand) of each constituent are used in conjunction with their respective mass attenuation coefficients (using Equation 3.2) to establish the target mass attenuation coefficient at the course-mesh energy points, Target(MAT), where MAT is the index (I = 1 to MAT) of the arrays.

Subroutine InputData. The InputData subroutine contains the input parameters of the model. These include: number of particles to track (IMAX),

minimum and maximum photon energies (EMIN, EMAX), and basic atomic data for the system components (H2O(MAT), KI(MAT), SIO2(MAT)). Bookkeeping items include counters and array sizes of the course-mesh and fine-mesh mass attenuation data arrays. The counters, Bounce and XrayCounter, are integer variables initially set to zero and updated with every Compton interaction, Bounce, or x-ray generation, XrayCounter.

Equation 2.7 is implemented after the coarse-mesh target mass attenuation coefficients have been established (Target(MAT)). It is also necessary that the mass concentration of iodide be known. The coded constants used to calculate the excitation factor, ESubI, are: JumpRatio (0.838), Fyield (0.869), and Gkalfa (0.810). A new array (Pxray(MAT)) is then constructed. The coded formulation is

$$Pxray(I) = MassConcI * ESubI * \left(\frac{IO(I)}{Target(I)} \right) \qquad 3.3$$

for I = 1 to MAT. *Pxray(I)* is later interpolated in the Prelim and Evaluate subroutines to form a fine-mesh grid of data points (Pkxray(JAT)).

Data Precalculation Subroutines

Subroutine Prelim. The primary function of the Prelim subroutine is a once-for-all calculation of data used during simulations. Sine and cosine tables (CCH(I), SCH(I): I = 1 to 360) are constructed on a 1-degree mesh width (calculated at mid-mesh point) since photons are tracked using spherical

trigonometric methods. EMIN and EMAX are converted to Compton

wavelengths, WMAX and WMIN, respectively (WMAX = 0.511/EMIN, WMIN =

0.511/EMAX). This establishes the upper and lower wavelength boundaries of

the simulation and maintains units when sampling the Klein-Nishina function.

Spectral resolution is obtained by creating a fine-wavelength mesh (WB(I):

I = 1 to N) since the original data consists of only 20 data points. Wavelength

bands (indexed by integer JGO) are created with varying mesh intervals from

band to band to preserve linearity. The mesh interval of each band is a function

of the integer number of steps required to fill between the endpoints while giving

the desired resolution. In this instance it was decided to use the same number of

discretized "channels" as the multichannel analyzer, 1024.

Subroutine Evaluate. Once the fine mesh is established subroutine

Evaluate is used to interpolate the mass coefficient data. Interpolation is done

using the Newton Divided Difference method. The coefficients are mapped one

on one to the Compton wavelength fine mesh grid. Before coefficient values are

passed to Evaluate they are natural log-transformed to linearize the data within

each wavelength band. On returning to the Prelim subroutine the values are

transformed back by taking the antilog. Each value is then multiplied by the

target density to yield the linear attenuation coefficient (cm^{-1}) at each wavelength

(Figure 3.5).
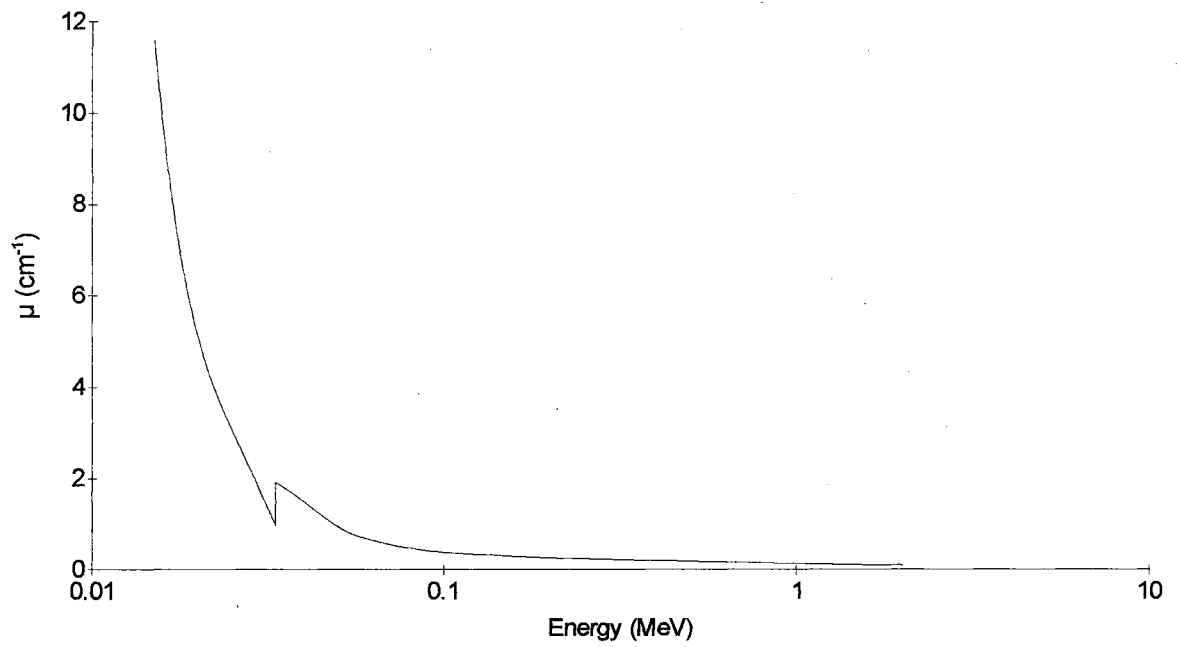
Figure 3.5 Linear Attenuation Coefficient of Target Matrix - Fine
Mesh Energy Grid.

Photon Life Histories

Subroutine Angles. An azimuthal scattering angle must be assigned after the photon has been given a new scattering angle in the Scatter subroutine. This new angle is drawn randomly to give a value lying between 0 and 360 degrees. A pathlength, based on the energy of the scattered particle, is then formulated in the NextStep subroutine.

Subroutine History. The History subroutine provides the overall program flow. A new photon is defined by calling Start. NextStep is then called to calculate the pathlength to the next collision. Score is called to determine whether the particle has exited the system, been absorbed, or scattered. If the particle has been absorbed a flag (Status) is set in Score and on return to History a new particle is initiated. If the particle is not absorbed the Scatter subroutine is called. The new wavelength is compared to WMAX (TestW = W - WMAX) and based on the sign of TestW the particle is passed to the Angles subroutine or it is terminated. The Angles subroutine is called if the test variable is positive and the particle is terminated if negative. If Angles is called a new set of direction cosines is formulated and the particles' history is resumed by again calling the NextStep subroutine. A new particle is initiated by calling Start if the test proved negative. This process continues until the target number of particles has been attained (PhotonNumber = 1 to IMAX).

Subroutine NextStep. As already noted a photon's history begins by defining the initial energy and position of the source (Subroutine: Start). The next

step is to calculate the random path length the particle will travel between collisions (Subroutine: NextStep). This is accomplished with a random number and the concept of the Mean Free Path (MFP). The MFP is defined as

$$\lambda = \frac{1}{\mu}$$
<div align="right">3.4</div>

where λ (cm) is the MFP and μ (cm.$^{-1}$) is the linear attenuation coefficient. MFP values for a target mixture (100,000 mg/l I and density of 2.04 g/cm^3) are shown in Figure 3.6 for E = 2.0 to 0.015 MeV.

Equation 3.4 actually represents the first moment of the probability density function (PDF) defining the probability for a collision at some distance, l, from the source. The derivation of the MFP may be found in Cashwell and Everett (1959) as well as Lux and Koblinger (1991). In practice it is desired to randomly select the path length the photon travels to the next collision. This is done by randomly sampling the uniform distribution which yields numbers in the interval $0 \leq RA \leq 1$. Positive-valued data is obtained by taking the negative natural logarithm of RA (in code, $-RAL$) which results in realistic values of path lengths. The random path length is calculated using

$$S = \frac{-RAL}{\mu}$$
<div align="right">3.5</div>

where S is the path length given the linear attenuation coefficient at some energy, E. The range of S is more a function of μ than $-RAL$ since the range of $-RAL$ is
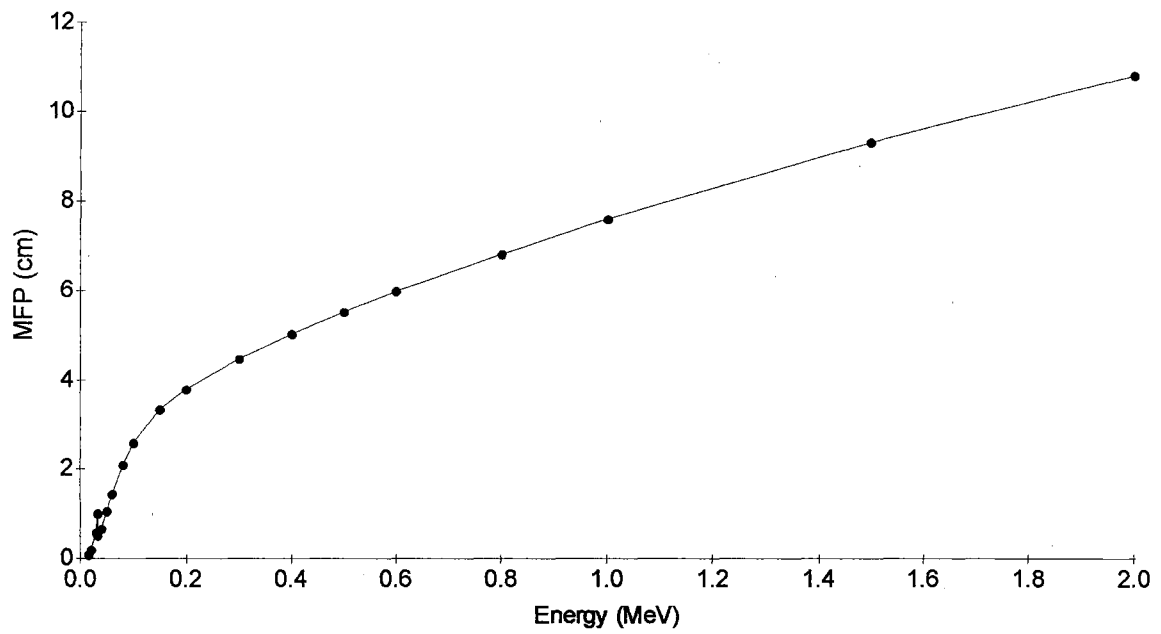
Figure 3.6 Mean Free Path for Target Mixture.

independent of μ and is the same regardless of whether the attenuation coefficient increases or decreases in value.

Subroutine Scatter. The primary function of the Scatter subroutine is the determination of the new wavelength of a scattered photon. The method used for sampling the Klein-Nishina pdf is that suggested by Kahn (1954) and implemented by Wood (1982). According to Wood it is valid for any energy of incident photon and does not rely on approximation.

If equation 2.1 is rewritten in terms of Compton wavelengths ($\lambda = 0.511/E$) it takes the form

$$\lambda - \lambda_o = 1 - \cos\theta \qquad\qquad 3.6$$

where λ_o and λ are the wavelengths of the incident and scattered photon, respectively. The maximum shift in wavelength is two Compton units and takes place when the photon has been scattered through 180°. In deriving the Klein-Nishina pdf, energy- and angular-dependence is removed by substituting $X = \lambda/\lambda_o$ and integrating with respect to the Compton cross section, σ_c. The function is now expressed in terms of X.

Subroutine Score. After S is established a new set of coordinates (XN, YN, ZN) are calculated and the Score subroutine is called. A set of conditions is then tested at the new coordinates: 1) Is the particle in or out of the target?, 2) If the particle is outside the target is it in scoring position?, 3) If the particle is inside the target what is the probability that an x-ray is generated?

The particle scoring procedure involves calculating the intersection of line (X, Y, Z)-(XN, YN, ZN) with the target boundaries. If the photon line of flight intersects the upper or lower target surfaces it is not scored. If the photon line of flight intersects the vertical target walls the exit angle is calculated and the energy-binned counter, EB(JE), is incremented for the detector whose field of view includes the exit angle.

Subroutine Start. The coding of the Start subroutine is straightforward. The wavelength, W, is set to WMIN which is the shortest wavelength that can occur during the simulation. The wavelength band (JGO) in which WMIN is located is also defined in order to save time. In addition to WMIN, source geometry, location, and direction cosines are defined for future use.

Subroutine Xray. There are three possible outcomes if the particle lies inside the target: 1) the photon is absorbed with resultant x-ray emission, 2) the photon is not absorbed, but scattered, and 3) the photon's energy has reached the minimum cut-off energy and is killed.

If the photon energy is greater than or equal to the energy required for x-ray generation subroutine XRAY is called to test for the probability of generating an x-ray. If x-ray generation tests true the coordinates are written to file and the photon is killed. At this point a new life history is begun. Should x-ray generation test false and the photon energy is greater than the cut-off energy the particle is scattered. If the photon's energy has reached a predefined cut-off point it is killed and a new history is started.

Results of Simulations

A total of 1.3 billion photons with an initial energy of 662 keV were simulated. All parameters but [KI] were held constant throughout these tests. Simulations of 100 million incident photons were conducted at four concentrations of iodide: 25,000, 50,000, 75,000, and 100,000 mg/l. All simulations placed the photon source/inline detector pair on the target centerline. Additional simulations were carried out at the highest concentration which simulated the target being passed through a beam of gamma rays as found in a tomography system. Since symmetry is assumed, the additional paths were spaced from the target edge to the centerline. Results were evaluated in terms of x-rays detected as a function of solute concentration, detector placement and pathlength of the incident beam through the target.

Site of X-ray Generation

As each x-ray was generated it's location was written to file. Each location was then treated as a point source for the next set of simulations. This data was later binned at 0.1 mm resolution to yield an x-ray generation distribution map. Figure 3.7 shows the distribution and intensity of x-rays at maximum solute concentration. Incident beam placement is on the column centerline. A total of 829,455 x-rays were generated. It can be seen that the majority of x-rays are generated along the axis of the incident beam. Also, the intensity of x-ray generation varies as the intensity of incident photons decreases. This is to be expected when the Lambert Law is considered.
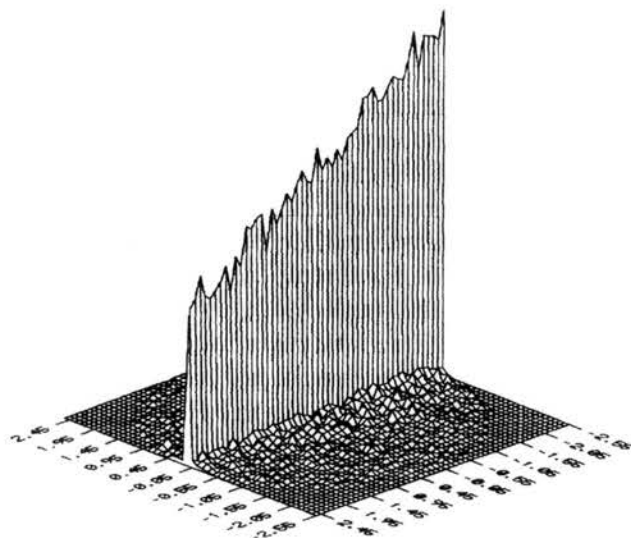
Figure 3.7 X-ray Generation Sites and Intensity Map.
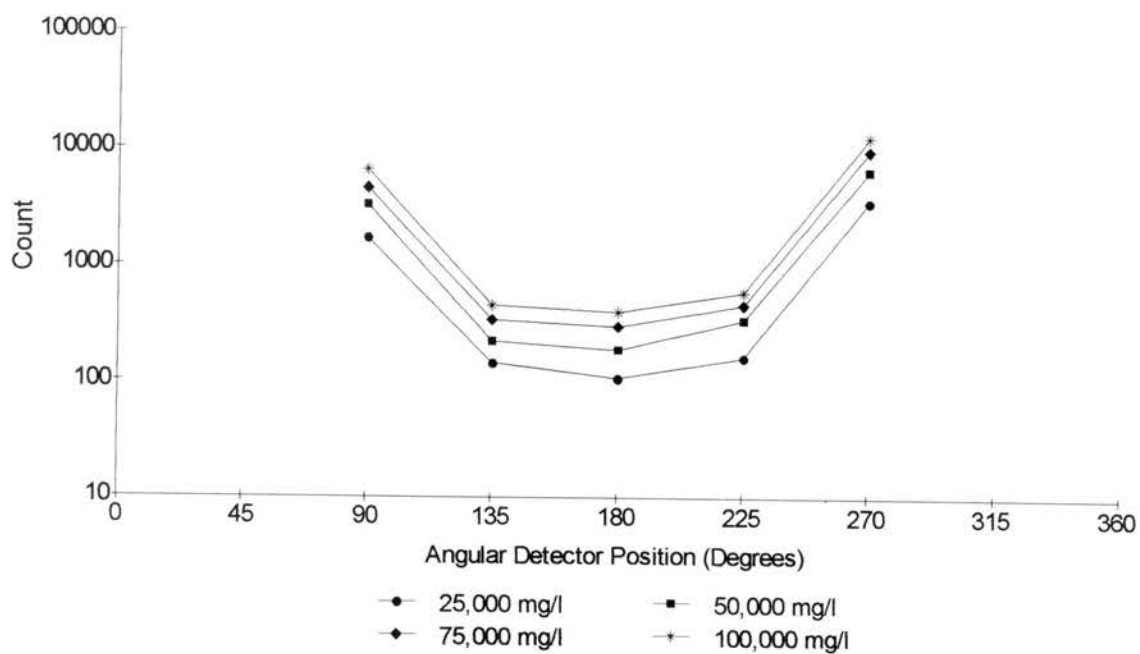
Figure 3.8 Detected X-rays as a Function of Concentration
and Detector Placement.

X-ray Detection as a Function of Concentration and Detector Placement

The intensity of x-rays varies with detector placement as well as solute concentration. A graph of detected x-rays as a function of concentration and detector placement is shown in Figure 3.8 (data in Table 3.4). Intensities range from highest to lowest at theta equal to 270, 90, 225, 135, and 180 degrees, respectively. This is a reasonable outcome when Figure 3.8 is compared to the distribution of x-ray generation (Figure 3.7).

The actual experiment was performed with the detector placed at 180 degrees. A plot of detected x-rays versus concentration at this position is shown in Figure 3.9. Data for the suite of centerline simulations is found in Table 3.4. Linear regression of count as a function of concentration leads to the expression

$$Count = 0.003972*[I] + 0.6 \qquad 3.7$$

where $[I]$ is in mg/l.

Comparison of Simulated to Measured X-ray Yields

To gain an understanding of how the simulation compared to the experiment, it was decided to compare the source fluxes in terms of x-rays detected/incident gamma ray. An estimated real time for the simulation can then be estimated. The incident flux at the column edge was 100 million photons for the simulation. No actual photon flux for the source in the experiment has been calculated due to the difficulty in the measurement. Although the apparent source strength with the collimation used has not been measured, measurements
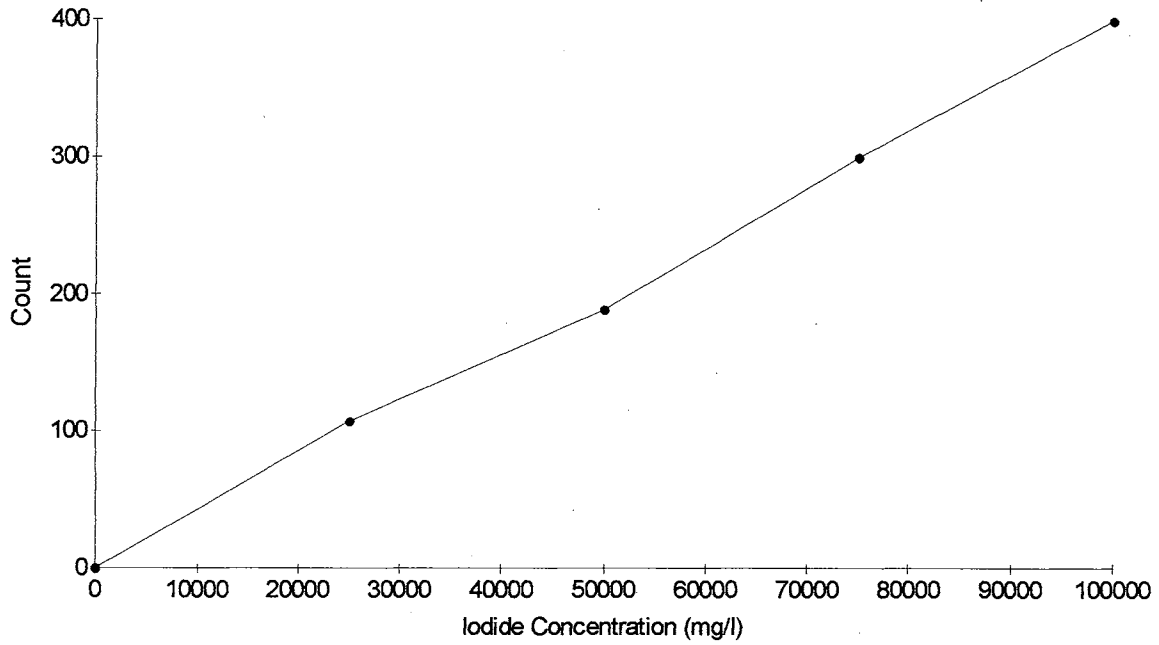
Figure 3.9   Xray Count vs Iodide Concentration.

TABLE 3.4

SUMMARY OF XRAY COUNT AS A FUNCTION OF
CONCENTRATION AND DETECTOR PLACEMENT

[I]	Detector Angular Position				
(mg/l)	90	135	180	225	270
25000	1724	145	107	163	3594
50000	3334	224	189	342	6639
75000	4632	342	300	457	9898
100000	6620	453	400	592	12887

with other collimations would indicate a strength of 1.0 Ci, or 3.7×10^{10} disintegrations/s. Cesium 137 has an efficient yield of 85.1% (Lide, 1995) which gives an effective activity of 0.851 Ci.

The rate of incident photons exiting the collimation can be estimated by calculating $d\Omega/4\pi$. With a source collimation of 5 mm and a distance from the source to the collimation edge of 7.1 cm, the flux is estimated to be approximately 9.6×10^6 photons/s. A mean net x-ray count of 21367 x-rays in 600 s was observed during the experiment that occurred at maximum iodide concentration. The ratio of detected x-rays per incident photon is estimated to be 3.7×10^{-6} x-rays/incident photon. A total of 400 x-rays were detected by the offset detector in the simulations. This yields an x-ray/incident photon ratio of 4.0×10^{-6} which is 7.5% higher than measured. The live time of the simulation is estimated to be approximately 10 s.

An x-ray detection rate of 3.2×10^{-6} x-rays/incident photon was measured. Simulations resulted in a rate of 4.0×10^{-6}. This implies that the real system has a lower x-ray measuring efficiency, as can be expected. The probable causes for the discrepancy can be attributed to the actual source collimation and detector efficiency. Although the source is collimated it is actually vertically divergent. The simulated collimation is "perfect" in that every incident photon's initial path is the same. Additionally, the simulation asssumed a perfect detector with 100% collection efficiency.

X-ray Detection as a Function of Pathlength

Five additional simulations were performed at maximum solute concentration. These runs were performed to illustrate how x-ray intensity varies with pathlength through the target. Symmetry was not assumed in these cases. Detectors at 0 and 180 degrees were used independently as the traverse was made from 0.10 cm to the centerline. This essentially allowed evaluation of x-ray penetration through the column diameter. Data is summarized in Table 3.5 and is shown graphically in Figure 3.10.

TABLE 3.5

SUMMARY OF OFFSET SOURCE SIMULATIONS

Offset (cm)	Count
0.10	31504
0.59	5916
1.08	1933
1.57	885
2.06	478
2.55	400
3.04	251
3.53	144
4.02	133
4.51	70
5.00	8
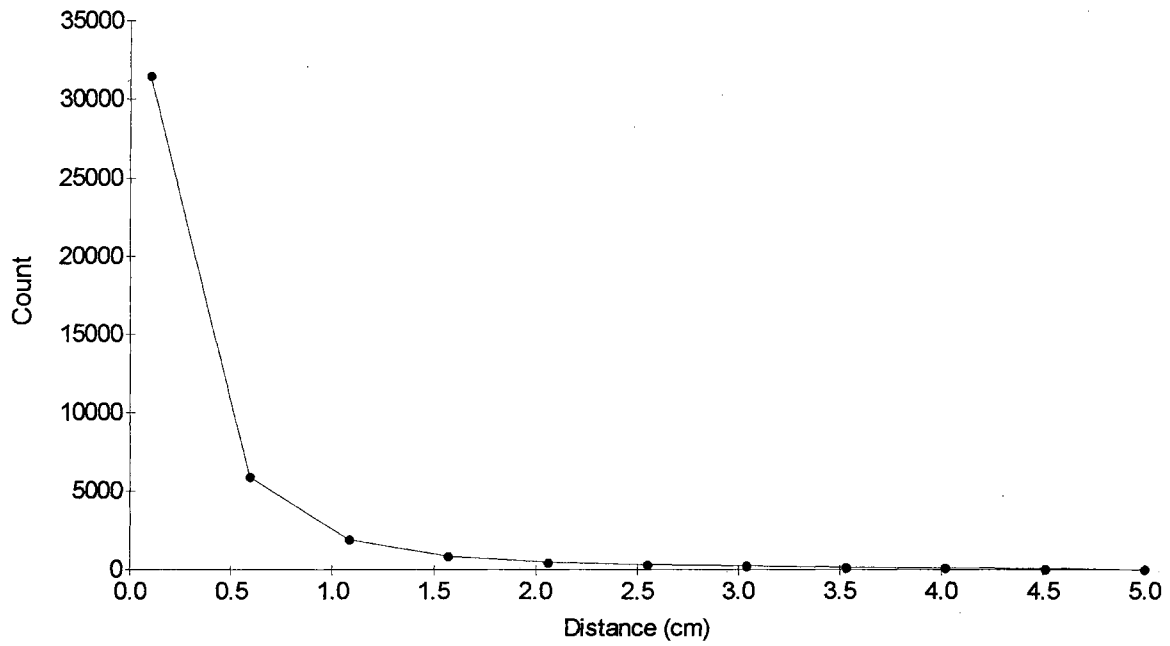
Figure 3.10 Xray Count as a Function of Distance.

Origin of Detected X-rays

The XRAY modification of GRATE tracked the origin of every scoring

particle regardless of energy. Analysis of the offset detector data ($\theta = 180°$)

shows that 0.175% (1454 particles) of the total x-rays generated scored. Of

these scoring particles, 400 (27.5%) were K_α x-rays. In terms of the total

number, only 0.048% of the x-rays generated were detected. The distribution of

scoring 28.612 keV x-rays is shown in Figure 3.11.

Only 3.6% of the scoring x-rays originate at the centerline. The majority of

scoring, 28.612 keV x-rays originate at a distance of greater than 2.0 cm from the

column centerline. It is assumed that Compton scattered photons are the primary

mechansim of generating xrays at this distance from the centerline.

The detector position located 45° from the in line detector was also

evaluated (Figure 3.12). A total of 2,359 (0.284% of the total generated) photons

scored. Of these, 453 (19.2%, 0.054% of the total) were 28.612 keV x-rays.

Among the scoring x-rays, approximately 15.2% originated at the column

centerline. Most of the remainder scored from near the column edge.

It could be interpreted from Figures 3.11 and 3.12 that scoring, 28.612 keV

x-rays are generated primarily along the column edge. This is not the case in this

instance. Output from GRATE consisted of the coordinates where x-rays were

generated. These were used as individual sources for XRAY. In keeping with

the randomness of the emission process, each x-ray's initial trajectory into a 4π

region was randomly computed. Those x-rays generated along the column edge

have a much greater probability of scoring than those lying away from the edge
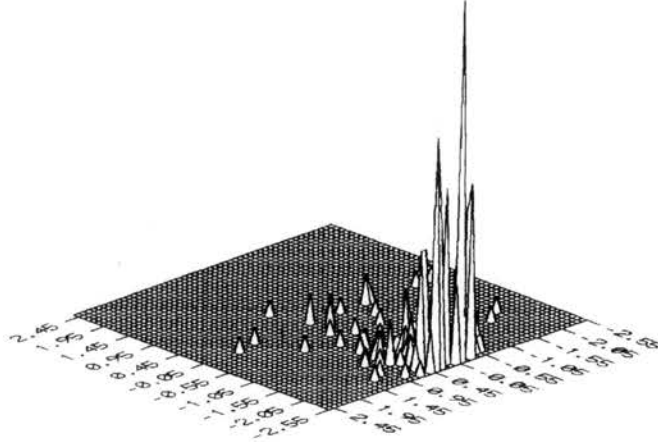
Figure 3.11 Origin of Scoring X-rays Detected Normal to Incident Beam.
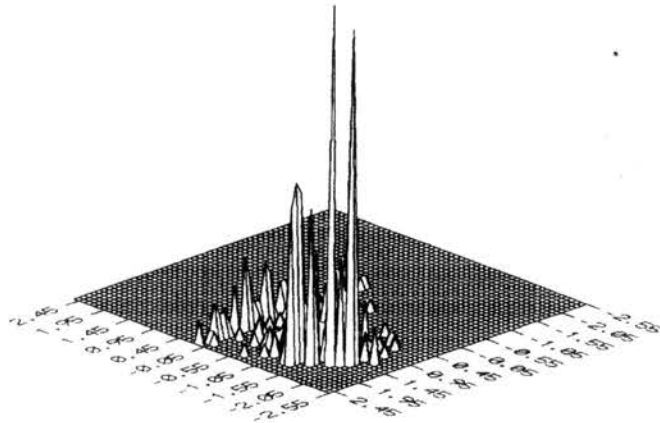
Figure 3.12 Origin of Scoring X-rays Detected Between In Line and Offset
Detectors.

since $d\Omega/4\pi$ is largest near the detector and decreases with distance.

Additionally, the probability of attenuation (scattering and absorption) is much

lower because of the shorter path length through the target.

Effects of Source Energy on Origin of Detected Xrays

An additional simulation of 50 million photons was implemented to

determine the effect of source energy on the distribution of the origin of x-rays.

The simulation was conducted on the column centerline at maximum iodide

concentration. Source energy was that of the gamma ray emitted by ^{241}Am,

59.536 keV. All other parameters were consistent with those of the previous

simulations.

Approximately 3% of the incident photons were detected by the in line

detector. The high attenuation resulted in the production of 29 million x-rays.

Sites of x-ray generation are shown in Figure 3.13. Detected x-rays as a function

of angular detector placement is found in Figure 3.14. To be consistent with

previous simulations, detected x-rays were evaluated at 45 and 90 degrees to the

incident beam.

A total of 40,000 x-rays scored at the detector positioned normal to the

incident beam. Of the scoring particles, 8300 (20.7%, 0.028% of total x-rays

generated) were 28.612 keV x-rays. The distribution of these particles is shown

in Figure 3.15. Photons scoring from the column center line accounted for 4.1%

(343) of the scoring 28.612 keV particles. This is approximately the same

percentage as that of the original simulations.
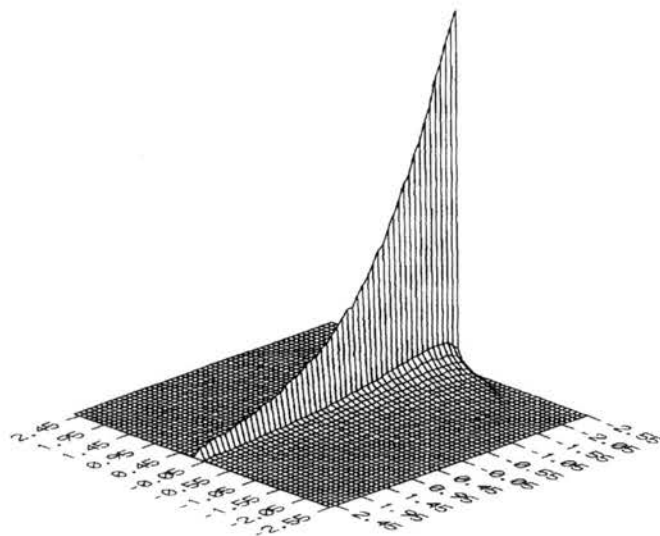
Figure 3.13 X-ray Generation Sites and Intensity Map - Americium Source.
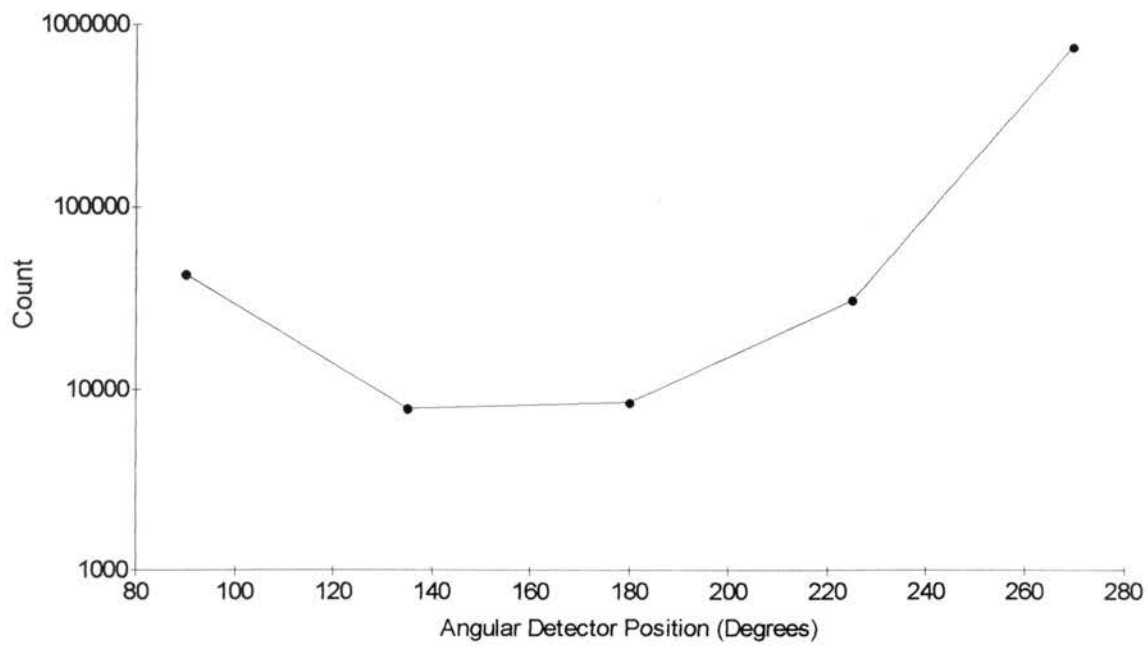
Figure 3.14 Detected X-rays as a Function of Detector Placement - Americium
Source.
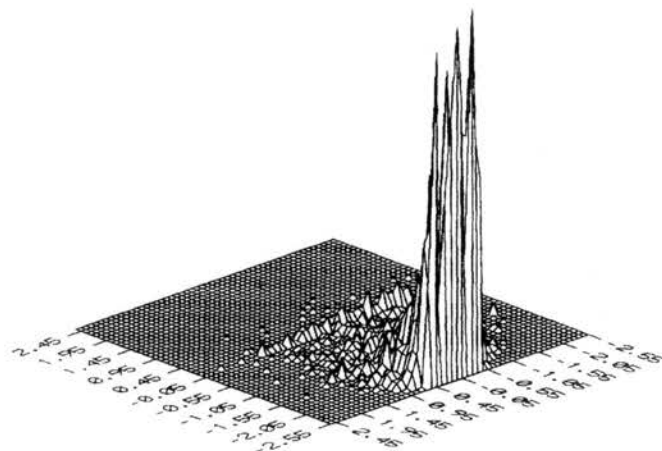
Figure 3.15 Origin of Scoring X-rays Detected Normal to Incident Beam - Americium Source.
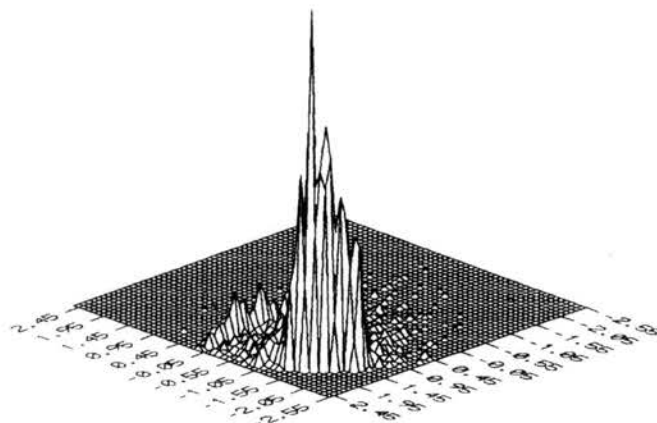
Figure 3.16 Origin of Scoring X-rays Detected Between In Line and Offset Detectors - Americium Source.

A total of 38,000 particles were detected at a position 45 degrees to the incident beam. The percentage of 28.612 keV x-rays scoring was 20.4% (0.026% of total generated) with 7.6% originating at the column center line (Figure 3.16). Percentages are approximately the same as those of the original simulations with one exception. On a percent basis, photons originating at the column center line are one-half that of the original simulations.

Summary

The application of GRATE proved beneficial in providing practical information concerning the laboratory column used in the current study. Results clearly indicate that x-rays are generated in sufficient quantity to be detected. Mapping of x-ray generation sites provided useful information in future detector placement and collimation.

Data clearly shows that x-ray generation decreases (following the Lambert Law) with distance through the column. This is directly related to the decrease in the number of incident photons as a function of the linear attenuation coefficient and pathlength into the column. Additionally, analysis of scoring photons indicate that a high percentage of scoring primary energy particles are Compton-generated.

Simulations using a lower energy source yielded predictable but significant information. Although only one-half the incident photons were simulated, there was a 21-fold increase in the number of 28.612 keV x-rays detected at the offset detector position. A 17-fold increase was noted at the position 45 degrees to the

incident beam.

Theoretically, the best detector placement would be either on the source or in line detector side of the test column. This is not possible in a practical sense. Compton haze would obscure any signal from the inline position. For obvious reasons the detector cannot be placed between the incident beam and the target. Positions 45 degrees off the incident beam on the source side of the target are likewise not possible given the current configuration. The size of the detector/shielding assembly precludes this location. There is room to place the detector 45 degrees off the inline detector but the potential for increased background is likely. This would decrease the signal to noise ratio. It is the opinion of the author that placement of the detector normal to the incident beam is the optimum for the current configuration.

Regression of data from the offset detector position (normal to the incident beam) shows that a linear relationship exists between detected x-rays and solute concentration. This allowed the construction of a theoretical calibration curve that is compared with the actual experimental data in Chapter 6. Finally, the data generated by simulating a CT scanner traversing the column indicates that fluoresced x-rays have sufficient energy to penetrate the diameter of the column.

CHAPTER 4

METHODS

AND

PROCEDURES

Introduction

Experimentation dealt exclusively with the quantitative, non-destructive

determination of the concentration of KI in solution passing through a saturated

porous medium of known bulk density. The concepts of the previous chapters,

x-ray generation and radiation transport modeling, are brought together to design

appropriate experimental techniques and procedures.

The current system arrangement consists of a pencil beam gamma

scanner modified to accept additional detectors and electronics. It is composed

of 1.2 Curie (Ci) ^{137}Cs and 0.20 Ci ^{241}Am gamma-ray sources, source shielding,

detector assemblies, data acquisition boards, positioning equipment, and

personal computer (Figure 4.1). Available photon energies are 662 and 60 keV

respectively, for cesium and americium sources.

An open-ended design was implemented to allow for a wider range of

modifications to the scanner with minimal investment in time and cost. This

proved valuable when adding components for conversion of the system to include

non-collinear, dual-source scanning and attenuation studies as well as x-ray
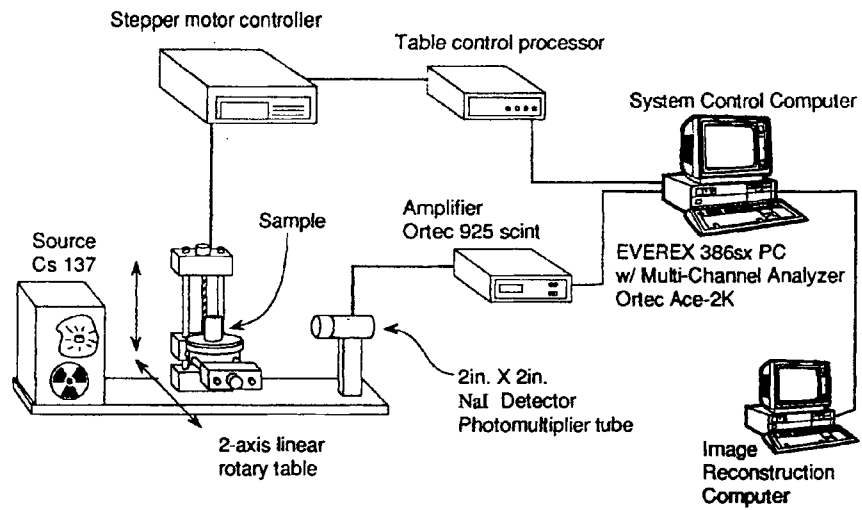
Figure 4.1 Schematic of System - Offset Detector Not Shown.

fluorescent x-ray spectroscopy. Additionally, source collimation was designed such that future modification to fan-beam geometry should be relatively simple.

Source and Detector Shielding

Source Shielding

Source shielding (Figure 4.2) is modular in nature to allow for relatively easy transport and assembly as well as maximum safety from exposure when modifying collimation or while in operation. Overall dimensions are 30.5 cm x 30.5 cm x 35.5 cm with a total weight of approximately 800 lbs. The housing consists of six lead components which were cast and machined for as accurate and tight a fit as possible to minimize leakage with the minimum shield thickness being approximately 13 cm on all but the detector side.

The detector side of the housing is composed of a 7 cm-thick plate through bolted to the main source housing. This front plate also serves as the collimation carrier. A 6.35 cm diameter lead insert is centrally located and designed to hold a removable 1.9 cm diameter by 5 cm long tungsten pencil beam collimator.

A ^{137}Cs source is situated in nested shielding and can be removed through the collimation insert without dissembling the overall shield. Again, this was done to minimize exposure while installing the source and during operation of the scanner. The source carrier, which is located in a two-part housing fabricated with the appropriate size cavity, consists of a 10 cm x 10 cm x 10 cm solid lead receptacle machined to accept the source. Both the bottom of the carrier and the cavity are lined with 0.6 cm-thick plates of polypropylene to provide a smooth
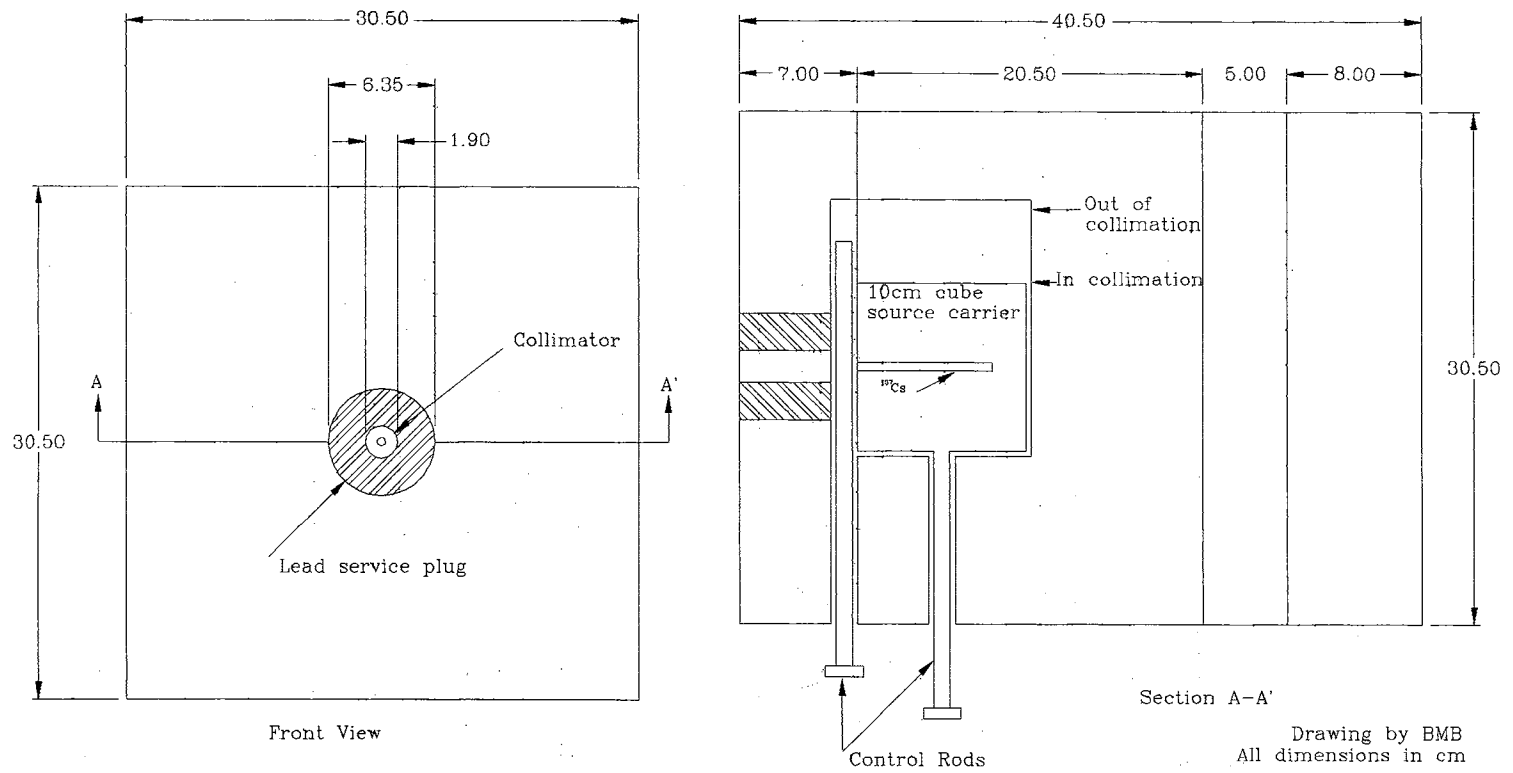
Figure 4.2 Source Shielding.

bearing for the source subassembly. It is moved in and out of alignment with the collimator by means of an attached brass bar that passes through the outer shielding.

The ^{241}Am source is mounted in a brass carrier rod and placed such that both sources can be used simultaneously. A slotted hole milled in the rod allows unimpeded transmission of cesium photons when the americium source is not in use. The carrier itself is mounted in a recess milled into the back of the front shielding plate. As designed, the source can be moved in and out of collimation without interfering with the primary ^{137}Cs source. This feature provides sub-stantial flexibility in allowing one to change sources without being exposed. The source is self-aligning with the shielding collimation and as with the ^{137}Cs source can be removed without dissembling any shielding.

Remaining shielding consists of two lead plates through-bolted to the back of the 2-part upper and lower primary housing. All plates average approximately 170 lbs weight and contain threaded inserts for attachment of eye bolts to aid in transport and setup.

Detector Shielding

An in line detector is located behind a 5 cm-thick lead shield in which the tungsten collimator is centrally located. Collimation is identical with that of the source. The detector and shielding are contained in an aluminum column mounted parallel to the primary photon beam. Attachment points allow substantial latitude in adjustment for the purpose of aligning the source and

detector collimation necessary for a pencil beam geometry.

An offset detector used for spectroscopy is shielded in a 1 cm-thick lead cap large enough to completely shield the detector crystal. Collimation consists of a 1 cm diameter by 3 cm long aperture which is centrally located in the cap face. The thickness of the cap shield is substantial in order to preclude Compton radiation reaching the detector.

Collimation Alignment

Collimation alignment must be as exact as possible in order to obtain maximum count rates as well as preserve the pencil beam geometry of the system. The author determined that this alignment could be done relatively easily by using an acrylic collimator in conjunction with a low-wattage laser.

An acrylic rod having the same diameter as the tungsten collimators but twice the length was procured. A 2 mm diameter hole was then drilled down the center and this acrylic collimator was placed in the source collimator carrier. A helium-neon laser with a beam diameter of approximately 2 mm was then situated on the posterior side of the detector collimator. The detector housing was aligned until the laser beam, after passing unobstructed through the detector collimator, only appeared at the terminal end of the hole that had been drilled in the acrylic rod. If the beam did not touch the sides of the hole, it was assumed that the two collimators were in alignment. This method appears to provide satisfactory accuracy.

The offset detector used for spectroscopy is located at a point equal to

one half the distance between the source and in line detector. This assembly is attached to a carrier which in turn is mounted to a floor-mounted frame that has been centered with respect to the pencil beam system. The geometry of the entire assembly forms a plane which is normal to the primary energy beam.

The carrier-frame attach point is a pivot which allows for tilting as well as rotation of the carrier assembly. Suspended from the pivot point attach plate is an aluminum beam which has had matching channels milled into both sides near the bottom edge. The original purpose of this beam was that of a detector-source carrier for non-collinear, dual-source scanning with the channels insuring proper alignment of source and detector. For spectroscopy purposes the carrier was rotated normal to the primary beam and lowered to the same elevation resulting in a three-point plane composed of the primary source collimator, primary detector, and offset detector.

The Positioning System

General Description

The positioning system consists of two stepper motor-driven rail tables and a stepper motor-driven rotary table. Two rail tables are attached perpendicularly to one another allowing 12" of travel in both the vertical and horizontal directions. A rotary table is mounted normal to the vertical rail table and the entire positioning assembly is located between the source and detector. This arrangement allows the target to be rotated and translated through the primary photon beam. The stepper motors are controlled by a stepper motor controller

which in turn is controlled by the host computer.

Table Characteristics

The following descriptions and specifications are those of the manufacturers, Daedal, Inc. Each rail table, which has overall dimensions of 6" width and 20" length, carries a 5" x 5" stage that is supported on twin rails the full length of travel. Drive is via a 0.20" (5 pitch) lead ball screw with a recirculating bearing system connected to a standard NEMA 23 motor flange. Maximum load capacities are 200 and 100 lbs. for horizontal and inverted orientations, respectively. Both linear tables have a positioning accuracy of ±0.0002" and repeatability of ±0.00025 in/in with incorporated limit and home switches.

The rotary table has overall dimensions of 6" x 6" with a 5" diameter rotating mounting plate which has a travel range of 360° continuous with accuracy and repeatability of 10.0 and 0.5 arc-minutes, respectively. Reported runout is 0.003" and concentricity 0.0005". Load capacities are 25 lbs. horizontal and 10 lbs. vertical. An input of 15 in.-oz. torque is required with the 90:1 gear ratio. As with the rail tables the rotary table is furnished with a NEMA 23 motor mount.

Stepper Motors

Each positioning table, linear and rotary, is driven by a 5Vdc/phase double shaft extension stepper motor. These motors have step angles of 1.8°/step with a total of 200 steps per revolution. With respect to the positioning tables this

results in a minimum translation of 0.0254 mm/step for the linear tables and 0.02°/step for the rotational table. Maximum axial and radial loads are 26.4 and 15.4 lbs. respectively, with a step angle tolerance of ±7%.

Stepper Motor Control. The basic stepper motor positioning system is composed of the stepper motor, power supply, and indexer. A power supply and associated electronics, composed of resistors and solid state relays, maintains the proper sequence of voltages to the stepper motor windings controlled by the indexer. The indexer as currently configured receives motion commands from a PC.

The indexer is an ACROSYSTEMS (now Analogic Corporation) ACRO-400, a 64180-based data acquisition and control unit. Programmable digital I/O lines (TTL, 1 load, user-definable direction by byte) are connected to the power supplies and a solid state relay (SSR) board populated with 12-5Vdc SSR's (four per stepper motor). Each stepper motor requires four I/O lines plus ground and 5Vdc power. A memory-resident ACRO-BASIC program, written in-house, configures the ports and controls each digital output line such that the stepper motor windings are energized in the proper sequence for the desired direction of motion.

The indexer receives its commands from a PC over the serial communications port (RS-232, 9600 baud). Direction and magnitude of movement is sent by the PC to the ACRO-400 basic program which then sequences the stepper motors. Synchronous communications are maintained via software handshaking.

Detection and Data Acquisition Components

General Description

Acquisition and subsequent spectral analysis of radiation data require a detector, amplifier, and multichannel analyzer (MCA). The system utilizes EG&G Ortec hardware consisting of a 2" sodium iodide, thallium-activated (NaI(Tl)) detector crystal connected to a photomultiplier tube (PMT) and Ortec 266 photomultiplier base (PMB) which is powered by an amplifier and bias supply. A single channel analyzer is incorporated into the control unit. The amplifier is spectroscopy shaping and provides a 10 volt linear output signal. This signal is transformed by the MCA into a histogram representing counts in the 0 to 10V range.

Amplifier and Bias Supply

The amplifier and bias supply in use is the EG&G Ortec ACE*Mate* Model 925 SCINT. A switchable preamplifier allows an external preamplifier to be coupled to the amplifier via a BNC input connector. The amplifier has a continuous adjustment from 5 to 1250 using a coarse-gain switch and fine-gain potentiometer. Pulse shape is semigaussian bipolar with a peaking time of 2 µs. The coarse- and fine-gain adjustments allow the user to center the desired energy spectrum in the 10 volt window.

A bias potentiometer, which is the high voltage output to the PMB, is continuously adjustable from 50 to 2000 volts and has an output load capacity of

1 mA, <0.02% regulation, <15 mV rms at 1 kV, 1 mA load and <0.01%/°C

stability. The unit also incorporates a single-channel analyzer (SCA) with user-

definable upper and lower limits (0.05-9.99 V) and LED rate meter with a range of

0-99.9 thousand counts per second (kcps). It is connected to the PMB by the

high voltage, linear input, and preamplifier lines and to the MCA by a linear output

line.

Settings for the amplifier and bias supply are generally dependent on the

individual system and source energy. The settings, which are the same for the

inline and offset detectors, are: bias - 0.8 kV, coarse gain - 10, and fine gain -

7.5. With this configuration both the gamma- and x-ray peaks are in the same

window.

Detector, PMT, and PMB

Detectors utilizing NaI(Tl) crystals are known as scintillation counters.

These types of detectors are generally used for high-energy gamma rays but also

function relatively well at ambient temperatures for higher energy x-rays

generated from the fluorescence of high-Z elements ($Z \geq 53$).

The NaI(Tl) crystal is an inorganic, impurity-activated phosphor with the

incorporated impurity serving as the source of the luminescent property of the

crystal. Typically, the crystal is enclosed in a thin aluminum canister approxi-

mately 0.1 mm thick. This housing isolates the crystal from light and moisture

contamination. The crystal is highly polished on one side and is optically

mounted to the photomultiplier using either oil or transparent grease having the

proper index of refraction to allow maximum light transmission.

When an incident photon strikes the crystal, a visible light photon is emitted. The visible light photon then strikes the photocathode of the photomultiplier where its intensity is increased multiplicatively at successive dynodes by secondary emission. This causes a negative charge at the anode which yields a voltage pulse. The pulse is then differentiated, amplified, and analyzed. Similar to a proportional counter the pulse is proportional to the energy of the incident photon.

The decay constant of the crystal is a measure of the time needed for luminescence to terminate. The total decay is composed of the principal and secondary luminescent decay times of 0.23 and 1.5, respectively.

Multichannel Analyzer

The PC board being used is the EG&G 916A MCB. This is a 1½ slot PC card consisting of a successive approximation analog-digital convertor (ADC), Z80A microprocessor, and memory. There is one card per detector used with data stored in a maximum of 2048 "channels" over a 10 volt range. The number of channels ranges from 2^8 to 2^{11} with intermediate values of 2^9 and 2^{10}. The maximum number of counts per channel is $2^{23}-1$.

Communication between the MCB and host PC is by dual-ported memory with base address HD000 (page D). Commands are sent to the MCB and read at this address. The dual-ported memory also allows the MCB to almost simultaneously dump its data to be read by the PC thereby providing real time

processing capabilities. Data is stored in either binary or decimal format at the discretion of the user.

MCA Characteristics

Two MCA's are currently being used, one for attenuation and imaging and one for spectroscopy. Since they are two different models there are some minor differences. The older model has a dead time of 25 versus 15 μs for the new as well as being hardware-dependent for the 10 volt discretization of channels.

As already stated, pulse height analysis is accomplished using successive approximation ADC. According to the manufacturer's specifications integral non-linearity is <±0.05% over 99% dynamic range and differential non-linearity is <±1% over the top 99% dynamic range.

Preparation and Experimental Procedures

Dougherty sand, a Thermic Arenic Haplustalf, was collected near Perkins, Oklahoma at a site not far from the north bank of the Cimmarron River. This soil was chosen because of its reported low clay and organic content. The collection site is a commercial sand quarry.

Analysis shows the soil to be composed of 98% sand and 2% silt and clay. It has a pH of 5.9, and a cation exchange capacity (CEC) of about 5 meq/100 g. There is an organic content of 0.07% with 0.7% ferric oxide present and a specific surface of 21.8 m^2/g. Extractable bases (meq/100 g) are: Na^+ - 1.4, K^+ - 0.14, Ca^{2+} - 2.4, and Mg^{2+} - 0.0.

Sample Preparation

A quantity of soil was triple-washed using de-ionized water and oven-dried. The triple-wash removed clays, silts, and much of the organics. After drying, the sand was sieved to isolate the fraction greater than 60- and less than 40-mesh (250 µm < sample fraction < 425 µm) to make the sample grain size distribution as homogeneous as practical. Finally, the soil sample was oven-stored to prevent moisture gain while preparing for the experiment.

Laboratory Column

The column used in the breakthrough curve experiment is a cylindrical flow cell 255 mm in length with an inside diameter of 51 mm. A water-tight column, made of acrylic (Lexan), was originally designed for transmission gamma ray tomographic imaging of moisture redistribution in an initially dry soil. The outside walls were milled down to give a final wall thickness of 3.2 mm to improve transmission of the 28 keV iodide K x-rays. Further reduction was not attempted for fear of breaking the flow cell during the milling process.

The cylinder has an incorporated base plate used for mounting the column to the positioning system. A 2° stilling well was milled into each cap to uniformly distribute flow. Mounting provisions are not required for the top cap so its diameter is the same as the O.D. of the column itself. Both are secured to the column with four recessed cap head screws. A neoprene gasket is placed between each cap and the column to provide a watertight seal. Each cap is fitted with a 1.4 mm I.D. nylon nipple with a tapered O.D. for accepting spaghetti

tubing.

The column is completed by the addition of a perforated Lexan flow plate and fine-mesh brass screen at each end. These are situated between the soil sample and the stilling well and serve to further distribute flow while keeping grains out of the cavities.

Pre-Test Preparation

Pre-test preparations can essentially be placed into four broad categories: column preparation, solution preparation, establishing test and data acquisition parameters and, finally, test set-up. The intention of this section is describe the steps taken and methodology used to prepare for the solute breakthrough curve experiment.

Column Preparation. Parameters such as target porosity and dry bulk density must be determined before actually packing the column. Due to the nature of the material, dry sand can pose problems when attempting to achieve too high a dry bulk density. For this reason, several practice columns were packed to obtain an optimal packing density. After several trials it became apparent that a ρ_b of 1.68 g cm^{-3} would be the optimum density. Assuming a mineral density of 2.65 g cm^{-3}, the porosity was calculated to be approximately 36.6%. The 520.9 cm^3 column was packed with 875.14 g of soil with a final packing density of 1.68 g cm^{-3}.

KI Solution. Solutions containing iodine compounds, usually potassium or sodium iodide, have been used extensively in gamma ray transmission studies. As previously mentioned, the original intent of this study was the gamma ray tomographic imaging of macropore flow and fingering effects in porous media. Both potassium and sodium iodide had been chosen as the initial solutes in order to enhance the contrast in density of the solution with that of the porous media and existing pore water. The potassium form was chosen over sodium based on cost and availability. Accordingly, a solution of KI ($[I] = 100,000$ mg/l) was prepared for the fluorescence breakthrough curve experiment.

The concentration of the solute was verified with 10 ml samples of the 100,000 mg/l KI as well as samples diluted to 75,000, 50,000, and 25,000 mg/l iodide. Total dissolved solids were measured by oven drying. The results are shown in Table 4.1.

Parameters. Test parameters for this particular experiment fall into three categories: electronics associated with counting, flow rate, and column packing. Parameters involved with column packing, namely dry bulk density, porosity, and pore volume were covered in the previous section and need no further discussion. There still remains to be some discussion of the data acquisition settings and flow rate, however.

TABLE 4.1

ANALYSIS OF TARGET SOLUTION`

Target [I] (mg/l)	Volume (ml)	Mass Solution (g)	Mass Precip. (g)	[K] (mg/l)	[I] (mg/l)
25000	10	10.1799	0.3312	7662	24872
50000	10	10.4004	0.6773	15338	49784
75000	10	10.6442	1.0383	22974	74571
100000	10	10.8907	1.4181	30668	99543

Electronics Settings. The basic detection system is composed of a detector assembly (detector crystal, photomultiplier tube, and base), linear preamp/amplifier, high voltage bias supply, and data acquisition board. The purpose of the bias supply is to provide high voltage to the dynode of the photomultiplier tube. An increase or decrease in voltage to the PMT results in an increase or decrease in gain of the PMT. The required high voltage setting changes with the energy of the incident photon and typically is found through a "trial and error" process if not known from past experience. In this case, both amplifiers are set at 800 volts which is sufficient to provide a good signal for both 667 keV and 28 keV photons.

The linear amplifier is responsible for pulse shaping and amplitude gain. The output is a shaped pulse over a 0 - 10 volt span and is variable over a wide range through fine- and coarse-gain controls. The desired energy peak can be centered in the 10-volt window by implementing the proper combination of gains. It should be noted that too high a gain setting results in distortion as well as greatly increased dead time. A coarse gain of 10.0 and fine gain of 7.0 was

found to work well with both detectors.

After centering using gain controls the signal can be discretized over the 10 volt range into a number of bins or "channels". The purpose of discretization is to control the energy resolution at which the incoming signal is binned. For example, coarse binning may result in minor peaks being lost in the accompanying Compton haze whereas finer binning may allow the peak to be discriminated. The options available with the current hardware allow a minimum of 256 and a maximum of 2048 channels. Given the peak energies of this study, 0.661 MeV and 0.028 MeV, both systems were set at 1024 channels.

Flow Rate.   Flow is provided by a detachable-head peristaltic pump set to 0.4 ml/min. A calibration run of the pump over a 64 minute period indicated a flow rate of 0.6 ml/min. The actual flow rate attained is determined during the experiment.

Test Setup.   The acrylic test column was packed in lifts to the predetermined dry-bulk density. Double-distilled, de-ionized water was then introduced to the column after deoxygenation. Removal of as much oxygen as possible was necessary to prevent the formation of microbubbles in the column while flushing preparatory to the experiment. Bubbles of any size would not only affect the uniformity of flow but attenuation data as well.

After mounting the column to the positioning tables the parastaltic pump was plumbed in and flow was initiated. Deaired, deionized water was flushed through the column to eliminate air bubbles. Flow was discontinued after two

pore volumes; this being considered sufficient to flush out any entrapped air. At this point the reservoir was switched over to the KI test solution source.

Data Collection. The experiment was designed to incorporate as many checks on data as possible. Data collected are from four sources: attenuation data of transmitted primary photons by the in-line detector, generated x-rays by the offset detector, conductivity probe analysis of the effluent, and oven-dried weight of the effluent. This allows three checks of the x-ray data. An additional check becomes available on comparing the experimental data with the theoretical breakthrough curve.

The data collection schedule had to be designed to accommodate two discrete and independent counting systems: the inline and offset detectors. It was decided to fix the sampling regimen based on a pre-determined live time of the inline detector. The live time used, 10 minutes, was based on an estimation of the time required to count 10^6 unimpeded 0.662 MeV photons. At the high count rates encountered, a dead time of approximately 35-40% could be expected resulting in a real time of around 14 minutes.

The data acquisition board was set to trigger at this live time. On triggering, software stopped acquisition of both the inline and offset detectors. The data acquisition boards controlling both were then reset and counting resumed. Data was downloaded from memory to hard disk.

Effluent was collected in 40 ml EPA volatile organic vials. The vial was replaced after triggering . Between sample changes the most recently collected sample was weighed, conductivity taken, and then weighed again. The

conductivity probe was checked for calibration at regular intervals throughout the

experiment. Also, the probe was checked against standards made up of the

reservoir solution.

CHAPTER 5

ERROR ANALYSIS

Introduction

Experimentation focused on steady-state, saturated flow regimes in which

transport mechanisms are limited to advection, mechanical dispersion, and

minimal molecular diffusion. These concepts are applied to the data in

breakthrough curve analysis. Several factors may affect the integrity of the

experimental data. Items needing some discussion are system error and bias,

counting error, and characteristics of the porous medium.

System Error and Bias

Unidentified bias results in errors and identified bias is dealt with through

calibration curves. Unless noted otherwise, it should be stressed that the

procedural elements were developed specifically for this system.

Potential sources of error should be identified before actually initiating data

collection. The sources of errors in the data will depend on the hardware being

used as well as preparation, experimental method, and procedures. This implies

that errors can be placed into two broad categories: those errors associated with

hardware and those associated with preparation, experimental method, and

procedures. Accuracy of the data will depend on knowledge of the accuracy of

the equipment and the procedures used.

System Error

The total error of a system can be decomposed into two components: bias and imprecision (Doebelin, 1990). If bias can be identified and removed by calibration or some other method then the total magnitude of the error is the result of the statistical imprecision associated with the measuring process. This implies that upper and lower limits of certainty, $\pm 3s$ or most probable error (e_p), can be placed on the quantity being measured.

The counting process is Poisson in nature (Jenkins and De Vries, 1973). Sample variance (σ^2) is equal to the sample mean (count, N) and sample standard deviation (σ) is the square root of count. The 3s precision of the system is therefore $N \pm 3^*(N)^{0.5}$. Precision has no meaning, however, if because of bias it does not accurately reflect the true estimate of the count. Accuracy is established by evaluating all practical sources of bias and removing them either through calibration or other methods. Having done this, accuracy can be said to equal count with a precision as defined above.

System Bias

As described in Chapter 4 the combined tomography and spectroscopy system is composed of five essential elements: source, collimation, positioning system, detectors with associated electronics, and data acquisition boards with multichannel analyzers. Each of these components is a potential source of

system error and should be evaluated.

Collimation. Additional bias can be attributable to improper or changing source collimation. Since x-ray generation is based on the flux of incident exciting photons, it is necessary to carry out experiments using the same collimation used in the construction of the calibration curves. Decreasing collimation by one half results in an approximate fourfold decrease in incident photons which decreases x-ray yield proportionately. Therefore, maintaining constant source and detector collimation is necessary.

Positioning System. Positioning system bias can be introduced in a number of ways. These errors are associated with two general categories: hardware and software. Assuming that software is sending the proper number of steps to the stepper motors and that hardware is in good condition, error in sample placement is controlled by the accuracy and repeatability of positioning tables and stepper motors. As discussed in Chapter 4, the linear tables have a bidirectional positional repeatability of ±0.0002 in. (0.005 mm) and a positional accuracy of ±0.00025 in./in. (0.00635 mm/mm). The stepper motors translate the linear tables at a rate of 0.0254 mm/step (stepper motor shaft revolution of 1.8°/step) which is more than 200 times less than the positional accuracy of the tables. It is concluded, therefore, that bias attributed to hardware can be effectively ignored as long as the linear positioning tables are maintained in proper working condition.

Detectors and Associated Electronics. That scintillation detectors are

subject to drift with changes in temperature is well documented in the literature. This was also noted with the current system while running long-term tests. To investigate count-rate variation as a function of temperature, thermocouples were placed at the detector, amplifier and bias supplies, computer, and on two walls at detector height. Temperatures were logged at constant time intervals while acquiring photon counts. Graphs were then constructed showing the variation in count with increasing temperature. The results showed a linear relationship between count and temperature.

There are at least three means of dealing with temperature-effect bias: construction of a detector response vs. temperature curve, detector cooling, and climate control. The first option is, in effect, the construction of calibration curves that are dependent not only on analyte concentration but temperature as well. Detector cooling can be accomplished by wrapping the detector in tubing which is connected to a constant temperature bath thereby providing a heat exchange mechanism. Climate control of the work space can be accomplished by means such as a dedicated air conditioner or by tapping a relatively constant-temperature reservoir.

Bias removal through construction of additional calibration curves is an unnecessary hindrance to data acquisition and a potential source of additional error. The installation of a dedicated air conditioner was considered but would have required structural changes to a load-bearing wall. After analyzing detector sensitivity vs. temperature, it was decided that the most practical means of climate control was to cycle air with the adjoining laboratory on a continuous

basis. This allowed air to be exchanged approximately ten times per hour with the relatively constant-temperature air of the outer laboratory.

Sources of Imprecision

With the removal of bias any imprecision in the data is a function of the randomness of photon emissions. Assuming a perfect sample, stable electronics, and an accurate counting interval, each individual count in a succession of intervals will still vary. This is an important consideration when quantitative analysis based on calibration curves is being implemented. The analysis of error associated with photon statistics is treated in the following sections.

Counting Error

Error analysis in fluorescence spectroscopy is straightforward assuming that neither wavelength enhancement nor secondary excitation of lower-Z elements is occurring due to matrix effects and incorporated similar-Z materials. The type of analysis, although similar in both cases, depends on whether the data is in the form of count as in this study, or intensity. In both cases the background count is taken into consideration.

Two types of error can be calculated: standard counting error (σ_N) and relative counting error (ξ_N) (Bertin, 1978). For a single count the standard counting error is given by

$$\sigma_N = N^{1/2} \qquad\qquad 5.1$$

and relative counting error as,

$$\xi_N = \frac{\sigma_N}{N} = \frac{N^{1/2}}{N} = \frac{1}{N^{1/2}} \qquad 5.2$$

Assuming the same live time for the peak and background counts the standard and relative errors are

$$\sigma_N = \left(\sigma_P^2 + \sigma_B^2\right)^{1/2} = \left(N_P + N_B\right)^{1/2} \qquad 5.3$$

and

$$\xi_N = \frac{\left(N_P + N_B\right)^{1/2}}{N_P - N_B} \qquad 5.4$$

where N_P is the net count and N_B is the background count.

In instances in which the accumulated count from a sample (N_x) is to be compared with that from a standard (N_S), assuming that both counts were acquired using the same live time, a ratio method is used for determining the relative counting error. For counts uncorrected for background the relative error is,

$$\xi_N = \left(\frac{1}{N_X} + \frac{1}{N_S}\right)^{1/2} \qquad 5.5$$

and the relative error corrected for background is given by,

$$\xi_N = \left(\frac{(N_P + N_B)_X}{(N_P - N_B)_X^2} + \frac{(N_P + N_B)_S}{(N_P - N_B)_S^2} \right)^{1/2}$$ 5.6

When replicate counts of the same standard or sample are made the standard counting error and relative fractional error is calculated as,

$$(\sigma_N)_n = \frac{1}{n^{1/2}} \sigma_N$$ 5.7

and

$$(\xi_N)_n = \frac{1}{n^{1/2}} \xi_N$$ 5.8

where n is the number of replicates.

System Precision, Accuracy and Sensitivity

System accuracy, precision, and sensitivity are determined through photon statistics and a calibration curve. A typical approach would be to construct a set of standards with a range of concentration equaling that of the expected distribution of the experiment. Statistical precision is then calculated based on fluorescence data of these standards. These same data points are then used to construct the calibration curve.

Precision. Repeated measurements are made at each concentration to determine the standard deviation, S, from the mean, $\bar{x}$, of the n results, x (Jenkins and De Vries, 1973). The coefficient of variation, ξ, is then calculated

based on the value of S. These are stated in equation form as,

$$S = \left(\frac{\sum d^2}{n-2} \right)^{1/2}$$

5.9

and

$$\xi = 100 \left(\frac{S}{\bar{x}} \right)$$

5.10

where d is the deviation from the individual result, x_i. Bertin (1978) states that the standard deviation, S, relates to absolute precision and the coefficient of variation, ξ, is a measure of precision relative to the concentration of analyte present.

Accuracy. A calibration curve must be established to determine concentration given an x-ray count. Linear regression is used to establish the best fit line describing the data after establishing a number of data points (x-ray count vs. concentration). The regression line is then assumed to represent the "true" representation of concentration given count, N. Accuracy, which is the degree of deviation of the measured concentration, c_i, and the true concentration, c, is expressed as

$$c_T = \left(\frac{c_i - c}{c} \right) 100$$

5.11

where c_T is the percent difference relative to the true value. Accuracy can be

tested by acquiring data on a standard composed of a concentration other than those used in the construction of the calibration curve. The concentration, c_i, calculated from the derived calibration curve

$$c_i = mx + b \qquad\qquad 5.12$$

where m is the slope, x is the count, and b is the background count (intercept) can then be used in equation 5.11 to obtain the percent accuracy.

Parameters are live time, sample position, sample dry bulk density, sample moisture content, and collimation of source and detector. Count rate not only depends on concentration but on position in the sample as well. Therefore, for multiple data points, a curve must be constructed for the expected count rate vs. concentration and position in the sample.

Sensitivity. There are essentially two goals in determining the sensitivity of a measurement in the counting process: establishing the minimum detectable limit (MDL) and the rate of change of count with respect to analyte concentration. Birks (1969) defines the MDL, based on a fixed counting time, as the amount of analyte giving a net count equal to three times the square root of the background count. Statistically this would be three times the standard error of the background count or, $3\sigma_B$. Sensitivity can be increased by decreasing the background count that lowers the MDL. This is accomplished through collimation and using a more sensitive detector.

Summary

The sources of bias discussed above can, in general, be removed without the aid of a calibration curve. Background interference as a result of interelement matrix effects, however, must be removed through the use of a calibration curve. Error from detector drift as a result of change in temperature is the only likely source of bias to be encountered and is easily checked by taking numerous air counts of the unattenuated beam during the data acquisition process. A steadily decreasing count rate is also indicative of temperature drift.

CHAPTER 6

RESULTS

AND

DISCUSSION

Introduction

The experiment resulted in 34 data sets acquired over a period of approximately eight hours. Data consists of gamma- and x-ray spectra, effluent mass flow rates, effluent conductivity, and total dissolved solids. Data analysis consists of plotting breakthrough curves (BTC) based on the five sets of experimental data. Relationships between these curves, as well as with the theoretical BTC are shown. Results of these comparisons are then used to determine the effectiveness of x-ray fluorescence as a quantitative tool in laboratory column breakthrough tests. A brief overview of breakthrough curve theory is given after presentation of experimental data. Comparisons between the experimental and theoretical curves are then presented based on concepts developed in the BTC overview.

Gamma and X-ray Results

Data collection intervals are based on a 10-minute live time trigger initiated by the in line detector. At the end of each interval spectral data is written to hard

disk and the effluent vial is replaced. Each sample has associated with it four experimental, and one theoretical, data sets. Attenuation and fluorescence data are acquired in real time while the conductivity and weight of the effluent are taken while the next data set is being acquired. Experimental parameters are summarized in Table 6.1.

TABLE 6.1

TEST PARAMETERS

Property	State
Column Position	Vertical
Flow Direction	Upwards
Flow Rate (ml/min)	0.483 ± 1.4%
Mass of Soil (g)	874.7
Bulk Density (g/cm^3)	1.68
Porosity (calculated)	0.366
Pore Volume (cm^3)	190.6
Initial Moisture Content	Saturated

Gamma Data

Inspection of the gamma data showed that peak shifting toward the high-energy end of the spectrum had occurred during the experiment. The electronic drift was a result of temperature changes and count rate variation. This shift resulted in widening the peak and decreasing the maximum channel count that in turn induced decreasing count with time. A post-count rubber band algorithm, which is the same algorithm used by the system during CT scanning (Brown, et al., 1996), was applied to correct this peak shift phenomenon. Maximum channel values vs. sample number for each peak are shown in Figure 6.1. The
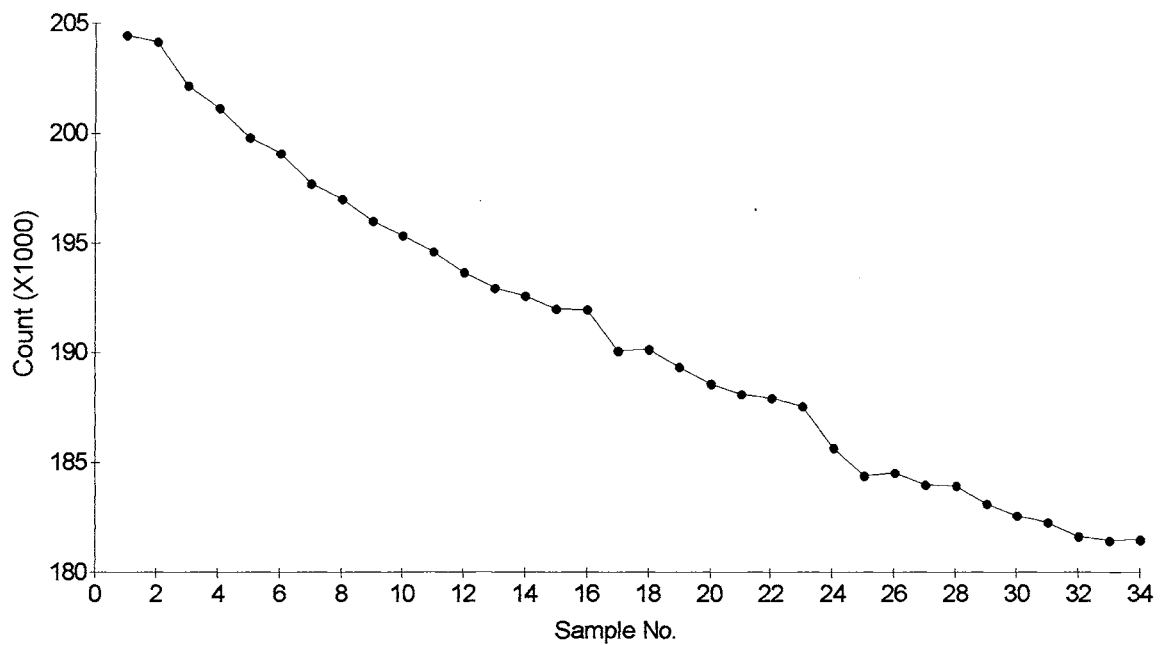
Figure 6.1 Maximum Peak Channel Count vs Sample Number.
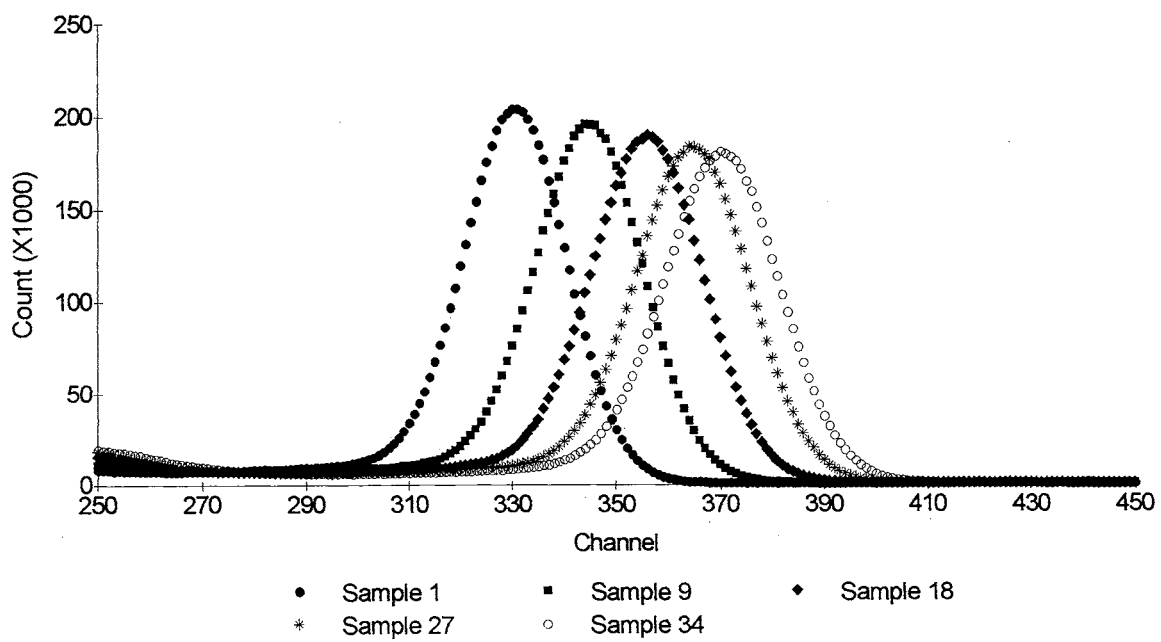
Figure 6.2 Peak Shift vs Channel Number.

degree of peak shift and change in peak geometry are illustrated in Figure 6.2.

The solute front was first detected by the in line detector during the time interval 5.35 < T < 5.58 hours (sample 24). Total attenuation of the primary 662 keV beam was approximately 0.85% the initial intensity at the point of maximum solute concentration beginning with sample 30 at T = 6.98 hours. Mean total peak areas corresponding to replicate samples of minimum and maximum solute concentrations are 5,432,643 and 5,386,308 counts, respectively. The minimal degree of attenuation is a strong indication that too high an energy was used for attenuation purposes.

A signal's magnitude is determined by the difference between the mean maximum and mean minimum counts. For this study, the standard counting error to signal ratio ranges from 5 to 15% (1 to 3σ). This translates into a ±3σ standard counting error spanning 10 to 30% of the signal. Although this study is not dependent on transmission-attenuation data it was hoped that it would serve as an additional independent, quantitative data set which would support the fluorescence data. This is not possible, however, due to insensitivity. Raw and adjusted values of gamma data versus sample number based on data found in Table 6.2 are presented graphically in Figure 6.3.

X-ray Data

X-ray data was much more stable than the attenuation data; no post test processing was required. Electronics had stabilized approximately 97 minutes into the experiment. Spectra 8 through 21 were used to establish the background

TABLE 6.2

ATTENUATION AND FLUORESCENCE DATA

Sample No.	Elapsed (mm:ss)	Gamma Count		X-Ray Count	
		Raw	Adjusted	Gross	Net
1	13:51	5505586	5456461	104294	0
2	27:50	5506127	5457435	103623	0
3	41:47	5506094	5457931	103258	0
4	55:45	5498993	5451040	102791	0
5	69:43	5494309	5456311	102382	0
6	83:41	5485878	5447557	102238	0
7	97:39	5481027	5443040	102561	0
8	111:37	5471917	5433736	101543	0
9	125:35	5478315	5440986	101906	0
10	139:33	5473499	5445685	102204	0
11	153:31	5463771	5435778	101630	0
12	167:29	5465436	5437120	102106	0
13	181:27	5458610	5430706	101552	0
14	195:26	5454796	5435968	101923	0
15	209:24	5450821	5432375	102054	0
16	223:22	5452878	5434440	101699	0
17	237:21	5445744	5427218	101655	0
18	251:20	5452127	5433893	101709	0
19	265:18	5446996	5428723	102225	0
20	278:17	5450632	5432346	101733	0
21	293:16	5438262	5429064	101554	0
22	307:15	5442640	5433572	102367	0
23	321:14	5445187	5436287	103792	1971
24	335:12	5434287	5425223	109933	8112
25	349:11	5410581	5401518	117945	16124
26	363:09	5401587	5392602	121874	20053
27	377:08	5399562	5390630	122743	20922
28	391:06	5388739	5388739	123233	21412
29	405:05	5393097	5393097	123040	21219
30	419:03	5384903	5384903	122979	21158
31	433:02	5384188	5384188	123340	21519
32	447:01	5389554	5389554	122812	20991
33	461:00	5384658	5384658	123338	21517
34	475:00	5388240	5388240	123576	21755
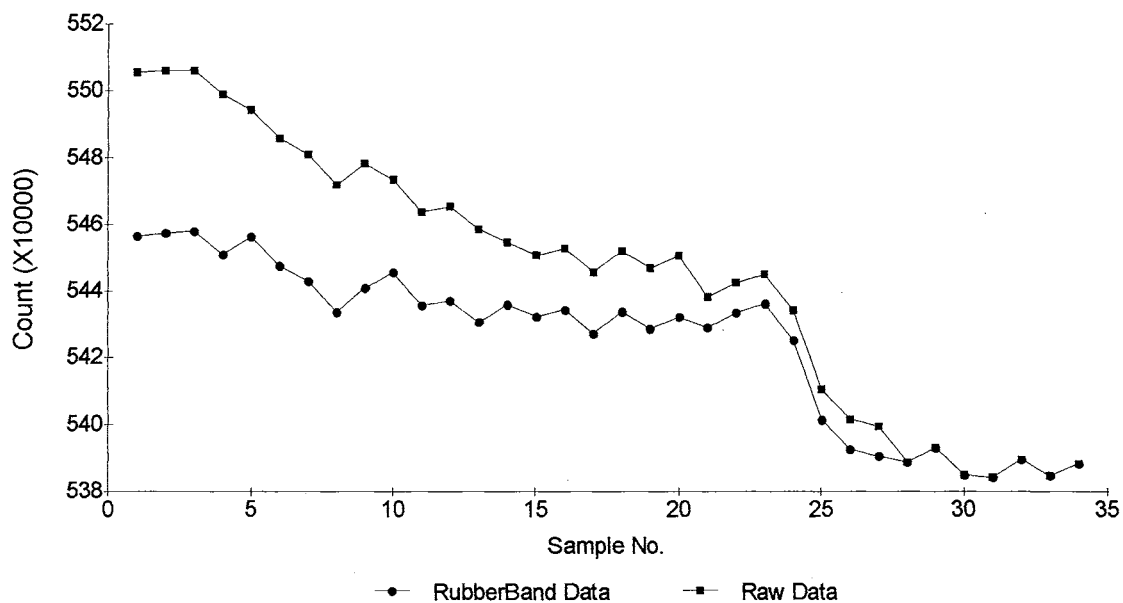
Figure 6.3 Gamma Peak Areas vs Sample No. - Raw and Adjusted Data.
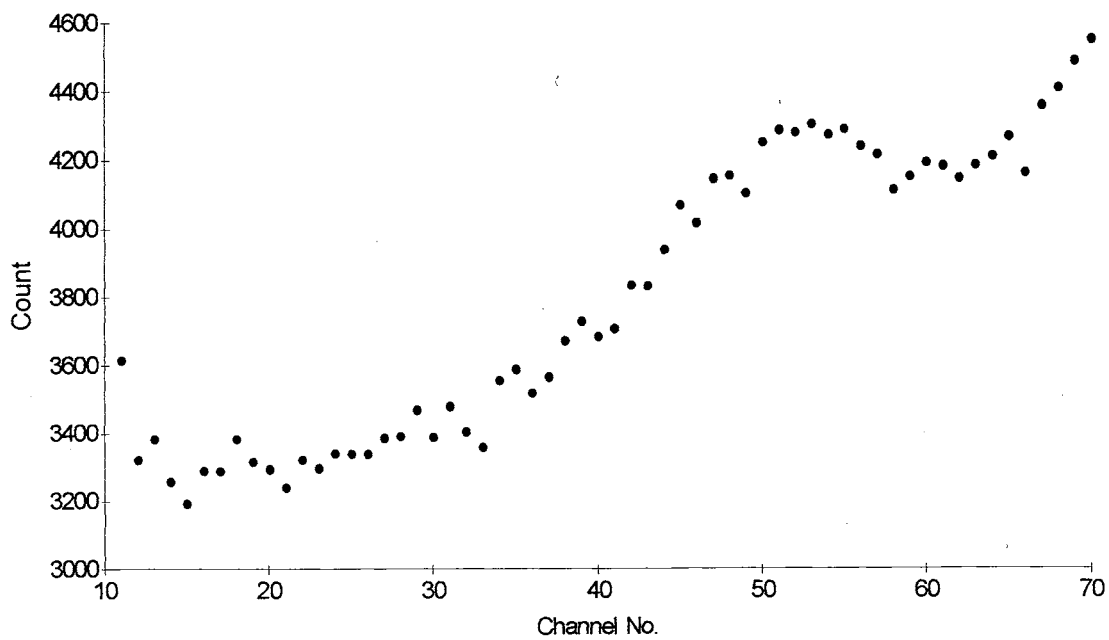
Figure 6.4   Example X-ray Background Spectrum.

count within the region of interest (ROI) containing the fluoresced x-ray peak (Table 6.2). The mean background count was established by summing the channel contents within the ROI for each spectrum and calculating the mean. A typical background spectrum with ROI is found in Figure 6.4.

The first statistically significant peak was detected during acquisition of sample 23. This was determined visually and by comparing the net peak area with the minimum detectable limit (MDL) defined in Chapter 5 as

$$MDL = N_B + 3\sigma_B \qquad\qquad 6.1$$

which states that a peak can be discriminated if its area exceeds the sum of the background and three times its standard counting error. Based on a mean background count of 101,821 and standard counting error of 319, the MDL was determined to be 102,778 counts. Background counts used in calculating the mean are presented in Figure 6.5 and x-ray data in the form of total count is found in Figure 6.6. A summary of counting statistics for spectra 22 through 34 is found in Table 6.3. Plots of N_P vs. σ and N_P vs. ξ are shown in Figures 6.7 and 6.8, respectively.

X-ray Peak Analysis. Theoretically, fluoresced net peak area is a linear function of solute concentration. This was illustrated by model output in Chapter 3. It was also shown that when net peak area is plotted versus concentration the slope varies with x-ray intensity. Intensity dependence is removed by using the ratio of fluoresced net to maximum (N_{max}) peak areas. Further determination of linearity was to have been made through construction of a calibration curve based on four standards (Chapter 5).
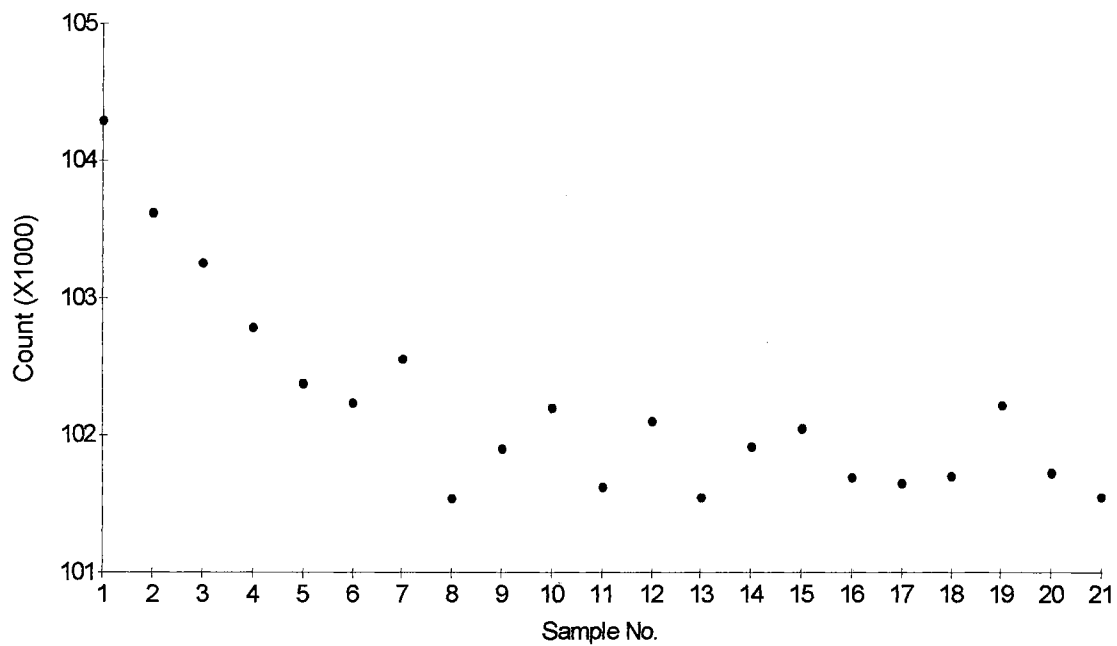
Figure 6.5 Background Peak Sums Used in Calculating Mean Background.
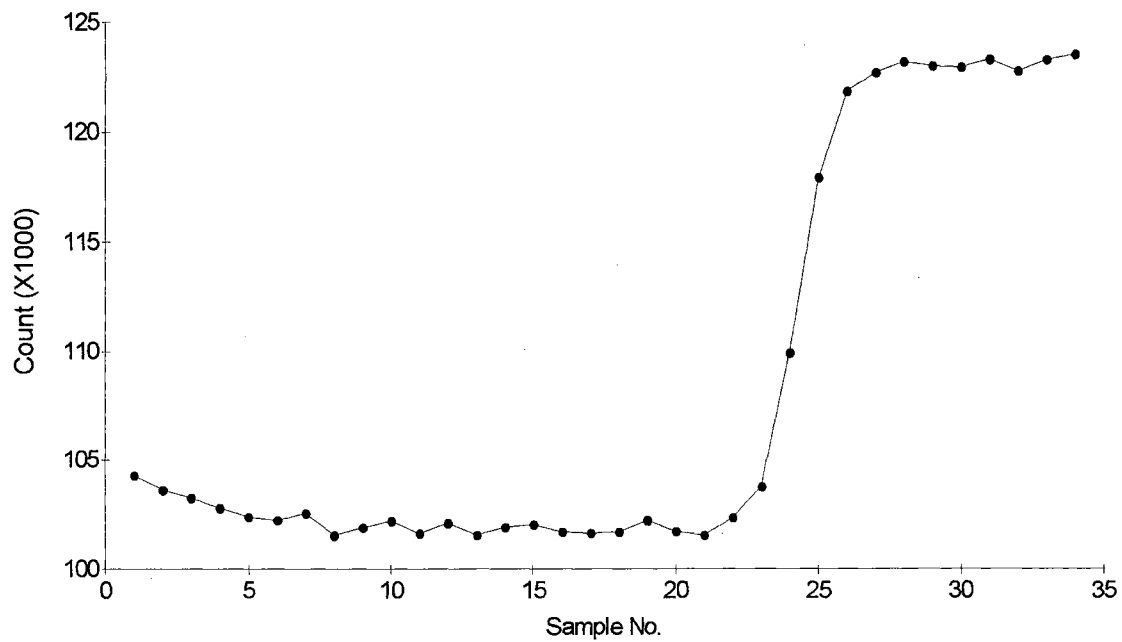
Figure 6.6 Total Count vs Sample Number.
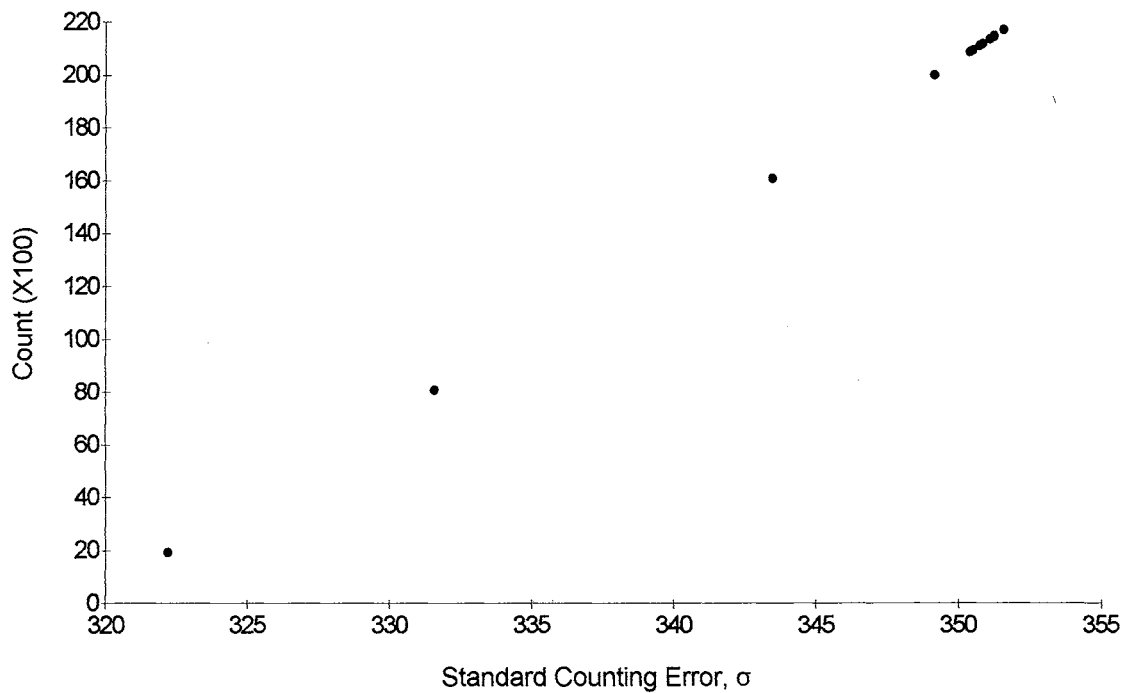
Figure 6.7 Net Peak Area vs Standard Counting Error.
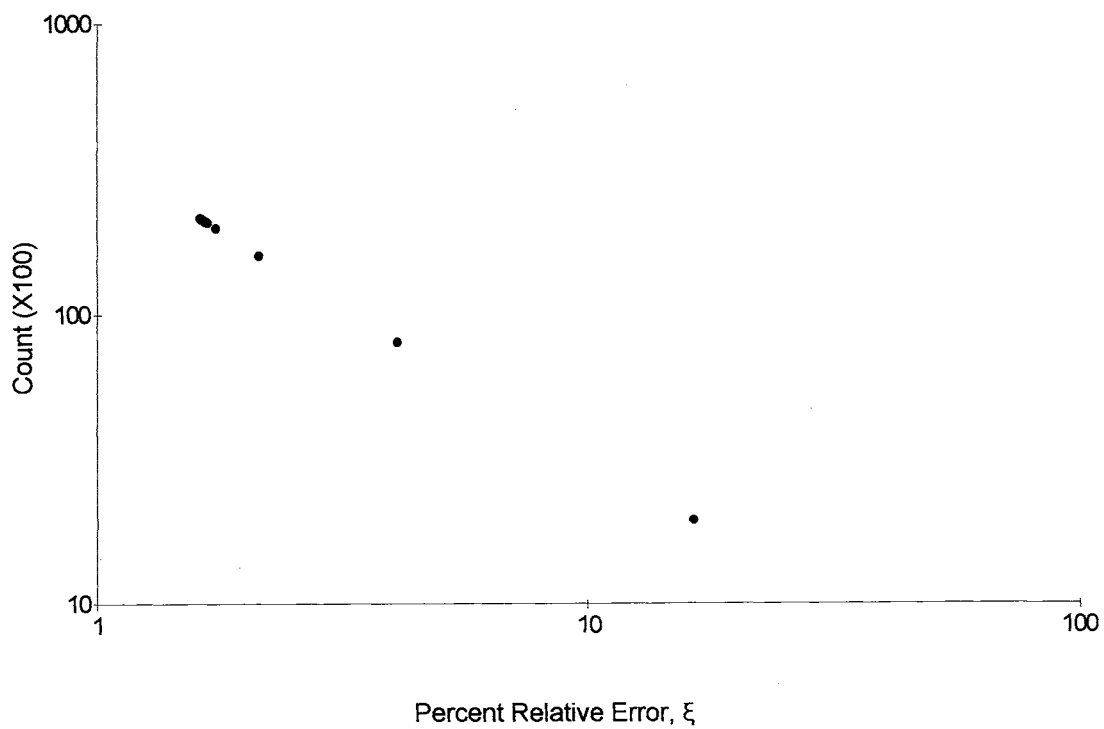
Figure 6.8 Net Peak Area vs Percent Relative Error.

TABLE 6.3

SUMMARY STATISTICS FOR FLUORESCENCE DATA

Sample No.	Gross Count $(N_B + N_P)$	Net Count (N_P)	Std. Error (σ)	% Rel. Error (ξ)
22	102367	0	N/A	N/A
23	103792	1971	322	16.35
24	109933	8112	332	4.09
25	117945	16124	343	2.13
26	121874	20053	349	1.74
27	122743	20922	350	1.67
28	123233	21412	351	1.64
29	123040	21219	351	1.65
30	122979	21158	351	1.66
31	123340	21519	351	1.63
32	122812	20991	350	1.67
33	123338	21517	351	1.63
34	123576	21755	352	1.62

The calibration curve was based on incorrect geometry and was not useful in determining count versus concentration of the experimental data. It did provide evidence for a linear relationship between concentration and x-ray net peak area, however. Therefore, it was decided to compare the theoretical calibration curve with BTC data. Linearity in both actual and modeled data implies the relationship

$$\frac{C}{C_0} = \frac{N_P}{N_{MAX}}$$

6.2

where C is the solute concentration at count N_P and C_0 is the maximum concentration at N_{MAX}.

Regression of the modeled output leads to the expression

$$\frac{C}{C_0} = N_p * 0.0025$$ 6.3

in which the slope term of 0.0025 corresponds to the inverse of N_{MAX} (=400

counts). This lends support to the relationship stated in Equation 6.2.

Rearranging Equation 6.3 to solve for C yields

$$C = C_0 * N_p * 0.0025$$ 6.4

Equation 6.4 shows that, given a net count, concentrations can be determined

without the aid of a calibration curve. The only *a priori* data needed is the

maximum concentration of solute introduced into the system.

A check on both modeled and experimental data was made by estimating

the counts at standard concentrations. Modeled counts are based on C_0 and

N_{MAX} values of 100,000 mg/l iodide and 400 counts, respectively. BTC values

were obtained with Equation 6.2. These are shown in Table 6.4. Also found in

the table is a scale factor determined by dividing the experimental count by the

modeled count at each standard concentration. This factor was then

incorporated into Equation 6.4 to predict counts of the same magnitude as those

found in the experimental data. A plot of N_p versus C for both data sets is shown

in Figure 6.9. Figure 6.10 represents concentrations based on Equation 6.6 and

N_p of Table 6.3.
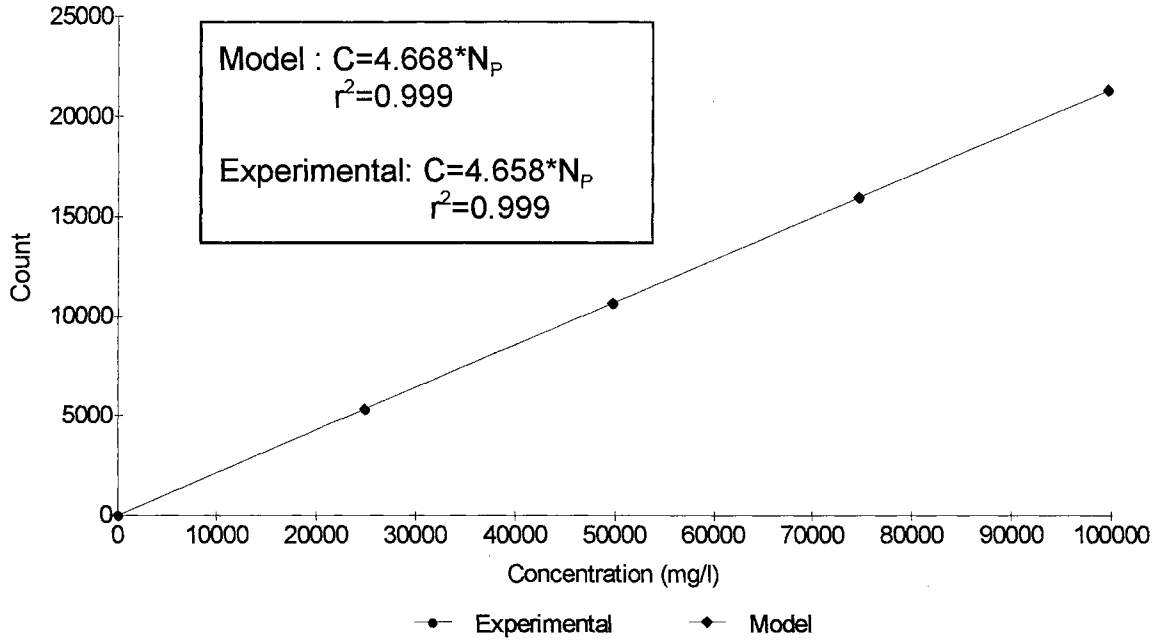
Figure 6.9 Net Peak Area vs Concentration - Modeled and Experimental Data.
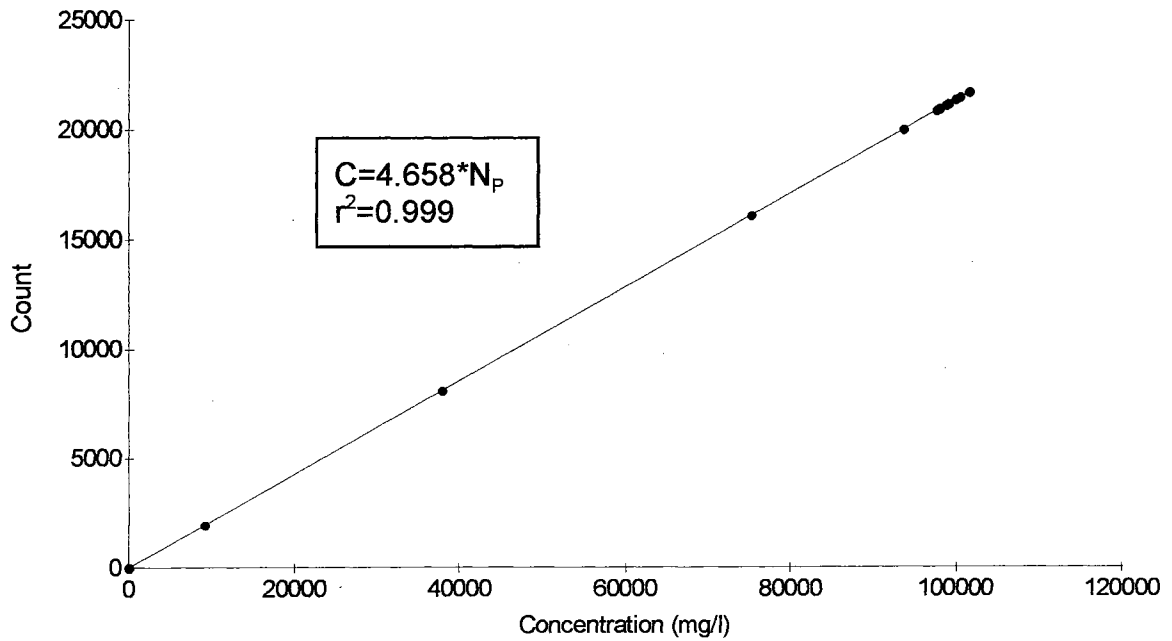
Figure 6.10 Net Peak Area vs Concentration - XRF Data.

TABLE 6.4

MODELED AND EXPERIMENTAL COUNTS

C	Net Count (N_P)			Scale	Percent
(mg/l)	Model	BTC	Scaled	Factor	Difference
24872	99	5325	5328	53.52	0.056
49784	199	10677	10665	53.65	0.065
74571	298	15965	15975	53.52	0.062
99543	398	21311	21324	53.52	0.061

Breakthrough Curve Theory

The solute BTC is a graphical representation of solute concentration versus transport time or distance. Time can be expressed in terms of pore volume. The shape of the curve is affected by advection, mechanical dispersion, and molecular diffusion. Initial moisture content ranges from oven dry to saturated with initial conditions based on the properties being evaluated.

In a saturated column, non-reactive solutes are transported by advection and dispersion. The governing equation for 1-D saturated flow with non-reactive solute (no retardation) is:

$$\frac{\partial C}{\partial t} = -\overline{v}\frac{\partial C}{\partial x} + D_L\frac{\partial^2 C}{\partial x^2}$$ 6.5

where D_L is the dispersion coefficient, a lumped sum combining the effects of dispersion and diffusion, t is time, x is distance and C is concentration. Determination of the dominant process, diffusion, dispersion or both, can be

obtained by calculating the Peclet number. This is defined as

$$P_e = \frac{\overline{v}D_p}{D}$$ 6.6

where D_p is the particle diameter. Diffusion dominates if P_e < 1; if 1<P_e<1000, diffusion transitions to dispersion with increasing values of P_e; and with P_e > 1000 dispersion dominates. Using the Peclet diagram, the ratio of D_L/D can then be determined. If dispersion is dominant, D_L can be approximated from the BTC as

$$D_L = \frac{1}{4t}\left((x-vt)^2{}_{.84} + (x-vt)^2{}_{.16}\right)$$ 6.7

where the subscripts .84 and .16 refer to the x-position at time t and C/C_o = .84 and .16 (assuming a Gaussian-distributed breakthrough curve). It should be noted that this method is valid only for sampling within the column. After calculating D_L, the solution to equation 6.1 is obtained by (van Genuchten, 1981)

$$\frac{C}{C_o} = \frac{1}{2}\left[erfc\left(\frac{L-v_x t}{2\sqrt{D_L t}}\right) + \left(\frac{v_x^2 t}{\pi D_l}\right)^{\frac{1}{2}} exp\left(-\frac{(L-v_x t)^2}{4D_L t}\right) - \frac{1}{2}\left(1 + \frac{v_x L}{D_L} + \frac{v_x^2 t}{D_L}\right) exp\left(\frac{v_x L}{D_L}\right) erfc\left(\frac{L-v_x t}{2\sqrt{D_L t}}\right)\right]$$ 6.8

where *erfc* is the complementary error function. With increasing flow length Equation 6.8 reduces to (Fetter, 1993)

$$C = \frac{C_o}{2}\left(erfc\left(\frac{L-v_x t}{2\sqrt{D_L t}}\right)\right)$$ 6.9

with initial condition

$$C(x,0) = 0$$

and boundary conditions

$$\left(-D\frac{\partial C}{\partial x} + v_x C \right)_{x=0} = v_x C_0$$

$$\left(\frac{\partial C}{\partial x} \right)_{x \to \infty} = (finite)$$

Breakthrough Curve Results

Experimental data used in BTC analysis consists of mass flow rates, total dissolved solids, and solute concentrations. Total dissolved solids were obtained from outlet samples with conductivities being used as a qualitative check. Gamma attenuation data was not used for reasons previously mentioned. Volumetric flow rates were derived from mass flow rates that were then used as one of the parameters in calculating the error function solution.

The first step in BTC analysis consists of determining the dominant transport process. This is done by plotting C/C_0 versus pore volume (Figure 6.11) and using equation 6.7 to establish D_L. Dispersion was the dominant process in this case. A theoretical breakthrough curve is then calculated using equation 6.8. The actual and calculated BTC's are plotted versus pore volume to determine the validity of the model. The two curves correspond if the experimental and modeled data describe the same process.
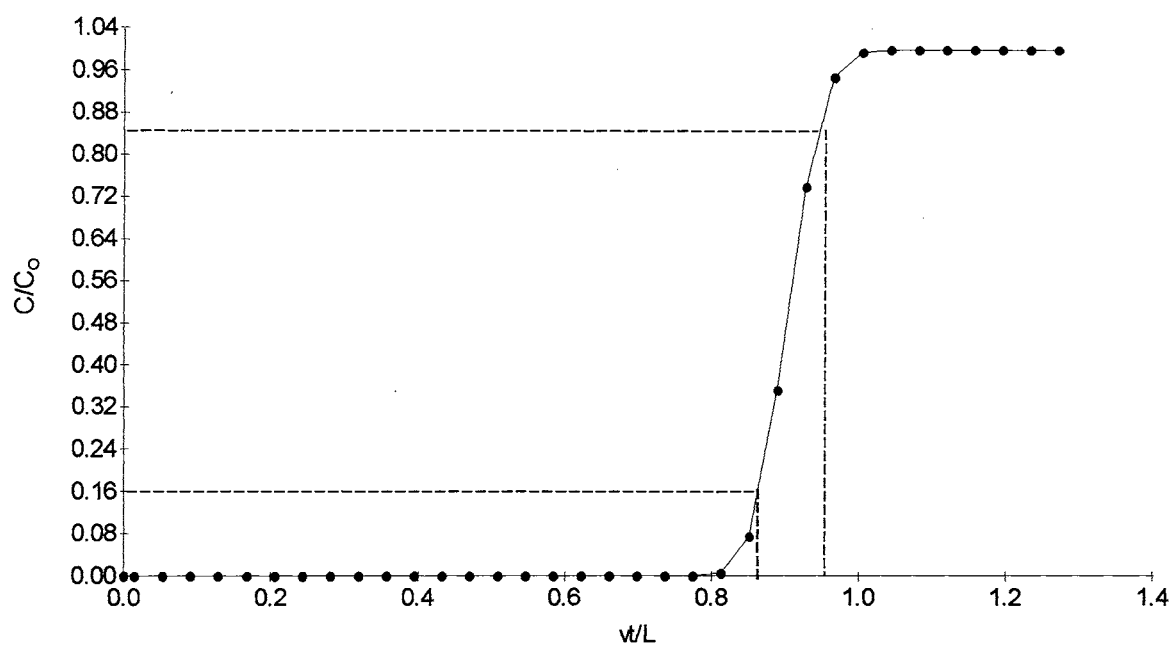
Figure 6.11 C/C_O vs Pore Volume for Determining D_L.

Presentation and Discussion of BTC Data

Data was analyzed at two positions in the column: x = 23.0 cm (fluor-

escence data) and x = L = 25.4 cm (effluent data). The error function solution

was calibrated using the derived D_L value (0.0013 cm^2/min) as a starting point.

The seepage velocity was varied iteratively until C/C_o = 0.5 at one pore volume

was obtained. Pore volumes were then calculated based on the predicted

velocity (v = 0.48362 cm/min). Resulting pore volumes, based on a porosity of

0.342 cm^3/cm^3, were 162.0 and 177.8 ml for the fluorescence and effluent sample

locations. These values correspond to column sample positions (x, and x = L) of

23.18 and 25.4 cm.

Plots of C/C_o versus pore volume for the fluorescence and effluent data

(Figures 6.12 and 6.13) were constructed based on these parameters. The

figures also show the calculated BTC based on the error function solution. Data

is presented in Table 6.5. Adjustment of the x-axis (pore volume) of both plots is

necessary because of dead space: the storage in the tubing, fittings, and wells at

the inlet and outlet. In the current configuration, this amounts to 2.4 ml at the

inlet and 1.5 ml at the outlet for a total of 3.9 ml.

The measured BTC is well fitted by the error function solution in both

instances. There is not a direct correspondence of individual data points

between the measured and fitted curves in either case, however. For the effluent

data this is most probably attributable to: 1) dispersion effects in the outlet cavity,

2) silt being washed from the sample, and 3) inadequate laboratory analytic

technique of the author. It should be noted that the curves themselves fit closely.
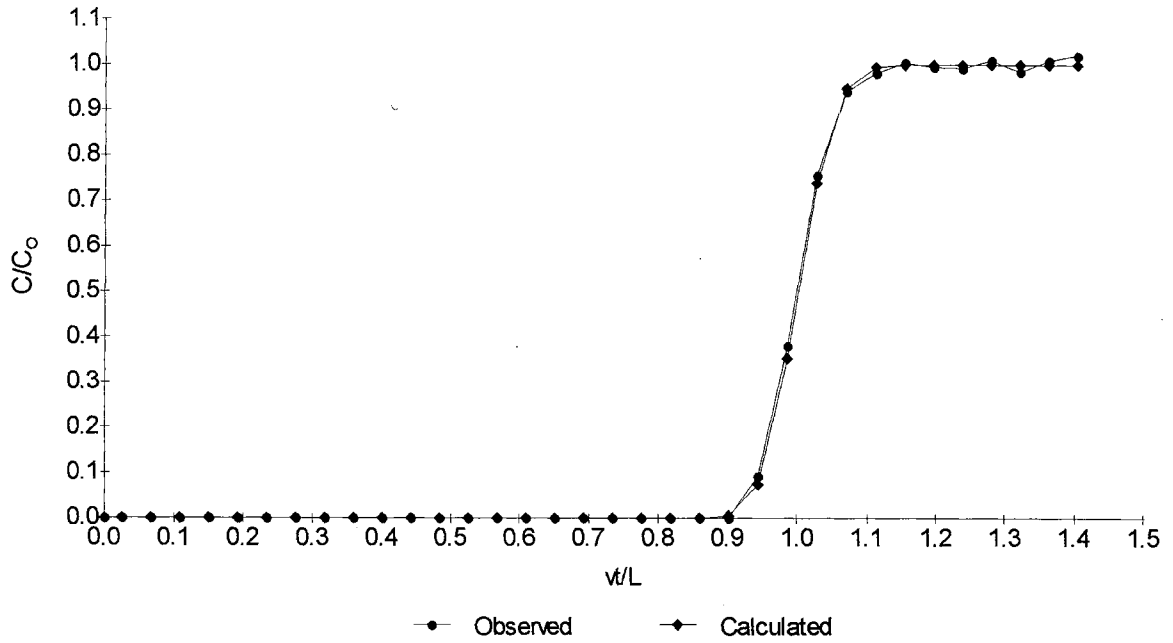
Figure 6.12 C/C$_O$ vs Pore Volume - Fluorescence Data.
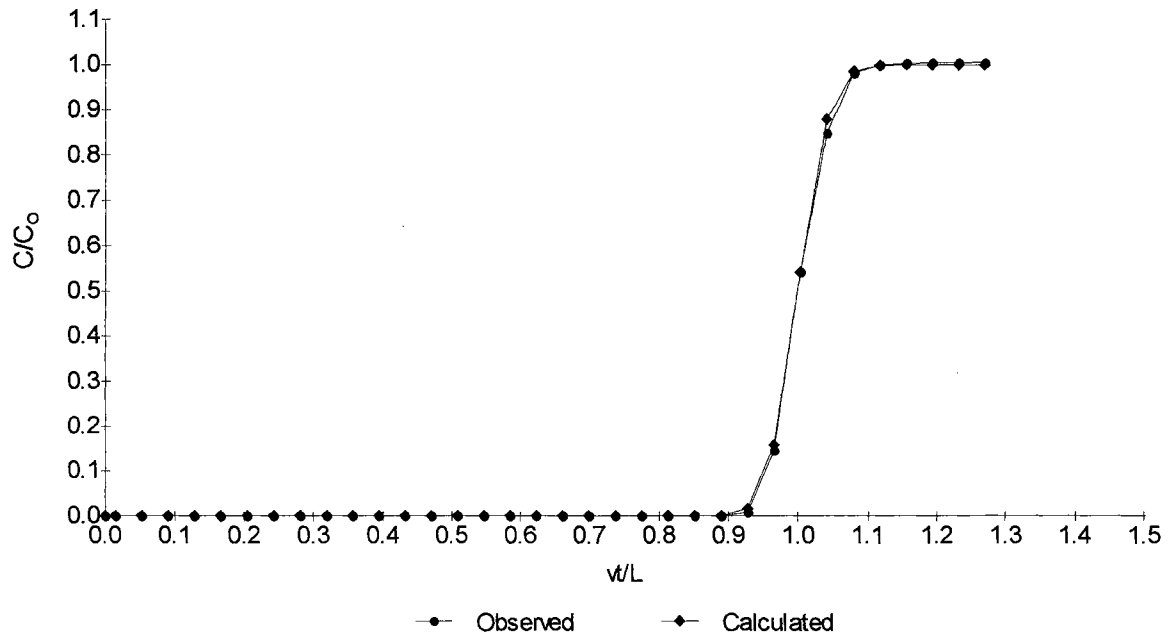
Figure 6.13 C/C$_O$ vs Pore Volume - Effluent Data.

TABLE 6.5

SUMMARY OF BREAKTHROUGH CURVE TEST DATA

Elapsed Time (min.)	Fluorescence Data			Effluent Data		
	vt/L	C (mg/l)	C/C_O	vt/L	C (mg/l)	C/C_O
0	0.000	0	0	0.000	0	0
13.51	0.026	0	0	0.015	0	0
27.50	0.067	0	0	0.053	0	0
41.47	0.109	0	0	0.091	0	0
55.45	0.151	0	0	0.129	0	0
69.43	0.192	0	0	0.167	0	0
83.41	0.234	0	0	0.205	0	0
97.39	0.276	0	0	0.243	0	0
111.37	0.318	0	0	0.281	0	0
125.35	0.359	0	0	0.319	0	0
139.33	0.401	0	0	0.357	0	0
153.31	0.443	0	0	0.395	0	0
167.29	0.485	0	0	0.433	0	0
181.27	0.526	0	0	0.471	0	0
195.26	0.568	0	0	0.509	0	0
209.24	0.610	0	0	0.547	0	0
223.22	0.652	0	0	0.585	0	0
237.21	0.693	0	0	0.623	0	0
251.20	0.735	0	0	0.661	0	0
265.18	0.777	0	0	0.699	0	0
279.17	0.819	0	0	0.737	0	0
293.16	0.860	0	0	0.775	0	0
307.15	0.902	0	0	0.813	0	0
321.14	0.944	9206	0.092	0.851	0	0
335.12	0.986	37889	0.380	0.889	0	0
349.11	1.027	75312	0.756	0.927	794	0.008
363.09	1.069	93664	0.940	0.965	14498	0.146
377.08	1.111	97723	0.981	1.004	53974	0.542
391.06	1.153	100011	1.004	1.042	84450	0.848
405.05	1.194	99110	0.995	1.080	97727	0.982
419.03	1.236	98825	0.992	1.118	99558	1.000
433.02	1.278	100511	1.009	1.156	99848	1.003
447.01	1.320	98045	0.984	1.194	99957	1.004
461.00	1.361	100502	1.009	1.232	99973	1.004
475.00	1.403	101613	1.020	1.270	100057	1.005

The differences between measured and fitted curves for the fluorescence

data is related to the resolution of the system. It was stated earlier that the offset

detector was placed at x = 24.9 cm that is 0.5 cm below the top of the column.

The effective position in terms of analysis was calculated to be x = 23.18 cm with

the actual position being x = 23.0 cm. This is shown is Figure 6.14. It can be

seen from the figure that the lower limit of the field of view (FOV) corresponds to

x = 23.0 cm where it crosses the centerline of the column. So, the effective FOV

corresponds to the position at x = 24.9 - 0.5 * 8 * Beam Diameter (= 0.5 cm) =

22.9 cm. Only one half the FOV is actually in the column. This means that a

substantial number of counts were missed. Proper placement would have

allowed the entire FOV to be in the column. Any discrepancies between the

curves, then, can be attributed to the averaging effect due to the volume of the

column in the detector's FOV. Volume averaging could probably be minimized by

decreasing the vertical collimation component.

SUMMARY

The use of x-ray fluorescence of high-z salts has been shown to be

feasible in nondestructive, in situ laboratory column BTC studies. BTC analysis

of effluent data confirmed results of fluorescence data acquired within the

column. Additionally, it was shown that in the current configuration it is

unnecessary to establish calibration curves to relate fluoresced x-ray count to

solute concentration. This is also verified by Monte Carlo modeling. Finally, BTC

analysis coupled with analysis of system geometry show that detector placement
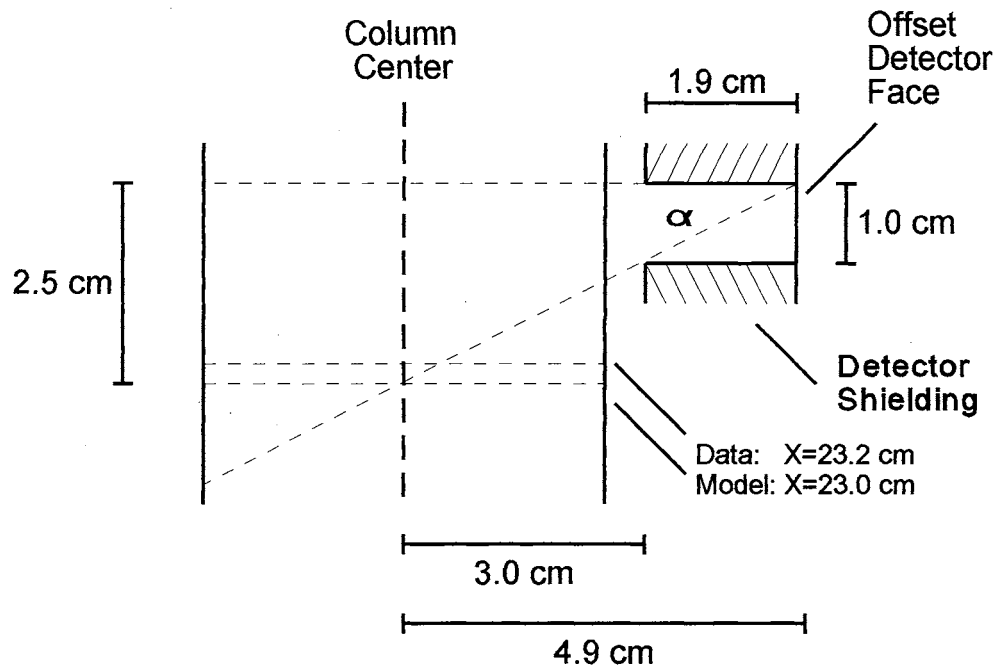
Figure 6.14 Detector Field of View.

should be at a position defined by

$$L = d * \tan(\alpha)$$
6.10

where L is the column length, d is the distance from the column centerline to the detector face, and α is the angle defining the point where one half the FOV intersects the column centerline.

CHAPTER 7

SUMMARY, CONCLUSIONS

AND

RECOMMENDATIONS

Summary

In situ, nondestructive examination of porous media is of interest to soil scientists and engineers studying transport processes. The common tool used in studying these processes has typically been some form of a laboratory column. The goal of this research has been to develop a new technique of nondestructively detecting and analyzing, by means of x-ray fluorescence, the transport of high-Z salts in saturated systems. X-ray fluorescence by itself is not new. However, application of this technique to the study of solute breakthrough curves in laboratory columns is new.

Theoretical evaluation of x-ray fluorescence processes showed that this approach would be feasible. The experimental system was simulated by using the theory of photon interactions in Monte Carlo modeling. Output provided important information concerning x-ray generation loci, detector response and construction of a theoretical calibration curve. The generated calibration curve was within approximately 0.065% that resulting from experimental data.

X-ray data from the BTC experiment was well fitted by the error function

solution. Effluent data was used to provide an independent check of the x-ray results. Gamma ray data was to have been used as well. Unfortunately, the source was too energetic and provided unacceptable error in signal response in terms of attenuation versus solute concentration. Fluorescence was more sensitive than gamma transmittance in this case. Lower concentrations of solute were measured with less error than with the traditional gamma attenuation method.

The feasibility of simultaneous CT imaging was considered throughout the progression of this research. Therefore, close attention was given to minimum data acquisition times and detector placement. It is the opinion of the author that simultaneous imaging/XRF is feasible with either the incorporation of more detectors or replacement of the current one with more sensitivity.

Conclusions

Breakthrough curve analysis is feasible with the system as currently configured. An understanding of the nature of photon interactions permitted data to be collected so that post acquisition processing was minimized. Problems normally associated with traditional x-ray fluorescence such as secondary and tertiary fluorescence, beam hardening, and non-monochromatic excitation were avoided through the use of a high-energy, high-activity radioisotope source and a single high-Z salt. Compton haze was minimized through the use of collimation on the source and detector.

Detector efficiency is the major limiting factor with this system. The lowest

fluoresced concentration of solute detected was approximately 9200 mg/l

compared with approximately 800 mg/l from effluent. This can be reduced to

about 4600 mg/l by repositioning the detector while keeping all other parameters

constant. The minimum detectable limit can be further lowered by either

incorporating more detectors or installing a more efficient detector.

Constraints affecting the overall success of this method as applied to

solute breakthrough curves are the need for a high-Z salt at large concentrations

and a high-activity, high-energy source. Considerations in source selection must

take into account the activity versus analyte excitation efficiency problem. An

additional constraint is one of time. The researcher must be aware of the time

needed for statistically significant data acquisition relative to the rate of

advancement of the solute front. Ideally, data should be acquired as quickly as

possible to construct a well-defined breakthrough curve.

CT imaging can be done simultaneously with XRF BTC testing if a more

efficient offset detector is incorporated. Photon emission tomography is possible

if a ring detector system is in place. This would allow two forms of imaging as

well as XRF.

Overall, system performance was as expected. Hardware, experimental

setup, and implementation were straightforward. The goal of providing a

multipurpose research tool requiring minimal specialized equipment was met.

Recommendations

Suggestions for future modifications are made in view of maintaining

simplicity and minimizing cost. As with computed tomography, time of data acquisition is one of the most important factors in dynamic fluorescence research. The four most important components concerning the rate of acquisition are: detector efficiency and collimation, source strength, and source activity.

1. **Investigate Improving the MDL.** Improving the total count by upgrading to a high-efficiency detector such as a large area geranium detector is a simple solution to part of the time problem. When considering efficiency it should be known what lower limit of detection is required and/or needed. If the lower limit is in the mg/l range, then a detector requiring cooling will probably be needed. That may not be the case if a lower limit in the hundreds of mg/l is required. It is the opinion of the author that trace analysis is not the concern in the type of research presented here.

2. **Investigate Improving System Resolution.** Signal strength can be improved by careful design of detector collimation. Background can be minimized by selecting a collimation geometry that will preclude most of the scattered radiation from reaching the detector. The horizontal collimation width of the current configuration is three cm. After analysis of the data it was determined that one cm would have been the optimum width. To some degree, this would result in lowering the MDL and increasing the relative net peak area of the fluoresced x-rays.

3. **Investigate Other Excitation Sources.** Excitation efficiency depends on source energy. The closer the incident photon energy is to the analyte absorption edge the greater the probability of excitation. To be remembered,

however, is that absorption increases with decreasing photon energy. So, although excitation efficiency may improve with a lower energy source, the overall rate of excitation will decrease because fewer incident photons will penetrate the target. A tradeoff must be reached between excitation efficiency as a function of incident photon energy and as a function of the rate of higher-energy incident photons.

Increasing the number of lower-energy incident photons is not just a matter of increasing the source size (activity). The source itself must be viewed as a high-Z absorber. There is a point at which the number of emitted photons cannot be increased despite source activity. Americium-241 is a good example of this limitation.

An additional consideration, when selecting the most effective source is the half-life. It is likely that the perfect source can be found but it may have a half-life of only a few days. Also, custom sources are usually extremely expensive and short-lived which would preclude long-term research projects.

4. Determine General Guidelines for MDL. The MDL, as a function of Z, concentration, counting time and excitation activity, can be evaluated using the equations and sources presented in Chapter 2 as well as the model described in Chapter 3. Optimizing all parameters for the most efficient fluorescence should be possible.

REFERENCES

Adams, F. and R. Dams, 1970. Applied gamma-ray spectrometry: Pergamon Press, Oxford.

Alemi, M.H., D.A. Goldhamer, and D.R. Nielsen, 1988. Selenate transport in steady-state, water-saturated soil columns: J. Environ. Qual., vol. 17, no. 4.

Appelt, H., K. Holtzclaw, and P.F. Pratt, 1975. Effect of anion exclusion on the movement of chloride through soils: Soil Sci. Soc. Am. Proc.: vol. 39, 264-267.

ASTM Data Series DS 37, 1965. X-ray Emission Line Wavelength and Two-Theta Tables.

Barrow, Gordon M., 1966. Physical chemistry: McGraw-Hill, N.Y.

Bearden, J.A., 1967. X-ray Wavelengths: Reviews of Modern Phyics: vol. 39, no. 1, 78-124.

Bearden, J.A., and A.F. Burr, 1967. Reevaluation of x-ray atomic energy levels: Reviews of Modern Physics: vol. 39, no. 1, 125-142.

Bertin, Eugene P., 1975. Principles and practice of x-ray spectrometric analysis: Plenum Press, N.Y.

Bertin, Eugene P., 1978. Introduction to x-ray spectrometric analysis: Plenum Press, N.Y., 485 p.

Beven, K., and P. Germann, 1981. Water flow in soil macropores: II. A combined flow model. Journal of Soil Science, v.32, no.1, 15-29.

Beven, K., and P. Germann, 1982. Macropores and water flow in soils: Water Resources Research, v.18, no.5, 1311-1325.

Beven, K.J., and R.T. Clarke, 1986. On the variation of infiltration into a homogeneous soil matrix containing a population of macropores: Water Resources Research, v.22, no.3, 383-388.

Birks, L. S., 1969. X-ray spectrochemical analysis, 2nd Ed.: Wiley-Interscience, N.Y.

Bond W.J., and I.R. Phillips, 1990. Ion transport during unsteady water flow in an unsaturated clay soil: Soil Sci. Soc. Am. J., 54:636-645.

Brown, G.O., M.L. Stone, and J.E. Gazin, 1993. Accuracy of gamma ray computerized tomography in porous media. Water Resour. Res. 29:479-486.

Brown, G.O., M.L. Stone, J.E. Gazin, and S.R. Clinkscales, 1994. Gamma ray tomography measurements of soil density variations in soil cores. Soil Sci. Soc. Am. J. Special Publication No. 36:87-97.

Bouma, J., 1981. Soil morphology and preferential flow along macropores: Agricultural Water Management, v.3, no.4, 235-250.

Cashwell, E.D., and C.J. Everett, 1959. A practical manual on the monte carlo method for random walk problems: Pergamon, Oxford.

Crestana, S., S. Mascarenhas, and R.S. Pozzi-Mucelli, 1985. Static and dynamic three-dimensional studies of water in soil using computed tomographic scanning: Soil Science, v. 140, no. 5, pp. 326-332.

Crestana, S., R. Cesareo, and S. Mascarenhas, 1986. Using a computed tomography miniscanner in soil science: Soil Science, v. 142, no. 1, pp. 56-61.

Devore, Jay L., 1987. Probability and statistics for engineering and the sciences: Brooks/Cole Publishing, Monterey.

De Vries, J. , 1969. In situ determination of physical properties of the surface layer of field soils. Soil Sci. Soc. Am. Proc. v. 33. 349-353.

Doeblin, E. O., 1990. Measurement Systems Application and Design - 4th Edition: McGraw Hill Publishing Co., N.Y.

Dyson, Norman A., 1973. X-rays in atomic and nuclear physics: Longman Group Ltd., London.

Elzeftawy, Atef, and R.S. Mansell, 1975. Hydraulic conductivity calculations for unsaturated steady-state and transient-state flow in sand. Soil Sci. Soc. Am. Proc., v. 39. pp. 599-603.

Etherington, Harold, Editor, 1958. Nuclear engineering handbook: McGraw-Hill, N.Y.

Fetter, C.W., 1993. Contaminant hydrogeology: Macmillan Publishing Company, N.Y.

Freeze, R. Allan, and John A. Cherry, 1979. Groundwater: Prentice-Hall, N.Y. 604 p.

Fritton, D.D., 1969. Resolving time, mass absorption coefficient and water content with gamma-ray attenuation. Soil Sci. Soc. Am. Proc., v. 33. pp. 651-655.

Gardner, Walter H., Gaylon S. Campbell, and C. Calissendorff, 1972. Systematic and random errors in dual gamma energy soil bulk density and water content measurements. Soil Sci. Soc. Am. Proc., v. 36. pp 393-398.

Gaston, L.A., and H.M. Selim, 1990. Transport of exchangeable cations in an aggregated soil: Soil Sci. Soc. Am. J., 54:31-38.

Germann, P. and K.Beven, 1981. Water flow in soil macropores: I. An experimental approach: Journal of Soil Science, v.32, no.1, 1-13.

Grevers, Mike C.J., and E. de Jong, 1994. Evaluation of soil-pore continuity using geostatistical analysis on macroporosity in serial sections obtained by compted tomography scanning. In Tomography of soil-water-root processes. Soil Sci. Soc. Am. Special Publication No. 36. pp. 73-86.

Grismer, M.E., 1984. Water and salt movement in relatively dry soils: PhD Dissertation, Colorado State University, Agricultural and Chemical Engineering Department, 130 p.

Hagedoorn, H.L., and A.H. Wapstra, 1960. Measurements of the fluorescent yield of the k-shell with a proportional counter. Nuclear Physics 15. North-Holland Publishing Co., Amsterdam, pp. 146-151.

Hainsworth, J.M., and Aylmore, L.A.G., 1983. The use of computer-assisted tomography to determine spatial distribution of soil water content: Aust. J. Soil Res., v.21, pp. 435-443.

Halliday, David, and Robert Resnick, 1970. Fundamentals of physics: John Wiley and Sons, Inc., N.Y.

Heinrich, Kurt F.J., Editor, 1966. Electron beam x-ray microanalysis: Van Nostrand Reinhold Company, N.Y., pp. 59-95.

Hem, John D., 1985. Study and Interpretation of the chemical characteristics of natural water: U.S. Geol. Survey Water-Supply Paper 2254, U.S. Govt. Printing Office, 263 p.

Hillel, Daniel, 1980. Fundamentals of soil physics: Academic Press, Inc., N.Y.

Hopmans, Jan W., Milena Cislerova, and Tomas Vogel, 1994. X-ray tomography of soil properties. In tomography of soil-water-root processes. Soil Sci. Soc. Am. Special Publication No. 36. pp 17-28.

Jaeger, R.G., Editor-in-Chief, 1968. Engineering compendium on radiation shielding, vol. 1: Springer-Verlag, N.Y.

Jenkins, Ron, and J.L. De Vries, 1969. Practical x-ray spectrometry: Springer-Verlag, N.Y.

Jenkins, Ron, R.W. Gould, and D. Gedcke, 1981. Quantitative x-ray spectrometry: Marcel Dekker, Inc., N.Y.

Kahn, H., 1954. Use of different monte carlo sampling techniques. Symposium on monte carlo methods, Wiley, N.Y.

Lide, David R., Editor-in-Chief, 1995. Handbook of chemistry and physics, 76th Edition: CRC Press, N.Y.

Nofziger, D.L.,1978. Errors in gamma-ray measurement of water content and bulk density in nonuniform soils. Soil Sci. Soc. Am. J. 42:845-850.

Petrovic, A.M., Siebert, and P.E. Rieke, 1982. Soil bulk density analysis in three dimensions by computed tomographic scanning: Soil Sci. Am. Journal, v. 46, no. 3, pp. 445-450.

Peyton, R. Lee, Stephen H. Anderson, Clark J. Ganzter, John W. Wigger, David J. Heinze, and Hong Wang, 1994. Soil-core breakthrough measured by x-ray computed tomography. In Tomography of soil-water-root processes. Soil Sci. Am. Special Publication No. 36. pp 59-71.

Radon, J., 1917. On the determination of functions from their integrals along certain manifolds, Berichte Saechsische Akad. Wissenschaft., Leipzig, v. 69.

Radulovich, R., E. Solorzano, and P. Sollins, 1989. Soil macropore size distribution from water breakthrough curves: Soil Sci. Soc. Am. J., v.53, 556-559.

Reginato, Robert J., and Ray D. Jackson, 1971. Field measurement of soil-water content by gamma-ray transmission compensated for temperature fluctuations. Soil Sci. Soc. Am. Proc., v.35. pp. 529-533.

Sienko, Michell J., and Robert A. Plane, 1979. Chemistry: principles and applications: McGraw-Hill, N.Y.

Smettem, K.R.J., 1986. Analysis of water flow from cylindrical macropores: Soil Sci. Soc. Am. J., v.50, 1139-1142.

So, H.B., and P.H. Nye, 1989. The effect of bulk density, water content, and soil type on the diffusion of chloride in soil: Journal of Soil Science, v. 40, 743-749.

Stillwater, R., and Klute, A., 1988. Improved methodology for a collinear dual-energy gamma radiation system: Water Resources Research, v. 24, no. 8, pp. 1411-1422.

Storm, Ellery, and Harvey I. Israel, 1970. Photon cross sections from 1 keV to 100 MeV for elements Z=1 to Z=100: Nuclear Data Tables, A7, no. 6, 565-681.

Tertian, R., and F. Claisse, 1982. Principles of quantitative x-ray fluorescence analysis: Heyden, London.

Topp, G.C. 1969. Soil-water hysteresis measured in a sandy loam and compared with the hysteretic domain model. Soil Sci. Soc. Am. Proc., v.33. pp 645-651.

van Bavel, C. H. M., N. Underwood, and S.R. Rager, 1957. Transmission of gamma radiation by soils and soil densitometry. Soil Sci. Soc. Am. Proc., v. 28. pp 588-591.

Van Genuchten, M.T., 1981. A comparison of numerical solutions of the one-dimensional unsaturated-saturated flow and mass transport equations: Adv. Water Resourc., v.5, 47-55.

van Genuchten, M.T., D.H. Tang, and R. Guennelon, 1984. Some exact solutions for solute transport through soils containing large cylindrical macropores: Water Resources Research, v.20, no.3, 335-346.

Veigele, Wm. J., 1973. Photon cross sections from 0.1 keV to 1 MeV for elements Z=1 to Z=94: Atomic Data Tables, vol. 5, no. 1, 51-111.

Warner, G.S., and Nieber, J.L., 1988. CT scanning of macropores in soil columns: Am. Soc. Ag. Eng. Presentation, Paper No. 88-2632, International Winter Meeting.

Wood, J.I., 1982. Computational methods in reactor shielding: Pergamon Press, N.Y.

Zachmann, J.E., D.R. Linden, and C.E. Clapp, 1987. Macroporous infiltration and redistribution as affected by earthworms, tillage, and residue: Soil Sci. Soc. Am. J., v.51, 1580-1586.

APPENDIX A

SOURCE CODE FOR GRATE

```
'QB TRANSLATION FROM FORTRAN OF MONTEREY MARK I BY
'J. WOOD, U. OF L., 1980. XLATION AND CHANGES BY J. GAZIN,
' OSU Biosystems Engineering.
'THIS PROGRAM APPLIES THE MONTE CARLO METHOD TO GAMMA
'PHOTON TRANSPORT. IT SIMULATES THE TRANSMISSION AND
'REFLECTION OF GAMMA RAYS INCIDENT ON A TARGET MATERIAL.
'PAIR PRODUCTION PHENOMENA ARE TREATED AS ABSORPTION.
'ANYTHING DEALING WITH DOSAGE AND ALBEDO HAVE BEEN RE-
'MOVED TO SPEED UP SIMULATIONS. MODEL CONVERTED TO DEAL
'WITH A CYLINDRICAL TARGET OF CONSTANT HETEROGENOUS COM-
'POSITION. IF XRAYS ARE GENERATED AN AUXILIARY FILE IS
'CREATED AND SIMULATIONS RAN AFTER INITIAL PHOTONS HAVE
'BEEN SCORED.
DECLARE SUB Angles ()
DECLARE SUB ConCalc ()
DECLARE SUB Evaluate ()
DECLARE SUB History ()
DECLARE SUB InputData ()
DECLARE SUB NextStep ()
DECLARE SUB Prelim ()
DECLARE SUB Scatter ()
DECLARE SUB Score ()
DECLARE SUB Start ()
DECLARE SUB XRay ()
DECLARE SUB WriteData ()
DIM SHARED Target(1300), Pkxray(1300), Y(1300), WB(1300)
DIM SHARED F(25), IO(25), K(25), KI(25), H2O(25), Pxray(25), SIO2(25), TargetMu(25), D(5)
DIM SHARED Escaping0(1025), Escaping45(1025), Escaping90(1025), EB(1025)
DIM SHARED Escaping225(1025), Escaping270(1025), CCH(360), SCH(360)
DIM SHARED CriticalW, CDPH, CIMAX, COSM, CPH, CPHN, CTH, CTHN
DIM SHARED EMAX, EMIN, ESubI, Height, I, IMAX, JAT, JAZ, JB, JGO, MassConcI, MAT
DIM SHARED MEN, Pi, PiOvr2, Radius, RadToDeg, Rho, R2, RhoI, SDPH, Status
DIM SHARED SOM, SPH, SPHN, StepCounter, STH, STHN, UX, UY, UZ
DIM SHARED W, WMAX, WMIN, X, XN, Y, YN, Z, ZN, ZSC,ZSubI
DIM SHARED PhotonNumber AS LONG, RecordNumber AS LONG, NoXrays AS LONG,
DIM SHARED Convert1, Convert2, Convert3, Convert4, Convert5, Convert6
DIM SHARED WB1Upper, WB1Lower, WB2Upper, WB2Lower, WB3Upper, WB3Lower
DIM SHARED WB4Upper, WB4Lower, WB5Upper, WB5Lower, WB6Upper, WB6Lower


        'OPEN FILE TO WHERE X-RAY COORDINATES WILL BE WRITTEN.


    TYPE XPosition
        X AS SINGLE
        Y AS SINGLE
        Z AS SINGLE
    END TYPE

DIM SHARED XRecord AS XPosition
OPEN FileName FOR RANDOM AS #6 LEN = LEN(XRecord)
RecordNumber = LOF(6) \ LEN(XRecord)

            'OPEN FILES FOR ENERGY SPECTRA AT EACH
            'DETECTOR POSITION.

OPEN "Path\0_100.DAT" FOR APPEND AS #1
```

```
OPEN "Path\45_100.DAT" FOR APPEND AS #2
OPEN "Path\90_100.DAT" FOR APPEND AS #3
OPEN "Path\225_100.DAT" FOR APPEND AS #4
OPEN "Path\270_100.DAT" FOR APPEND AS #5

        InputData
        Prelim
            FOR PhotonNumber = 1 TO IMAX
                History
            NEXT PhotonNumber
            WriteData
        CLOSE #1
        CLOSE #2
        CLOSE #3
        CLOSE #4
        CLOSE #5
        CLOSE #6
END

SUB Angles


            'AZIMUTHAL ANGLE OF SCATTERING IS RANDOMLY CHOSEN
            'BETWEEN 0 - 360 DEGREES.


        RA = RND
        JAZ = INT(360! * RA)


            'NEW VALUES OF PHOTON'S DIRECTION VARIABLES ARE OBTAINED
            'FROM STD. RELATIONSHIPS IN SPHERICAL TRIG. USE IS MADE
            'OF PREVIOUSLY CONSTRUCTED COS AND SIN TABLES TO EVAL.
            'NECESSARY TRIG FUNCTIONS.

                            'VARIABLES USED
        'CCH/SCH      - COS(PHI)...LOCAL AZIMUTHAL ANGLE OF COMPTON SCATTERING
        'CDPH/SDPH  - COS(PHI(N+1) - PHI(N))...PHOTON'S DIRECTION OF MOTION
        '                     BEFORE AND AFTER NTH SCATTERING.
        'COSM/SOM  - COS(THETA)...DEFLECTION ANGLE OF COMPTON SCATTERING
        'CPH/SPH      - COS(PHI)...AZIMUTHAL ANGLE OF PARTICLES'S DIR. OF MOTION
        'CPHN/SPHN  - NEW VALUE AFTER A SCATTERING
        'CTH/STH      - COS(THETA)...OBLIQUITY ANGLE OF PARTICLE'S DIR. OF MOTION
        'CTHN/STHN  - NEW VALUES AFTER A COLLISION
        'JAZ          - INDEX FOR PICKING COS AND SIN OF AN ANGLE UNIFORMLY
        '                     DISTRIBUTED BETWEEN 0 - 360 DEGREES
        'UX          - DIRECTION COSINE...COS(PHI)*SIN(THETA)
        'UY          - DIRECTION COSINE...SIN(THETA)*SIN(PHI)
        'UZ          - DIRECTION COSINE...COS(THETA)
        'X/Y/Z        - X, Y AND Z COORDINATES (CM.) OF PHOTON
        'XN/YN/ZN   - POSTULATED COORD.S AT NEXT COLLISION
        'ZSC          - HGT. (CM.) OF PHOTON EMERGING FROM TARGET

        CTHN = CTH * COSM + STH * SOM * CCH(JAZ + 1)
        FixIt = 1! - CTHN * CTHN
        STHN = SQR(FixIt)
        DENOM = STH * STHN
```

```
                    'IF THE DENOMINATOR IS TOO LOW AN ALTERNATIVE PROC.
                    'IS FOLLOWED TO PRESERVE ACCURACY.

Condition = ABS(DENOM) - .000001
SELECT CASE Condition
    CASE IS <= 0
        CDPH = -CCH(JAZ + 1)
        SDPH = SCH(JAZ + 1)
    CASE IS > 0
        CDPH = (COSM - CTH * CTHN) / DENOM
        SDPH = SOM * SCH(JAZ + 1) / STHN
    CASE ELSE
END SELECT
CPHN = CPH * CDPH - SPH * SDPH
SPHN = SPH * CDPH + CPH * SDPH


            'UPDATE VALUES OF ANGULAR VARIABLES


CTH = CTHN
STH = STHN
CPH = CPHN
SPH = SPHN


            'PHOTON'S NEW DIRECTION COSINES ARE COMPUTED.  THIS IS
            'ESSENTIAL INFO REQ. BY SUBS NextStep AND Score.
            'EQ. 7.16, P. 277, COMPUTATIONAL METHODS IN REACTOR
            'SHIELDING.

UZ = CTH
UY = STH * SPH
UX = STH * CPH


            'EXIT TO History
END SUB

SUB ConCalc
                'GIVEN CONC. OF IODIDE IN MG/L, THIS MODULE
                'CALCULATES THE MASS OF I AND K IN THE SYSTEM
                'WHICH ALLOWS MuOvrRho OF THE SYSTEM TO BE
                'CALCULATED.  THIS IS ONLY FOR THIS SYSTEM.

ConcI = 100000
MassSand = 43.79: MassWater = 8!: VolumeSample = 26.066
GramsPerMolI = 126.9045: GramsPerMolK = 39.0983
ConcI = ConcI / 1000          'MG OR PPM TO GRAMS
MassI = ConcI * (MassWater / 1000) 'G/L * # OF LITERS (8/1000)
MolsI = ConcI / GramsPerMolI
MassK = MolsI * GramsPerMolK * (MassWater / 1000)
MassKI = MassK + MassI


                'CALCULATE MASS CONCENTRATIONS OF ALL
                'COMPONENTS IN THE SYSTEM

MassSystem = MassSand + MassWater + MassKI
MassConcI = MassI / MassSystem
```

```
            MassConcKI = MassKI / MassSystem
            MassConcWater = MassWater / MassSystem
            MassConcSand = MassSand / MassSystem

                   'CALCULATE DENSITY OF SAMPLE

            Rho = MassSystem / VolumeSample

                   'CALCULATE Mu/Rho OF MIXTURE BASED ON C[I].

            FOR I = 1 TO MAT
                  TargetMu(I) = SIO2(I) * MassConcSand + KI(I) * MassConcKI + H2O(I) *
                             MassConcWater
            NEXT I
      END SUB

      SUB Evaluate
      DIM J, StartValue AS INTEGER
                  'CONSTRUCT FINE MESH TABLE FOR THE VARIOUS ATTEN. COEFF.
                  'USING NEWTON DIVIDED DIFFERENCE INTERPOLATION OF COARSE
                  'MESH DATA IN BOTH THE INDEPENDENT VARIABLE AND FUNCTION.
                  'USE A 3RD DEGREE FIT ON 4 KNOWN POINTS AT A TIME TO MIN-
                  'IMIZE ERROR. X(3) BECOMES X(0) OF THE NEXT GROUP OF POINTS
                  'EXCEPT AT THE ABSORPTION EDGE WHERE X(0) HAS BEEN ARBITRAR-
                  'ILY SET AT 0.0331 SO THAT THE SAME POINT WILL NOT HAVE 2
                  'F(I)'S. ALL VALUES IN MeV.
                  '
                  '       A     B     C      D      E          F
                  'X(0)  2.0   0.8   0.40   0.15   0.06        0.0331
                  'X(1)  1.5   0.6   0.30   0.10   0.05        0.03
                  'X(2)  1.0   0.5   0.20   0.08   0.04        0.02
                  'X(3)  0.8   0.4   0.15   0.06   0.033166    0.015
                  '
                  'DeltaX = -0.0025 MeV FOR GROUPS A THRU D AND -0.0001 MeV
                  'FOR GROUPS E THRU F.

                  'COARSE MESH PHOTON ENERGY TABLE (MeV)

      EB(1) = 2!: EB(2) = 1.5: EB(3) = 1!: EB(4) = .8: EB(5) = .6: EB(6) = .5
      EB(7) = .4: EB(8) = .3: EB(9) = .2: EB(10) = .15: EB(11) = .1: EB(12) = .08
      EB(13) = .06: EB(14) = .05: EB(15) = .04: EB(16) = .033166: EB(17) = .0331
      EB(18) = .03: EB(19) = .02: EB(20) = .015

                  A = 1: B = 2: C = 3: D = 4: E = 5: F = 6
                  GROUP = A
                  StepCounter = 0
                  DEGREE = 3
      DO
            SELECT CASE GROUP
                  CASE IS = A
                        UPPER = EB(1): LOWER = EB(4)
                        NumberOfSteps = 480: StartValue = 1
                        DeltaX = -(UPPER - LOWER)/NumberOfSteps
                        GROUP = B
                  CASE IS = B
```

```
                    UPPER = LOWER: LOWER = EB(7)
                    NumberOfSteps = 160: StartValue = 4
                      DeltaX = -(UPPER - LOWER)/NumberOfSteps
                      GROUP = C
                CASE IS = C
                    UPPER = LOWER: LOWER = EB(10)
                    NumberOfSteps = 100: StartValue = 7
                      DeltaX = -(UPPER - LOWER)/NumberOfSteps
                      GROUP = D
                CASE IS = D
                    UPPER = LOWER: LOWER = EB(13)
                    NumberOfSteps = 36: StartValue = 10
                      DeltaX = -(UPPER - LOWER)/NumberOfSteps
                      GROUP = E
                CASE IS = E
                    UPPER = LOWER: LOWER = EB(16)
                    NumberOfSteps = 267: StartValue = 13
                      DeltaX = -(UPPER - LOWER)/NumberOfSteps
                    GROUP = F
                CASE IS = F
                    UPPER = EB(17): LOWER = EB(20)
                    NumberOfSteps = 181: StartValue = 17
                      DeltaX = -(UPPER - LOWER)/NumberOfSteps
                      GROUP = Z
                CASE ELSE
                    EXIT DO
            END SELECT

            FOR I = 0 TO DEGREE
                D(I) = F(StartValue + I)
                EB(I) = EB(StartValue + I)
            NEXT I

                    'CONSTRUCT DIVIDED DIFFERENCE TABLE
                    'FOR HIGHER ORDER DIFFERENCES.

            FOR I = 1 TO DEGREE
                FOR J = DEGREE TO I STEP -1
                    D(J) = (D(J) - D(J - 1)) / (EB(J) - EB(J - I))
                NEXT J
            NEXT I

                    'EVALUATE AT DESIRED POINTS

            FOR J = 1 TO NumberOfSteps
                K = UPPER + (J - 1) * DeltaX
                StepCounter = StepCounter + 1
                Answer = D(3)
                FOR I = (DEGREE - 1) TO 0 STEP -1
                    Answer = D(I) + (K - EB(I)) * Answer
                    Y(StepCounter) = Answer
                NEXT I
            NEXT J
        LOOP
```

```
        K = UPPER + (J - 1) * DeltaX
        StepCounter = StepCounter + 1
        Answer = D(3)
        FOR I = (DEGREE - 1) TO 0 STEP -1
            Answer = D(I) + (K - EB(I)) * Answer
            Y(StepCounter) = Answer
        NEXT I
END SUB


SUB History
        Start           'A PHOTON'S INITIAL STATE IS DEFINED
5       NextStep        'PATHLENGTH TO NEXT COLLISION IS FOUND


                'SEE IF PHOTON CROSSES BOUNDARIES. IF IT DOES, STATUS
                'IS SET TO 1.  IF NOT STATUS IS SET TO 0 AND PHOTON
                'IS SCATTERED AGAIN. IF AN XRAY IS GENERATED, XN, YN, ZN
                'ARE WRITTEN TO FILE SO THAT THE SCATTERED PHOTON'S LIFE
                'CAN STILL BE FOLLOWED.  AFTERWARDS, THE XRAY FILE WILL
                'BE READ AND SIMULATIONS STARTED AT COORDINATES OF EACH
                'XRAY WITH E = 28 keV.


        Score
        IF Status = 1 THEN GOTO 500
        Scatter


                'IF E < EMIN THEN HISTORY IS TERMINATED


        TestW = W - WMAX
        SELECT CASE TestW
            CASE IS <= 0
                'ASCERTAIN PHOTON'S DIRECTIONS
                Angles
                GOTO 5
            CASE ELSE
        END SELECT


500             'EXIT TO PARTICLE FOR START OF NEW PHOTON
END SUB


SUB InputData
IMAX = 1000000  'NUMBER OF PARTICLES TO TRACK.
RhoI = 4.94     'DENSITY OF IODIDE
EMAX = .662     'MAX. ENERGY IN MeV (EMAX LTE. 10)
EMIN = .02      'CUT-OFF ENERGY (MeV). PHOTON'S LIFE HISTORY IS TERMINATED
                'WHEN ITS ENERGY IS REDUCED TO < EMIN (EMIN GTE. 0.018)
MEN = 1024      'NO. OF INTERVALS REQUIRED IN PHOTON ENERGY SPECTRUM TABLE
MAT = 20        'TOTAL NO. OF COARSH MESH ENERGIES FOR BASIC X-SECTION DATA
Radius = 2.55   'RADIUS OF TARGET (CM.)
R2 = Radius * Radius
Height = .638   'HALF-HEIGHT OF TARGET (CM.)
Bounce = 0      'COUNTER THAT KEEPS TRACK OF TOTAL NUMBER OF INTERACTIONS.

XRayCounter = 0 'COUNTER THAT KEEPS TRACK OF NUMBER OF X-RAYS GENERATED.
JumpRatio = .838 'ABSORPTION JUMP RATIO: (R - 1) / R
FYield = .869   'FLUORESCENCE YIELD OF IODIDE K SHELLS
```

GKalfa = .8108   'RATIO OF K ALFA X-RAYS TO TOTAL K X-RAYS (INTENSITIES)
ESubl = JumpRatio * FYield * GKalfa

'ALL ATTENUATION COEFF'S OBTAINED EITHER DIRECTLY OR DERIVED
'FROM 4.1-3, PP. 173-177 IN ENGINEERING COMPENDIUM ON RADI-
'ATION SHIELDING, VOL. 1 (1968). THIS Mu/Rho DATA DO NOT
'INCLUDE COHERENT SCATTERING (RAYLEIGH X-SECTION) BECAUSE
'PAIR PRODUCTION WILL NOT OCCUR AT Cs137 ENERGIES.

'COARSE MESH MASS ATTEN. COEFF. FOR IODIDE (CM^2/G)

IO(1) = .0409: IO(2) = .0459: IO(3) = .0574: IO(4) = .066: IO(5) = .0807
IO(6) = .0936: IO(7) = .116: IO(8) = .168: IO(9) = .349: IO(10) = .673
IO(11) = 1.91: IO(12) = 3.52: IO(13) = 7.55: IO(14) = 12.3: IO(15) = 22.3
IO(16) = 35.8397: IO(17) = 6.0509: IO(18) = 7.98: IO(19) = 24.7: IO(20) = 53.4

'COARSE MESH MASS ATTEN. COEFF. FOR POTASSIUM (CM^2/G)

K(1) = .0439: K(2) = .0505: K(3) = .0619: K(4) = .0689: K(5) = .0786
K(6) = .0852: K(7) = .0938: K(8) = .106: K(9) = .128: K(10) = .15
K(11) = .216: K(12) = .296: K(13) = .512: K(14) = .777: K(15) = 1.39
K(16) = 1.4305: K(17) = 1.4313: K(18) = 3.14: K(19) = 10.5: K(20) = 24.6

'COARSE MESH MASS ATTEN. COEFF. FOR KI (CM^2/G)

KI(1) = .0416: KI(2) = .047: KI(3) = .0585: KI(4) = .0667: KI(5) = .0802
KI(6) = .0916: KI(7) = .1108: KI(8) = .1534: KI(9) = .2969: KI(10) = .5498
KI(11) = 1.511: KI(12) = 2.7607: KI(13) = 5.8924: KI(14) = 9.586: KI(15) = 17.3751
KI(16) = 27.7354: KI(17) = 4.2971: KI(18) = 6.84: KI(19) = 21.3555: KI(20) = 46.618

'COARSE MESH MASS ATTEN. COEFF. FOR SILICA (CM^2/G)

SIO2(1) = .0446: SIO2(2) = .0518: SIO2(3) = .0635: SIO2(4) = .0707: SIO2(5) = .0805
SIO2(6) = .0871: SIO2(7) = .0954: SIO2(8) = .107: SIO2(9) = .1239: SIO2(10) = .1368
SIO2(11) = .1618: SIO2(12) = .1836 SIO2(13) = .2329: SIO2(14) = .2911: SIO2(15) = .4225
SIO2(16) = .4287: SIO2(17) = .429 SIO2(18) = .7907: SIO2(19) = 2.3648: SIO2(20) = 5.5231

'COARSE MESH MASS ATTEN. COEFF. FOR WATER (CM^2/G)

H2O(1) = .0493: H2O(2) = .0575: H2O(3) = .0706: H2O(4) = .0785: H2O(5) = .0894
H2O(6) = .0966: H2O(7) = .106: H2O(8) = .118: H2O(9) = .136: H2O(10) = .149
H2O(11) = .168: H2O(12) = .179: H2O(13) = .197: H2O(14) = .214: H2O(15) = .248
H2O(16) = .2845: HO(17) = .2851: H2O(18) = .337: H2O(19) = .711: H2O(20) = 1.48

'GOTO SUB ConCalc TO CALCULATE TargetMu(I)

ConCalc

'FRACTION ABSORBED BY IODIDE AND P(X-RAY) WILL BE EQUAL TO
'C[I] * ESubl * (Mu/Rho (I))/ (Mu/Rho (Sample))

FOR I = 1 TO MAT
    Pxray(I) = MassConcl * ESubl * (IO(I) / TargetMu(I))
NEXT I

```
                    'EXIT TO PARTICLE
END SUB

SUB NextStep
        'JGO HELPS TABLE LOOK-UP BY CAUSING SEARCH FOR JAT
        'TO START WITHIN APPROPRIATE BAND TO PHOTONS PREV-
        'IOUS VALUE OF W.  LOWER VALUES OF JGO ARE EXCLUDED
        'SINCE W CAN ONLY INCREASE WITH SCATTERING.

TempE = .5110034 / W
DO
    SELECT CASE JGO
        CASE IS = 1
                'FIRST BAND SEARCHED
            Test1 = TempE - WB1Lower
            SELECT CASE Test1
                CASE IS >= 0
                    JAT = Convert1 * ABS(TempE - WB1Upper)
                    JAT = CINT(JAT + 1)
                    EXIT DO
                CASE IS < 0
                    JGO = 2
                CASE ELSE
            END SELECT
        CASE IS = 2
                'SECOND BAND SEARCHED
            Test2 = TempE - WB2Lower
            SELECT CASE Test2
                CASE IS >= 0
                    JAT = Convert2 * ABS(TempE - WB2Upper)
                    JAT = CINT(JAT + 480)
                    EXIT DO
                CASE IS < 0
                    JGO = 3
                CASE ELSE
            END SELECT
        CASE IS = 3
                'THIRD BAND SEARCHED
            Test3 = TempE - WB3Lower
            SELECT CASE Test3
                CASE IS >= 0
                    JAT = Convert3 * ABS(TempE - WB3Upper)
                    JAT = CINT(JAT + 640)
                    EXIT DO
                CASE IS < 0
                    JGO = 4
                CASE ELSE
            END SELECT
        CASE IS = 4
                'FOURTH BAND SEARCHED
            Test4 = TempE - WB4Lower
            SELECT CASE Test4
                CASE IS >= 0
                    JAT = Convert4 * ABS(TempE - WB4Upper)
                    JAT = CINT(JAT + 740)
```

```
                        EXIT DO
                    CASE IS < 0
                        JGO = 5
                    CASE ELSE
                END SELECT
            CASE IS = 5
                'FIFTH BAND SEARCHED
                Test5 = TempE - WB5Lower
                SELECT CASE Test5
                    CASE IS >= 0
                        JAT = Convert5 * ABS(TempE - WB5Upper)
                        JAT = CINT(JAT + 776)
                        EXIT DO
                    CASE IS < 0
                        JGO = 6
                    CASE ELSE
                END SELECT
            CASE IS = 6
                'SIXTH BAND SEARCHED
                JAT = Convert6 * ABS(TempE - WB6Upper)
                JAT = CINT(JAT + 1044)
                EXIT DO
            CASE ELSE
        END SELECT
LOOP


            'S, PATHLENGTH TO NEXT COLLISION IS DETERMINED
            'BY RANDOM SAMPLING.

RA = RND
RAL = LOG(RA)
S = -RAL / Target(JAT)


            'COORD'S OF NEXT COLLISION POINT ARE TENT. FIXED

XN = X + S * UX
YN = Y + S * UY
ZN = Z + S * UZ



            'EXIT TO HISTORY
END SUB

SUB Prelim
DIM J, StartValue, XCounter AS INTEGER
Pi = 3.141592
PiOvr2 = Pi / 2
RadToDeg = 180 / Pi
CIMAX = IMAX          'NO. OF PARTICLE HISTORIES TO BE TRACKED

            'CONDITION FOR CASE JB = 1
RANDOMIZE TIMER

            'EVALUATE MAX AND MIN PHOTON WAVELENGTHS IN COMPTON UNITS
```

```
WMIN = .5110034# / EMAX
WMAX = .5110034# / EMIN
CriticalW = .5110034# / .033167

'CONSTRUCT SINE AND COSINE TABLES FOR MESH WIDTH = 1 DEGREE

'COMPUTED AT MID-MESH POINT

CH = -.5
FOR I = 1 TO 360
    CH = CH + 1
    CCH(I) = COS(Pi * CH / 180)
    SCH(I) = SIN(Pi * CH / 180)
NEXT I

'CONSTRUCT FINE WAVELENGTH MESH OF 6 BANDS.
'BANDS 1 THRU 4 HAVE THE SAME ENERGY MESH WIDTH.
'BANDS 5 AND 6 HAVE THE SAME ENERGY MESH WIDTH.

'JGO   ENERGY RANGE      WB RANGE      MESH INTERVAL
'          (MeV)
' 1     2.0   - .8025     0.26 -  0.63         0.0008
' 2     0.8   - .4025     0.63 -  1.27         0.004
' 3     0.4   - .1525     1.27 -  3.35         0.02
' 4     0.15  - .0625     3.35 -  8.17         0.13
' 5     0.06  - .033166   8.51 - 15.34         0.025
' 6     0.0331 - .015    15.43 - 34.06         0.102

            'BAND 1

WB(1) = 2!
FOR I = 2 TO 480
    WB(I) = 2! + ((I - 1) * -.0025)
NEXT I
WB1Upper = 2!: WB1Lower = .8025
MeshInterval1 = (WB(1) - WB(480)) / 479
Convert1 = 1 / MeshInterval1

            'BAND 2

FOR I = 481 TO 640
    WB(I) = 2! + ((I - 1) * -.0025)
NEXT I
WB2Upper = .8: WB2Lower = .4025
MeshInterval2 = (WB(481) - WB(640)) / 158
Convert2 = 1 / MeshInterval2

            'BAND 3

FOR I = 641 TO 740
    WB(I) = 2! + ((I - 1) * -.0025)
NEXT I
WB3Upper = .4: WB3Lower = .1525
MeshInterval3 = (WB(641) - WB(740)) / 98
Convert3 = 1 / MeshInterval3
```

```
                    'BAND 4

FOR I = 741 TO 776
    WB(I) = 2! + ((I - 1) * -.0025)
NEXT I
WB4Upper = .15: WB4Lower = .0625
MeshInterval4 = (WB(741) - WB(776)) / 34
Convert4 = 1 / MeshInterval4

                    'BAND 5

Stepper = 1
WB(777) = .06
FOR I = 778 TO 1044
    WB(I) = .06 + (Stepper * -.000100502#)
    Stepper = Stepper + 1
NEXT I
WB5Upper = .06: WB5Lower = .033166
MeshInterval5 = (WB(777) - WB(1044)) / 266
Convert5 = 1 / MeshInterval5

                    'BAND 6

Stepper = 1
WB(1045) = .0331
FOR I = 1046 TO 1226
    WB(I) = .0331 + (Stepper * -.0001)
    Stepper = Stepper + 1
NEXT I
WB6Upper = .0331: WB6Lower = .015
MeshInterval6 = (WB(1045) - WB(1226)) / 180
Convert6 = 1 / MeshInterval6

            'INTERPOLATE DATA ONE SET AT A TIME.

SetNumber = 1
DO
    SELECT CASE SetNumber
        CASE IS = 0
            EXIT DO
        CASE IS = 1
            FOR I = 1 TO MAT
                F(I) = LOG(Pxray(I))
            NEXT I
            Evaluate
            FOR I = 1 TO StepCounter
                Pkxray(I) = EXP(Y(I))
                IF Xray(I) > 1! THEN Pkxray(I) = 1!
            NEXT I
            SetNumber = 2
        CASE IS = 2
            FOR I = 1 TO MAT
                F(I) = LOG(TargetMu(I))
            NEXT I
            Evaluate
```

```
                    FOR I = 1 TO StepCounter
                        Target(I) = Rho *EXP( Y(I))
                    NEXT I
                    SetNumber = 0
                CASE ELSE
            END SELECT
    LOOP

    'PHOTON CURRENT ENERGY SPECTRUM MESH CONSTRUCTED
    'IN EB WITH INTERVAL = EMAX/MEN (Energy bins).

    MATO = MEN
    MEN = MEN + 1
    EB(1) = EMAX
    FOR JE = 1 TO MEN
        IF JE > MATO THEN GOTO 80
        EB(JE + 1) = EB(JE) - EMAX / MATO
80      NEXT JE
        EB(MEN) = 0!

        'PHOTON LIFE HISTORIES CAN START NOW. EXIT TO PARTICLE
END SUB

SUB Scatter
        'WAVELENGTH, W, OF SCATTERED PHOTON IS OBTAINED BY THE
        'METHOD SUGGESTED BY KAHN FOR SAMPLING THE KLEIN-NISHINA
        'PDF. THIS RELIES ON A REJECTION/ACCEPTANCE TECHNIQUE
        'TO FIND A SUITABLE VALUE OF R = (NEW W)/(OLD W) AND
        'HENCE THE NEW W.
DO
    RA = RND
    T = 2! / W
    Condition1 = RA - (1! + T) / (9! + T)
    SELECT CASE Condition1
        CASE IS <= 0
            RA = RND
            R = 1! + RA * T
            RA = RND
            Condition1A = RA - 4! * (R - 1!) / (R * R)
            SELECT CASE Condition1A
                CASE IS <= 0
                    EXIT DO
                CASE ELSE
            END SELECT
        CASE IS > 0
            RA = RND
            R = (1! + T) / (1! + RA * T)
            RA = RND
            Condition1A = RA - .5 * ((W - R * W + 1!) ^ 2 + (1! / R))
            SELECT CASE Condition1A
                CASE IS <= 0
                    EXIT DO
                CASE ELSE
            END SELECT
        CASE ELSE
```

```
            END SELECT
LOOP

            'ACCEPTABLE VALUE OF R FOUND. NEW WAVELENGTH IS COMPUTED
            'FROM WHICH THE COMPTON ANGLE OF SCATTERING CAN BE DET.

        WOLD = W
        W = R * WOLD
        COSM = 1! - W + WOLD
        SOM = SQR(1! - COSM * COSM)

            'EXIT TO HISTORY
END SUB

SUB Score
    R2Prime = XN * XN + YN * YN
    SELECT CASE R2Prime
        CASE IS < R2
            SELECT CASE ABS(ZN)
                CASE IS < Height
                    X = XN: Y = YN: Z = ZN
                    SELECT CASE W
                        CASE IS <= CriticalW
                        XRay
                        CASE ELSE
                    END SELECT
                    Status = 0
                    GOTO 400
                CASE IS >= Height
                    SELECT CASE ZN
                        CASE IS <= -Height
                            'ZSC = -Height:Theta = 362
                            GOTO 395
                        CASE IS >= Height
                            'ZSC = Height:Theta = 361
                            GOTO 395
                        CASE ELSE
                    END SELECT
                CASE ELSE
            END SELECT
        CASE IS >= R2
            RPrime = SQR(R2Prime)
            PhiPrime = ATN(ZN / RPrime)
            SELECT CASE ABS(PhiPrime)
                CASE IS > .2451632
                    SELECT CASE PhiPrime
                        CASE IS < -.2451632
                            'ZSC = -Height: Theta = 362
                            GOTO 395
                        CASE IS > .2451632
                            'ZSC = Height: Theta = 361
                            GOTO 395
                        CASE ELSE
                    END SELECT
                CASE IS <= .2451632
```

```
                    ZSC = 2.55 * TAN(PhiPrime)
               CASE ELSE
          END SELECT
          XP = X: YP = Y: XPN = XN: YPN = YN
          DO
               MPX = (XP + XPN) / 2!: MPY = (YP + YPN) / 2!
               MPX2 = MPX * MPX: MPY2 = MPY * MPY
               RP2 = MPX2 + MPY2
               R2High = R2 + .001
               R2Low = R2 - .001
               SELECT CASE RP2
                    CASE IS < R2Low
                         XP = MPX: YP = MPY
                    CASE IS > R2High
                         XPN = MPX: YPN = MPY
                    CASE ELSE
                         XSC = MPX: YSC = MPY
                         Theta = ATN(YSC / XSC) * RadToDeg
                         EXIT DO
               END SELECT
          LOOP
     CASE ELSE
END SELECT

'BASED ON XSC, YSC, AND E DETERMINE ANGLE WITH ORIGIN
'THAT SCORING COMPTON PHOTON LEAVES SYSTEM.  UNCOLLIDED
'FLUX IS ASSUMED TO LIE ON POSITIVE Y-AXIS.
'ORIGIN = 0,0,0 BASED ON CYLINDRICAL COORDINATES.

E = .5110034# / W
     SELECT CASE E
          CASE IS = .662
               Theta = 90!
               XSC = 0!
               YSC = 2.55
               ZSC = 0!
          CASE IS < .662
               SELECT CASE XSC
                    CASE IS >= 0
                         SELECT CASE YSC
                    'QUADRANT 1
                              CASE IS >= 0
                                   Theta = INT(Theta)
                    'QUADRANT 4
                              CASE IS < 0
                                   Theta = INT(360 + Theta)
                              CASE ELSE
                         END SELECT
                    CASE IS < 0
                         SELECT CASE YSC
                    'QUADRANT 2
                              CASE IS >= 0
                                   Theta = INT(180 + Theta)
                    'QUADRANT 3
                              CASE IS < 0
```

```
                              Theta = INT(180 + Theta)
                        CASE ELSE
                      END SELECT
                 CASE ELSE
               END SELECT
          CASE ELSE
        END SELECT

        'BIN THE ENERGY LEVEL

FOR JE = 1 TO MEN
    IF E >= EB(JE) THEN EXIT FOR
NEXT JE

        'DETECTOR IS AT 3 POSITIONS. ARC LENGTH CORRESPONDING
        'TO DETECTOR COLLIMATION IS 1 CM.  WINDOW OF INTEREST
        'IS 90,135, AND 180 DEGREES +/- 11 DEGREES. ZSC RANGE
        'IS ALSO 1 CM. THEREFORE, ZSC RANGE IS -.5 TO .5 CM.

        SELECT CASE Theta
             CASE 79 TO 101
                  Escaping90(JE) = Escaping90(JE) + 1
             CASE 0 TO 11
                  Escaping0(JE) = Escaping0(JE) + 1
             CASE 34 TO 56
                  Escaping45(JE) = Escaping45(JE) + 1
             CASE 124 TO 146
                  Escaping45(JE) = Escaping45(JE) + 1
             CASE 169 TO 191
                  Escaping0(JE) = Escaping90(JE) + 1
             CASE 214 TO 236
                  Escaping225(JE) = Escaping225(JE) + 1
             CASE 259 TO 281
                  Escaping270(JE) = Escaping270(JE) + 1
             CASE 304 TO 326
                  Escaping225(JE) = Escaping225(JE) + 1
             CASE 349 TO 360
                  Escaping0(JE) = Escaping0(JE) + 1
             CASE ELSE
        END SELECT
395     Status = 1
400              'EXIT TO HISTORY

END SUB

SUB Start
        'INITIAL WAVELENGTH

        W = WMIN

        'INITIAL WAVELENGTH BAND

        JGO = 2

        'DEFINE SOURCE GEOMETRY
```

```
CTH = COS(.5 * Pi): STH = SIN(.5 * Pi)
CPH = COS(.5 * Pi): SPH = SIN(.5 * Pi)

        'INITIALIZE COORDINATES OF SOURCE

X = 0!: Y = -2.55: Z = 0!

        'DEFINE DIRECTION COSINES

UZ = CTH: UY = STH * SPH: UX = STH * CPH
COSM = 1!

        'EXIT TO HISTORY
END SUB

SUB WriteData

            'SPECTRUM FOR THETA = 349 TO 11 AND 169 TO 191 DEG.

    WRITE #1, Rho,NoXrays:
    FOR JE = 1 TO MEN
        WRITE #1, EB(JE); Escaping0(JE):
    NEXT JE

            'SPECTRUM FOR THETA = 34 TO 56 AND 124 TO 146 DEG.

    WRITE #2, Rho, NoXrays:
    FOR JE = 1 TO MEN
        WRITE #2, EB(JE); Escaping45(JE):
    NEXT JE

            'SPECTRUM SPECTRUM FOR 79 TO 91 DEG.

    WRITE #3, Rho, NoXrays:
    FOR JE = 1 TO MEN
        WRITE #3, EB(JE); Escaping90(JE):
    NEXT JE

            'SPECTRUM SPECTRUM FOR 214 TO 236 AND 324 TO 346 DEG.

    WRITE #4, Rho, NoXrays:
    FOR JE = 1 TO MEN
        WRITE #4, EB(JE); Escaping225(JE):
    NEXT JE

            'SPECTRUM FOR BACKSCATTER THETA = 259 TO 281 DEG.

    WRITE #5, Rho, NoXrays:
    FOR JE = 1 TO MEN
        WRITE #5, EB(JE); Escaping270(JE):
    NEXT JE
END SUB

SUB XRay
    RA = RND
```

```
TestRA = Pkxray(JAT)
SELECT CASE RA
    CASE IS <= TestRA
        RecordNumber = RecordNumber + 1&
        XRecord.X = X
        XRecord.Y = Y
        XRecord.Z = Z
        PUT #6, RecordNumber, XRecord
        NoXrays = NoXrays + 1
    CASE ELSE
END SELECT
END SUB
```

Note: The following changes are made to GRATE to run simulations on the generated x-rays. Also, the author is aware that the random number generator in QuickBasic is banded. It was the author's opinion that effects would be neglible in this type of model. The results bore this out.

PROGRAM NAME : XRAY

Sub InputData Changes

1. Change EMAX to 0.028612
2. Omit IMAX, JumpRatio, Fyield
3. Omit For..Next loop

Sub Main Changes

```
Open "Path\File" for Random as # LEN = LEN(XRecord)
NumberOfRecords = LOF(#)\LEN(XRecord)
I = 0
For RecordNumber = 1 to NumberOfRecords
        Get #, RecordNumber, Xrecord
        X=XRecord.X : Y=XRecord.Y: Z=XRecord.Z
        XO = X: YO = Y: ZO = Z
        History
Next RecordNumber
Close #
```

Sub Score Changes

```
Select Case Theta
        CASE 79 TO 101
                Escaping90(JE) = Escaping90(JE) + 1
                Write #, XO, YO, ZO, E
        CASE 124 TO 135
                Escaping135(JE) = Escaping135(JE) + 1
                Write #, XO, YO, ZO, E
        CASE 169 TO 191
                Escaping180(JE) = Escaping180(JE) + 1
                Write #, XO, YO, ZO, E
        CASE 214 TO 236
                Escaping225(JE) = Escaping225(JE) + 1
                Write #, XO, YO, ZO, E
        CASE 259 TO 281
                Escaping270(JE) = Escaping270(JE) + 1
                Write #, XO, YO, ZO, E
        CASE ELSE
END SELECT
```

Sub Start Changes

```
Ra = RND
RaTheta = Ra * Pi
Ra = RND
RaPhi = Ra * Pi

        Define Source Geometry
```

CTH = COS(RaTheta): STH = SIN(RaTheta)
CPH = COS(RaPhi): SPH = SIN(RaPhi)

Define Direction Cosines

UZ = CTH: UY = STH*SPH: UX = STH*CPH
COSM = 1!

Initial energy is in Band 6

JGO = 6

VITA

Jack E. Gazin

Candidate for the Degree of

Doctor of Philosophy

Thesis: LABORATORY COLUMN SOLUTE CONCENTRATION MEASURE-
   MENT USING X-RAY FLUORESCENCE SPECTROSCOPY

Major Field: Biosystems Engineering

Biographical:

   Personal Data: Born in Kingfisher, Oklahoma, July 19, 1957, the son of John
      H. and Docia I. Gazin.

   Education: Graduated from Kingfisher High School, Kingfisher, Oklahoma,
      1975; Defense Language Institute, Presidio of Monterey, Monterey,
      California, 1976; U.S. Air Force School of Applied Cryptologic
      Sciences, 1976; received Bachelor of Science Degree in Geology from
      Oklahoma State University in Stillwater, Oklahoma in July, 1984;
      received Master of Science Degree in Geology from Oklahoma State
      University in Stillwater, Oklahoma in May, 1992. Completed the
      requirements for the Doctor of Philosophy Degree in May, 1998.

   Professional Experience: Research Assistant, Department of Geology,
      Oklahoma State University, May 1985, to December, 1985;
      Engineering Aid, USDA-ARS Outdoor Hydraulics Laboratory, Lake
      Carl Blackwell, Stillwater, Oklahoma, May 1986, to August, 1987;
      Teaching Assistant, Department of Geology, Oklahoma State
      University, May 1986, to August 1987; Teaching Assistant,
      Department of Biosystems and Agricultural Engineering, Oklahoma
      State University, January 1987, to May, 1987; Research Assistant,
      Department of Biosystems and Agricultural Engineering, Oklahoma
      State University, June 1987, to September, 1992; Research Engineer,
      Department of Biosystems and Agricultural Engineering, Oklahoma
      State University, May 1993, to December, 1993.